Doctoral theses at NTNU, 2023:417

Abba Elizabeth Coron

Novel and Established Alginate Hydrogel Beads for Cell Therapy

Fibrotic and Inflammatory Responses with Insights from Proteomics

Doctoral thesis

NTNU
Norwegian University of Science and Technology
Thesis for the Degree of
Philosophiae Doctor
Faculty of Natural Sciences
Department of Biotechnology and Food Science

NTNU
Norwegian University of
Science and Technology

Abba Elizabeth Coron

Novel and Established Alginate Hydrogel Beads for Cell Therapy

Fibrotic and Inflammatory Responses with Insights from Proteomics

Thesis for the Degree of Philosophiae Doctor

Trondheim, November 2023

Norwegian University of Science and Technology
Faculty of Natural Sciences
Department of Biotechnology and Food Science

NTNU
Norwegian University of
Science and Technology

NTNU
Norwegian University of Science and Technology

Thesis for the Degree of Philosophiae Doctor

Faculty of Natural Sciences
Department of Biotechnology and Food Science

ISBN 978-82-326-7534-0 (printed ver.)
ISBN 978-82-326-7533-3 (electronic ver.)
ISSN 1503-8181 (printed ver.)
ISSN 2703-8084 (online ver.)

IMT-rapport 2023:417

Doctoral theses at NTNU, 2023:417

Printed by NTNU Grafisk senter

Acknowledgments

First and foremost, I would like to extend my profound gratitude to Prof. Berit L. Strand, for being an exceptional supervisor. Your extensive knowledge in the biopolymer and alginate field, combined with your ability to educate and motivate, has significantly encouraged my academic growth. Despite the many challenges along this journey, your unwavering support has been a constant. Truly, you have been the most inspirational, supportive, and kind-hearted supervisor I could have ever wished for. I extend my utmost respect and admiration to you as not only a great leader and scientist but also as a remarkable person. I would also like to extend my heartfelt gratitude to my co-supervisor, Assoc. Prof. Anne Mari A. Rokstad, whose guidance, expertise, and support have been invaluable throughout this doctoral journey. Thank you for introducing me to the field of immunology; your profound knowledge has been instrumental in shaping both my work and academic growth. Your scientific dedication serves as a true inspiration. Equally significant are your qualities of empathy and kindness, which I sincerely value. I consider myself extremely fortunate to have had such wonderful supervisors.

I would further like to thank my friends and co-workers at NTNU. Special thanks to my closest colleague and dear friend Joachim S. Kjesbu. Since we started working together, we were pretty much glued at the hip – with our surprisingly similar mindset and borderline OCD, it was hard to not get along. You are an outstanding scientist, and it has been a true pleasure working with you. Thank you for always being extremely helpful and such a good friend. George Kopplin, thank you for adding joy to my time at NTNU. I really appreciate all our get-togethers and, of course, your excellent vegetarian cooking. Your consistently positive spirit and amazing company made a significant impact. Aman S. Chahal, I am grateful that you joined our group in Trondheim. Your kind and remarkably creative spirit is truly admirable. Thank you for all the fruitful and heartfelt discussions and for being such a nice guy. I would also like to thank the rest of the “alginate group”, Line A. Omtvedt, Anita A. Solbu, and Daria Zaytseva-Zotova, for their scientific expertise and for making such a great working environment. I really enjoyed working with all of you.

I would like to extend my sincere gratitude to Prof. Geir Slupphaug, Dr. Davi Fonseca, and Dr. Animesh Sharma at PROMEC for our excellent collaboration. I am grateful for your support and guidance through the vast and intricate world of proteomics; it has truly been an enlightening and, undeniably, challenging journey.

I extend my gratitude to senior engineer Wenche I. Strand for her exceptional support in the biopolymer lab during my time at NTNU, and for always being so friendly and caring. I would also like to thank Ann-Sissel T. Ulset and Dr. Olav Aarstad, as well as Bjørg Steinkjer and Liv Ryan at IKOM, for their technical assistance.

I extend my gratitude to the Chicago Diabetes Project and Prof. Jose Oberholzer and the group in Chicago, Dr. Peter Rios, Dr. Matt Bochenek, Jenny Cook, Doug Isa, Ira Joshi, and Sofia Ghani. Thank you for our great collaboration and for making my time in Chicago truly memorable. I would also like to express my sincere gratitude to Prof. Igor Lacík and Dr. Michal Pelach at the Slovak Academy of Sciences. Your warm welcome made for a very nice experience, both scientifically and culturally, for which I am truly thankful.

I would like to thank Robin D. Andersen, my beloved fiancé, for your endless support and for always taking such good care of me. Without you, I would be lost – I could not have done this without you. I also want to thank my mother, Anna, as well as my sisters, Ida and Sylvianna, and my brother, Dodou, for all their love and support over the years. I would also like to thank my extended family – Rolf, Yu, Joakim, Chenxing, Adrian, Rebekka, Benjamin, and the kids. I am truly grateful to my cherished and supportive friends in Oslo – Nayab, Elnaz, Ingvild, Haddy, and Beatriz. I would also like to express my heartfelt gratitude to my dear friends in Trondheim – Hilde, Carina, and Kjersti. We started our Biotechnology studies together many years ago, and your continuous support throughout this long journey means a lot to me. Thank you for all the memorable times we shared along the way. To my former PhD roommates, Ewa and Vishnu – thank you for all the good times we shared and for being part of this journey.

Finally, I offer my sincere gratitude to those who supported me in any way during the completion of my PhD, and to all my colleagues at the Department of Biotechnology who made my time at NTNU so memorable.

Preface

This thesis is submitted in partial fulfilment of the requirements for the academic title Philosophiae Doctor at the Norwegian University of Science and Technology (NTNU). The work was performed at the Norwegian Biopolymer Laboratory (NOBIPOL) at the Department of Biotechnology and Food Science, as well as the Centre of Molecular Inflammation Research (CEMIR) and the Proteomics and Modomics Experimental Core Facility (PROMEC) at the Department of Clinical and Molecular Medicine (IKOM). Part of the work was carried out at the CellTrans research laboratory at the University of Illinois Chicago (UIC). The current work was conducted under the supervision of Prof. Berit Løkensgard Strand and the co-supervision of Assoc. Prof. Anne Mari Aukan Rokstad.

The project was funded by NTNU (SO), Faculty of Natural Sciences. Parts of the work were financed by the Chicago Diabetes Project (chicagodiabetesproject.org), including proteomic analyses at PROMEC and the collaborative work with CellTrans at UIC.

The thesis includes a general introduction, an outline of the research scope, summaries of the research articles, and a general discussion based on the four scientific papers presented in the appendix.

Summary

Encapsulation of pancreatic islets in immunoprotective alginate hydrogel microspheres represents a promising alternative to current therapies for type 1 diabetes. By providing a semipermeable barrier, this strategy protects the graft from immediate immune attack and eliminates the need for immunosuppression with its inherent health risks. However, no clinical trial has yet succeeded in maintaining the long-term function of grafted islets. Several challenges associated with alginate microsphere encapsulation have been identified, including hydrogel instability and pericapsular fibrotic overgrowth (PFO), which may lead to graft failure. While foreign body reactions to biomaterials are well-documented and begin with protein adsorption, the specific proteins that adsorb to alginate microspheres and their role in PFO development remain to be elucidated.

One primary objective of this thesis was to develop alginate microbeads with sustained efficacy for cell encapsulation therapy in the treatment of type 1 diabetes. This involved formulating and characterising alginate microbeads with high stability and minimal PFO. Stable microbeads were achieved using intermediate guluronate (G) alginate and chemically modified alginate with sulfate groups. Importantly, these microbeads demonstrated minimal PFO in C57BL/6J mice compared to high G microbeads used in previous clinical trials. Additionally, a human whole blood model revealed no significant increases in complement activation or cytokine induction for all microbeads compared to a saline control. Furthermore, the immunoprotective capabilities of both high G and sulfated alginate beads were demonstrated through encapsulated rat islets transplanted into diabetic C57BL/6J mice, which exhibited glucose-responsive islets for the study duration of 120 days. The evaluation of intermediate G alginate beads was obstructed due to precipitate of hydroxyapatite, however maintained normoglycemia for 50 days in the same mouse model.

We also hypothesised that investigating the adsorbed proteins on specific alginate microspheres could provide valuable insights into the different host responses observed for these microspheres. To gain these insights, we developed a novel mass spectrometry

(MS)-based proteomics approach for in-depth protein profiling of the materials, which included high G alginate and sulfated alginate microbeads, along with poly-L-lysine-coated microbeads. Incubation in lepirudin-anticoagulated human plasma enabled the investigation of acute-phase proteins within the complement and coagulation systems, which are critical in biomaterial-mediated host responses. Importantly, sulfated alginate microbeads were highly enriched with complement inhibitors (e.g. factor H and C1 inhibitor) and coagulation factors (e.g. factor XII and antithrombin). In addition, several proteins with potential anti-fibrotic effects, such as matrix metalloproteinases and fibrinolytic factors (e.g. factor XII and plasma kallikrein) were found. This conforms to the low-inflammatory and anti-fibrotic profile of sulfated alginate microbeads. High G alginate microbeads were enriched with moderate levels of complement inhibitors, conforming to a low-inflammatory but fibrotic profile. In contrast, the pro-inflammatory poly-L-lysine-coated microbeads, known to be prone to PFO, displayed increased binding of complement activating factors such as C3 and properdin.

In summary, this research has demonstrated alginate microbeads that hold promise for the future treatment of type 1 diabetes. It has provided new tools and knowledge to further our understanding of initial protein adsorption and its role in the development of PFO on alginate microspheres.

Symbols and abbreviations

CLSM	Confocal laser scanning microscopy
Da	Dalton
DS	Degree of substitution
E	Young's modulus
ECM	Extracellular matrix
EDTA	Ethylene diamine tetra-acetic acid
ELISA	Enzyme-linked immunosorbent assay
G	α-L-guluronate
GAG	Glycosaminoglycan
HPLC	High-performance liquid chromatography
hPSC	Human pluripotent stem cell
hWB	Human whole blood
HR-ICP-MS	High-resolution inductively coupled plasma mass spectrometry
hWB	Human whole blood
LC-MS/MS	Liquid chromatography-tandem mass spectrometry
M	β-D-mannuronate
$(\overline{M_n})$	Number average molecular weight
MS	Mass spectrometry
$(\overline{M_w})$	Weight average molecular weight
$N_{G>1}$	Average G-block length
NMR	Nuclear magnetic resonance
OGTT	Oral glucose tolerance test
PFO	Pericapsular fibrotic overgrowth
PLL	Poly-L-lysine
PTF1.2	Prothrombin fragment 1+2
SEC-MALLS	Size exclusion chromatography with inline multi-angle laser light scattering
STZ	Streptozotocin
TCC	Terminal complement complex

List of papers

I. Strand, B. L., **Coron, A. E.**, & Skjåk-Bræk, G. (2017). Current and Future Perspectives on Alginate Encapsulated Pancreatic Islet. *Stem cells translational medicine*, *6*(4), 1053-1058.

II. **Coron, A. E.***, Kjesbu, J. S.*****, Kjærnsmo, F., Oberholzer, J., Rokstad, A. M. A., & Strand, B. L. (2022). Pericapsular fibrotic overgrowth mitigated in immunocompetent mice through microbead formulations based on sulfated or intermediate G alginates. *Acta biomaterialia*, *137*, 172-185.

III. **Coron, A. E.**, Fonseca D. M., Sharma A., Slupphaug G., Strand B. L., & Rokstad A. M. A. (2022). MS-proteomics provides insight into the host responses towards alginate microspheres. *Materials Today Bio*, *17*, 100490.

IV. Kjesbu, J. S.*, **Coron, A. E.***, Bochenek M., Rios P., Isa D., Joshi I., Ghani S., Oberholzer J., Rokstad, A. M. A., & Strand, B. L. Function of encapsulated rat islets in sulfated and intermediate G alginate in diabetic immunocompetent and immunodeficient mice. *Manuscript ready for submission.*

***** The authors contributed equally to this work.

Contributions to publications not included in this thesis:

Ørning, P., Hoem, K. S., **Coron, A. E.**, Skjåk-Bræk, G., Mollnes, T. E., Brekke, O. L., Espevik, T., & Rokstad, A. M. (2016). Alginate microsphere compositions dictate different mechanisms of complement activation with consequences for cytokine release and leukocyte activation. *Journal of controlled release*, *229*, 58-69.

Syanda, A.M., Kringstad, V.I., Blackford, S.J.I., Kjesbu, J.S., Ng, S.S., Ma, L., Xiao, F., **Coron**, **A.E.**, Rokstad, A.M.A., Modi, S., Rashid, S.T., & Strand, B.L. (2022). Sulfated Alginate Reduces Pericapsular Fibrotic Overgrowth on Encapsulated cGMP-Compliant hPSC-Hepatocytes in Mice. *Frontiers in Bioengineering and Biotechnology*, *9*, 816542.

Contents

1 Introduction

1.1 Background

Islet transplantation holds great promise as a treatment for type 1 diabetes, a disease which causes significant morbidity worldwide. However, current clinical practice faces challenges from graft rejection, impairing islet function. Long-term immunosuppressive medication is therefore necessary for sustained graft function, although it carries the risk of infections and cancer. Encapsulation of therapeutic cells within semipermeable biomaterials offers a viable strategy to protect the graft from the host immune system while permitting the diffusion of nutrients, oxygen, and secreted hormones such as insulin through the membrane. This approach may thus facilitate long-term graft survival and eliminate the need for immunosuppressive therapy. The field of biomaterials has recently made strides in optimising hydrogel-based materials for islet cell transplantation, and for various applications in tissue engineering and drug delivery. Alginate hydrogel microspheres have been extensively researched as immunoisolating materials in cell therapy, due to their general biocompatible characteristics and cell-friendly crosslinking conditions. However, a persistent obstacle in using alginate microspheres for cell encapsulation is pericapsular fibrotic overgrowth (PFO). This involves the overgrowth of host cells on the microsphere surface as part of a foreign body response, disrupting nutrient and oxygen exchange and thereby limiting graft viability. Understanding the interactions at the host–biomaterial interface is, however, not a trivial task. Both the causal factors leading to PFO on alginate hydrogel microbeads as well as the mechanisms by which certain alginate-based materials resist or mitigate fibrosis remain poorly understood. Protein adsorption to the biomaterial surface occurs immediately after implantation and plays a pivotal role in the interaction between the material and cells or tissues, ultimately governing the subsequent host responses. Consequently, characterising protein adsorption on biomaterials may prove critical in our understanding of host–biomaterial interactions and in the development of new biomaterials. Indeed, recent studies have revealed the role of adsorbed proteins in modulating inflammatory responses. However, there is a notable knowledge gap regarding the protein adsorption profiles of alginate

hydrogel microspheres. Addressing this gap could significantly advance the design of high-performing, non-fibrotic alginate materials for cell encapsulation therapies. Hence, the present work has focused on the production of novel alginate hydrogel materials with reduced host responses. Firstly, the work herein entailed a detailed characterisation of various alginate formulations with respect to their physicochemical and inflammatory properties, as well as PFO. Furthermore, we investigated protein adsorption both *in vitro* and *in vivo*, including in-depth proteomic profiling of alginate microspheres eliciting different host responses. Lastly, we evaluated the efficacy of alginate materials as immune barriers, along with their ability to support transplanted islet function *in vivo*. These investigations have revealed alginate microbeads with minimal PFO, which are promising for cell encapsulation therapy in the treatment of type 1 diabetes.

1.2 Diabetes

Diabetes, also known as diabetes mellitus, is a group of metabolic diseases characterised by hyperglycaemia resulting from impaired insulin production, insulin resistance, or both [1]. The majority of diabetes cases can be divided into two main categories, namely type 1 and type 2 diabetes. An estimated 5–10% of diabetics suffer from type 1 diabetes while type 2 diabetes constitutes approximately 90–95% of cases. Type 1 diabetes results from a cellular-mediated autoimmune destruction of the pancreatic islet cells (β-cells) responsible for insulin production. This leads to complete absence or inadequate levels of insulin necessary for maintaining normoglycemia, thereby requiring treatment through exogenous insulin administration [2]. Type 2 diabetes involves insulin resistance and relative insulin deficiency. Since autoimmune β-cell destruction is absent, insulin treatment is not always essential. Management can range from lifestyle changes to medications or insulin [3]. Despite advances, managing type 1 diabetes remains a significant challenge due to long-term complications resulting from hyperglycaemia as well as acute and recurring episodes of hypoglycaemia [1, 2]. Diabetes and the complications that follow constitute a significant cause of morbidity and mortality worldwide. Persistent hyperglycaemia is associated with long-term damage and dysfunction of multiple organs, including the eyes, kidneys, nerves, heart, and blood vessels, as well as a notable reduction in life expectancy [1, 4]. Given the

estimated global diabetes prevalence of 10.5% in the adult population (aged 20–79 years), representing 536.6 million individuals (2021; [5]), there is a clear need for novel therapeutic interventions to mitigate this significant health and economic burden.

1.2.1 Transplantation therapies for diabetes

Whole-organ pancreas and islet transplantations are primarily performed on type 1 diabetes patients, particularly those with recurrent severe hypoglycaemia or kidney failure that requires transplantation [4, 6]. While whole-pancreas transplants are highly effective in achieving insulin independence, they come with significant surgical risks, making the less invasive procedure of islet transplantation a more attractive alternative [7]. Recent years have brought significant advancements in clinical islet transplantation, leading to high success rates in normalising glycaemic control, although this often requires multiple pancreas donors. It offers long-term clinical outcomes similar to whole-pancreas transplantation, with insulin independence observed in 50–70% of patients after 5 years [4]. In another significant milestone, the U.S. Food and Drug Administration recently approved [8] the first allogeneic pancreatic islet cellular therapy (*Lantidra*) derived from deceased donors, for treating type 1 diabetes. This approval enhances the accessibility of islet transplantation for diabetic patients, albeit limited to the U.S. at present. Despite the efficacy of traditional transplantation treatments, their widespread use is restricted by a shortage in donors and the need for lifelong immunosuppression [9]. While allogeneic islets remain the clinical gold standard, their scarcity fails to meet patient demand. Alternative sources like stem cell-derived β-cells offer a potential solution [10, 11] to satisfy this demand, although concerns regarding efficacy, safety, and regulation still persist [9]. Cell encapsulation represents a viable strategy for islet transplantation by providing an immune barrier, thereby eliminating the need for immunosuppression [12, 13]. Despite the potential of cell encapsulation therapy in the treatment of diabetes, its long-term efficacy has yet to be achieved.

1.3 Immunoisolation in cell therapy

In cell-based therapies, the concept of immunoisolation involves restoring lost or impaired functions by protecting grafted tissue or cells from the host immune system using biocompatible materials. The transplanted cells are encapsulated in a semi-permeable membrane that allows for free diffusion of oxygen, nutrients, and effector molecules, while preventing the ingress of immune cells and molecules that may be detrimental to the therapeutic cells [14, 15] (**Figure 1**). Key considerations for developing an implantable device encompass the type of encapsulation material, the device size, and the site of implantation. Encapsulation devices are generally classified as macro-, micro-, or nanoscale and can be implanted into intravascular or extravascular sites in the body [16, 17].

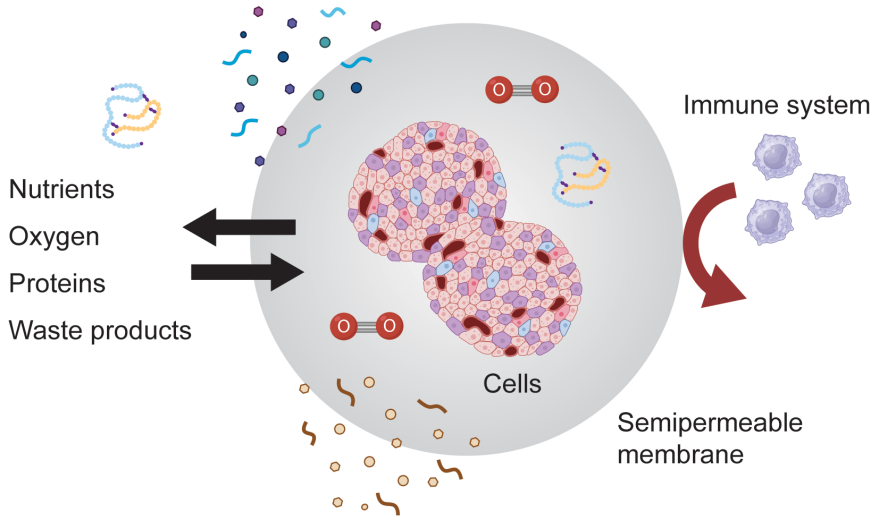

Figure 1. The principle of immunoisolation. Using a semipermeable membrane, this technique allows for the exchange of nutrients, oxygen, therapeutic proteins (e.g. insulin), and waste products, while protecting the transplanted cells from the host immune system. Adapted from [18, 19] and partly includes artwork from BioRender.

Similar to whole-organ transplants, transplanted tissues or cells (allo- or xenograft) are identified as foreign by the host immune system, triggering a response that may ultimately destroy the graft if left unprotected. Prolonged graft function is achieved by immunosuppressive therapy to modulate the immune system. However, the non-

specific nature of these medications can compromise the patient's overall immunity, increasing the likelihood of infections, cancer, and other malignancies [4, 20]. Thus, immunoisolation therapy presents a promising solution not only for circumventing the challenges of graft rejection, but also for eliminating the need and side effects of immunosuppression. Immunoisolation devices can be used to transplant cells for treating a variety of human diseases. Pancreatic islet transplants for treating type 1 diabetes is a key area of research, where these devices may potentially provide protection to encapsulated islet cells against autoimmunity and allo- or xenograft rejection [9]. In particular, microencapsulation in alginate-based hydrogel microspheres has been widely explored as a potential treatment modality [13, 21, 22]. This is attributed to their biocompatibility and capability to form hydrogels under physiological conditions conducive to cell function. Several clinical trials have established the safety of transplanting human islets in alginate microspheres [23-27]. However, long-term graft survival remains to be achieved, with fibrosis identified as one significant challenge [23, 24]. Recent advancements in producing low-fibrotic alginate microspheres have shown promise in pre-clinical studies for long-term immunoprotection of transplanted islets in mice and non-human primates [22, 28-30].

1.4 Biomaterials

Biomaterials serve as a cornerstone in the development of new medical technologies and therapies, aiming to replace, restore, or enhance the function of impaired tissues or organs [31, 32]. A biomaterial may be defined as "a substance that has been engineered to take a form which, alone or as part of a complex system, is used to direct, by control of interactions with components of living systems, the course of any therapeutic or diagnostic procedure, in human or veterinary medicine" [33]. Biomaterials may either be natural or synthetic, encompassing a range of materials such as metals, polymers (e.g. alginate), ceramics, and composites [34]. Given their diversity, biomaterials can be tailored for specific applications, whether it be drug delivery, tissue engineering, or implantable devices. Some examples include heart valves, hip replacements, ocular lenses, and materials employed in dentistry and surgery [33, 34]. Notably, a biomaterial of particular interest in the context of the current work is alginate hydrogel microspheres for cell encapsulation therapy. The

performance of biomaterials is highly influenced by the host response after implantation, emphasising the necessity for in-depth knowledge and management of host–material interactions to ensure successful integration and long-term efficacy.

1.4.1 The concept of biocompatibility

Biocompatibility is a widely used term in the field of biomaterials science, referring to the interactions between foreign materials and the body. Despite its common usage, the precise definition and underlying mechanisms of biocompatibility remain an ongoing subject of discussion [35-38]. Historically, the conception of biocompatibility has generally been limited to the inertness of long-term implantable devices, specifically their ability to cause no harm to the surrounding tissues. Consequently, the selection and development of biomaterials have adhered to certain standards, including non-toxicity, non-immunogenicity, and non-carcinogenicity, among others [35, 39]. With the expanding use of biomaterials in diverse and complex applications, our understanding of biocompatibility has evolved and continues to evolve with time [35]. Many definitions have been offered for biocompatibility over the years. The most commonly cited among these is: "the ability of a material to perform with an appropriate host response in a specific application" [37, 40, 41]. Although this definition is accurate, it fails to shed light on the intrinsic aspects of biocompatibility, including its mechanisms, testing, or enhancement. Accordingly, the term exhibits considerable variance in usage and interpretation. For instance, an uncomplicated foreign body reaction with a thin fibrous capsule surrounding the implant is considered today to be the hallmark of a "biocompatible" biomaterial [39]. However, in encapsulated cell therapy, this fibrotic formation is detrimental and can lead to graft failure, thereby rendering the therapy ineffective. Thus, for this specific application true biocompatibility includes the absence of fibrosis.

1.4.2 Inflammation, the foreign body reaction, and protein adsorption

The innate immune response, encompassing acute and chronic inflammation as well as the foreign body reaction, typically occurs within the initial 14 days after the implantation of a biomaterial [42, 43]. The extent of the response depends on the location and procedure of the implantation, and the biomaterial properties [44]. Acute

inflammation, which persists from minutes to days, is generally characterised by the exudation of fluid and plasma proteins as well as the predominant recruitment of neutrophils, as well as monocytes, to the implantation site [43-45]. Chronic inflammation is caused by sustained inflammatory stimuli and is marked by the presence of macrophages and lymphocytes, including the proliferation of blood vessels and connective tissue [43, 44]. Initiated by the adsorption of plasma proteins, the foreign body reaction includes monocyte/macrophage adhesion, macrophage fusion to form foreign body giant cells, and crosstalk between macrophages/foreign body giant cells and inflammatory/wound healing cells [42]. In general, inflammatory responses involve the cellular secretion of chemical factors like cytokines (small proteins), which modulate cell recruitment and activity [44]. The foreign body reaction is characterised by the presence of foreign-body giant cells and the components of granulation tissue (e.g. macrophages, fibroblasts, and capillaries) [43]. Fibrosis represents the end-stage of the inflammatory and wound healing responses after biomaterial implantation [42, 43], wherein myofibroblasts and fibrocytes have been shown to have central roles in collagenous fibrous encapsulation [43].

Following biomaterial implantation, injury to vascularised connective tissue occurs with ensuing blood–material interactions and provisional matrix formation [42]. The provisional matrix is the initial thrombus or blood clot at the host–biomaterial interface, which involves the activation of the intrinsic and extrinsic coagulation systems, as well as the complement, fibrinolytic, and kallikrein–kinin systems, and platelets [42, 46]. The different cascade systems are in tight crosstalk with platelets and leukocytes during clotting and inflammation [42, 46]. Platelets play a critical role in maintaining haemostasis, and their activation is closely associated with inflammatory responses, including complement activation and the release of chemoattractants (e.g. growth factors) that recruit immune cells to the site of injury [42, 47]. The immediate adsorption of blood proteins to a biomaterial surface plays a critical role in determining the subsequent host responses [42, 46, 48]. Protein adsorption is a complex and dynamic process wherein the adsorption and desorption to the biomaterial depends on the properties of the surface [49-51], the proteins, and the surrounding solution, as well as the exposure time [48, 52]. The competitive displacement of surface-adsorbed proteins by other proteins with higher binding

affinities is commonly referred to as the Vroman effect [53, 54], providing a dynamic surface for the interacting host cells that facilitate wound healing and foreign body responses [42]. Importantly, the types, concentrations, and conformations of the surface-adsorbed proteins modulate these cellular events [42]. The adsorption of proteins to a biomaterial surface may result in conformational changes that affect their bioactivity [46]. The complement (e.g. C3, IgG) and contact/coagulation (e.g. factor [F]XII) systems, which are critical in biomaterial-mediated host responses, are examples of protein cascades that are activated through conformational changes upon binding to nonself surfaces [46].

1.4.3 The complement and coagulation systems

The complement system, an integral component of the innate immune system, comprises an intricate network of soluble and cell-surface bound proteins that enable the recognition and elimination of foreign intruders [55, 56]. The primary role of the coagulation system is to initiate haemostasis following vascular injury [57, 58]. The complement and coagulation systems are finely orchestrated to form two distinct multi-component protein networks, both of which engage in the sequential activation of zymogens to form active proteinases during inflammatory and thrombotic events, respectively, and are known to have several crossover points [58, 59]. In the following, the complement and coagulation systems will be further detailed.

The complement system [55, 56] is activated through three distinct routes, namely the classical, lectin, and alternative pathways (**Figure 2**). The classical pathway is initiated by C1q recognition of pathogen- or damage-associated pattern recognition molecules, such as IgG, IgM, and C-reactive protein (CRP), on foreign or self surfaces. C1q with its associated proteases C1r and C1s constitute the C1 complex, which cleaves C2 and C4 and forms the classical C3-convertase (C4b2a). In the lectin pathway, mannose-binding lectin (MBL), ficolins (FCN), and collectins (COLEC) recognise specific carbohydrate patterns and assemble with MBL-associated serine proteases (MASPs), which also result in the formation of C4b2a. C4b2a cleaves C3 and generates the active fragments C3a and C3b. In the alternative pathway, surface deposited C3b form the alternative C3-convertase (C3bBb) in the presence of complement factor B (CFB) and D (CFD). This generates more C3b and amplifies the

complement response. Properdin (CFP) is a central protein in the alternative pathway with several roles, including recognising target surfaces, recruiting fluid-phase C3b to enable *de novo* assembly of C3bBbP, and stabilising surface-deposited alternative C3-convertases (C3bBbP). A low-grade complement activity is maintained in solution ("tick-over"), involving hydrolysed C3 (C3[H2O]), CFB, and CFD, which form the fluid-phase C3-convertase (C3[H2O]Bb). The increased surface deposition of C3b by the alternative pathway leads to the formation of convertases that contain an additional C3b molecule (C4b2a3b or C3bBb3b[P]), and a shift in the substrate specificity from C3 to C5 occurs. These C5-convertases cleave C5 into C5a and C5b. Both C5a and C3a (anaphylatoxins) serve as potent chemoattractants that guide immune cells towards sites of complement activation, subsequently promoting phagocytosis of opsonised, e.g. with C1q or C3b, components. C5b initiates the assembly of the terminal complement complex (TCC; C5b-9) by associating with C6, C7, C8, and several C9, which can be membrane inserted or released to the fluid-phase in its soluble form (sTCC) by associating with vitronectin (VTN) and clusterin (CLU). Complement-independent cleavage of C3 and C5 by proteases thrombin and plasmin has also been described in the literature [56], although the physiological relevance is debated [60, 61].

Soluble, as well as cell-bound (not shown), complement regulators act at different stages to modulate the severity, propagation, and terminal endpoints of complement. At the level of initiation, C1 inhibitor (C1-INH) inhibits the proteases of the classical (C1r, C1s) and lectin (MASPs) pathways. C4b-binding protein (C4BP) acts on the classical C3-convertase (C4b2a), accelerating its decay and functioning as a cofactor for factor I (CFI) in the inactivation of C4b which restricts further convertase formation. In the alternative pathway, activation is mainly controlled by factor H (CFH). CFH acts on alternative C3-convertases, either competitively removing Bb from the C3bBb complex (decay acceleration) or serving as a cofactor for CFI-mediated inactivation of C3b (iC3b). VTN and CLU regulates TCC by preventing its assembly. Lastly, carboxypeptidase-N (CPN) degrades C3a and C5a to their desArg-forms, thereby impairing proinflammatory signalling.

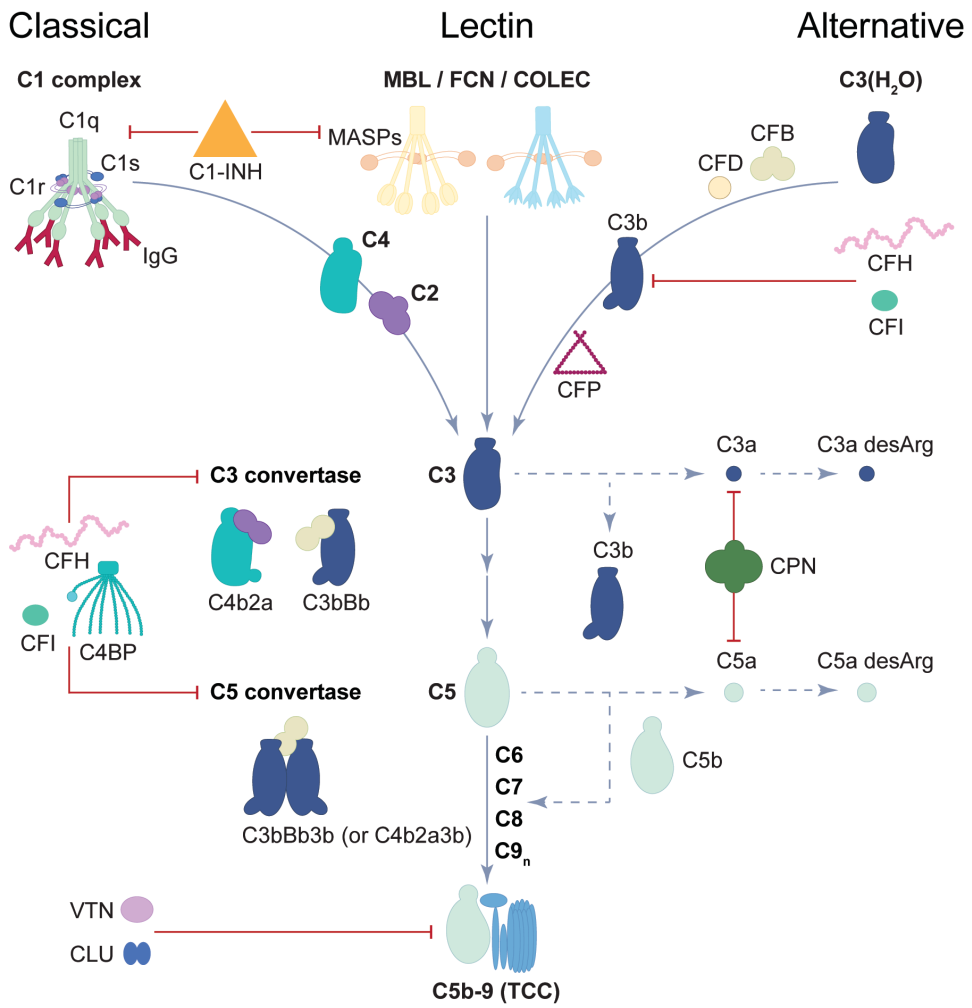

Figure 2. The complement system [55, 56].

The coagulation system is activated through two mechanisms, namely the extrinsic pathway and the intrinsic (contact activation) pathway. The extrinsic pathway consists of the transmembrane receptor tissue factor (TF), found on perivascular and epithelial cells, as well as activated monocytes, and plasma factor (F)VII [62, 63]. The contact system [57, 64, 65] is initiated by FXII, which is activated (FXIIa) when it comes into contact with negatively charged surfaces. FXIIa converts plasma prekallikrein (PPK) to plasma kallikrein (PK), which in turn activates FXII, creating a positive feedback loop for FXII activation. This activates both the proinflammatory

kallikrein–kinin system (not shown) and the intrinsic pathway of coagulation (**Figure 3**). The intrinsic pathway is propagated through FXIIa-mediated cleavage and activation of FXI to generate FXIa. Subsequently, FXIa initiates a series of sequential cleavage events leading to the downstream activation of FIX, FVIII, FX, and FV (activated factors denoted with a), which result in the cleavage of prothrombin (FII) to thrombin (FIIa). Finally, thrombin converts fibrinogen to fibrin and thereby facilitates clot formation. Inhibitors of the coagulation cascade, involved at different levels (outlined in **Figure 3**), include C1-INH, antithrombin (AT3), heparin cofactor 2 (HCF2), tissue factor pathway inhibitor (TFPI), vitamin K-dependent protein C (PROC) and its cofactor vitamin K-dependent protein S (PROS), and protein Z-dependent protease inhibitor (ZPI).

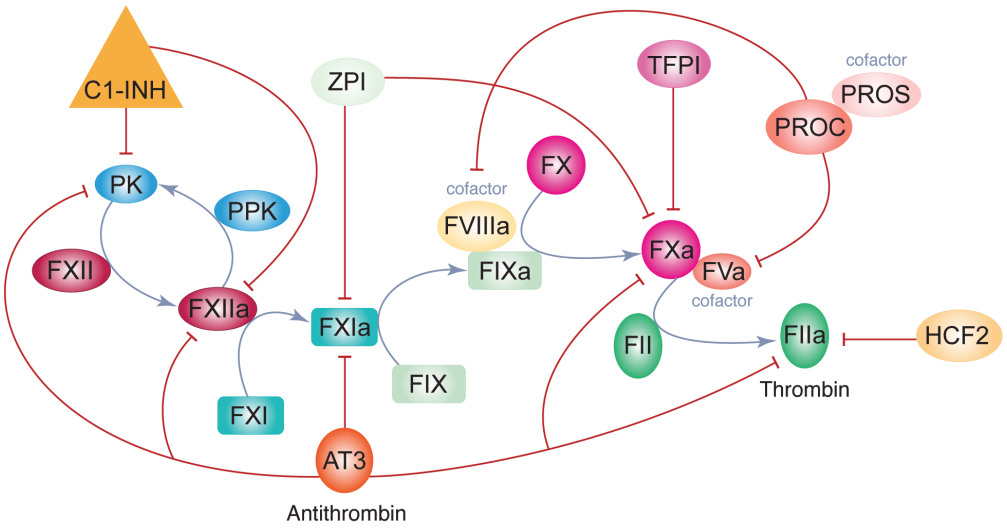

Figure 3. The contact system and the intrinsic pathway of coagulation, initiated by FXII [57, 64-66].

1.5 Alginate

1.5.1 Sources and applications

Alginate is a naturally occurring polysaccharide primarily found in marine brown algae (*Phaeophycea*) and comprises up to 40% of the dry matter [67]. The polymer serves as a structural component, located in the intercellular matrix as a gel containing various cations, providing strength and flexibility to the plant tissue [67, 68]. Specific bacteria within the *Azotobacter* and *Pseudomonas* genera produce alginates as exopolysaccharides, which exhibit structural differences from algae-derived alginates [69, 70]. At present, commercial alginates are produced solely from brown seaweeds, including the genera *Laminaria*, *Macrocystis, Saccharina*, *Lessonia*, *Durvillaea*, *Ecklonia* and *Ascophyllum* [71]. The physicochemical properties of alginate, including water retention, gel formation, viscosity enhancement, and stabilisation, have made it a widely utilised material in various industries such as food, agriculture, cosmetics, pharmaceuticals, and biomedicine [68, 72]. In the biomedical field, alginate has shown great utility and potential as a biomaterial due to its biocompatibility and gelation characteristics, finding applications in cell encapsulation, tissue engineering, wound healing, and drug delivery [73, 74].

1.5.2 Chemical composition, structure, and molecular weight

Alginates are unbranched polymers consisting of (1→4)-linked β-D-mannuronate (M) and its C5 epimer, α-L-guluronate (G) (**Figure 4 A**). The M and G residues are distributed along the polymer chain in a block-wise pattern, forming homopolymeric M-blocks and G-blocks interspersed with regions of strictly alternating sequence, known as MG-blocks [75] (**Figure 4 B**). The M residues exist in a $^{4}C_{1}$ ring conformation (–COOH and all –OH except –OH[2] are equatorial) while the epimerisation at C5 for the G residues renders the carboxylic acid group axial, leading to a transition to the $^{1}C_{4}$ conformation [76-78]. These conformational differences result in the formation of four possible glycosidic linkages, including di-equatorial (MM), equatorial-axial (MG), axial-equatorial (GM) and di-axial (GG) (**Figure 4 C**). The structure and, in turn, the functional properties of alginate are determined by the M/G ratio and the distribution of the uronic acid groups [79].

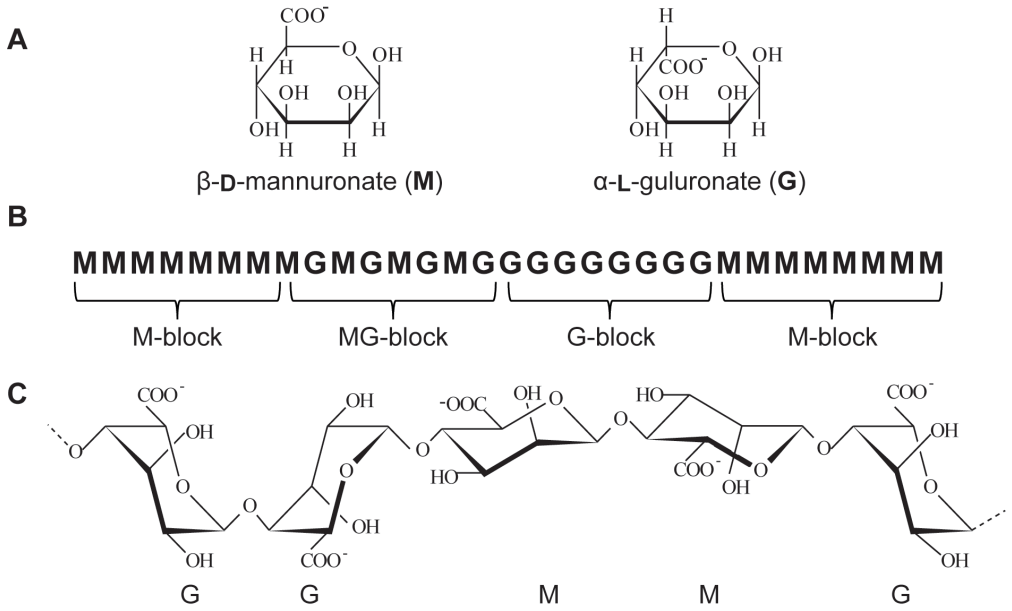

Figure 4. Alginate chemical structure. **A**) Haworth formula of the two monomers, β-D-mannuronate (M) and α-L-guluronate(G). **B**) Block compositions in alginate, including G-, M-, and MG-blocks. **C**) Chair conformations in alginate chain ($^4C_1$ for M and $^1C_4$ for G). Ring protons not shown. Adapted from [18].

Due to the extended conformation of the alginate polymer, solutions containing alginate generally exhibit high viscosity [80]. Alginate is a polyelectrolyte which is typically obtained in its water-soluble sodium form [81]. The polymer is negatively charged at neutral pH due to the unprotonated carboxylate ($–COO^-$) groups, as the pKa-values for the M and G monomers are 3.38 and 3.65, respectively, with the effective pKa of the alginate polymer only varying slightly from these values [67, 80].

Given the heterogeneous block-like structure of alginate, its compositional characterisation requires information beyond the frequency of monomers (M/G). High-resolution ^1H and ^{13}C nuclear magnetic resonance (NMR) spectroscopy is commonly employed for detailed analysis of the composition and sequence of alginates, yielding average frequencies of monads (F_G and F_M), diads (F_{GG}, F_{MG}, F_{GM} and F_{MM}), and triads (F_{GGG}, F_{MMM}, F_{MMG}, F_{GGM}, F_{MGG}, F_{GMM}, F_{MGM} and F_{GMG}) [82, 83]. The obtained data allow for the determination of the average G-block length ($N_{G>1}$) [82]. In addition,

enzymatic digestion using specific alginate lyases, followed by analysis of block structure through high-performance liquid chromatography (HPLC), has provided further insight into the presence of extensively long G-blocks in seaweed alginates [84]. Alginates are non-uniform polymers of high molecular weight, typically ranging from 10^5 to 10^6 Da, which corresponds to about 500 to 5000 uronic acid residues per chain [85]. Accordingly, the molecular weight of alginate is given as an average over the whole distribution of molecular weights, such as the number average molecular weight ($\overline{M_n}$) or weight average molecular weight ($\overline{M_w}$) [86]. The molecular weight distribution of alginates can be characterised using size exclusion chromatography with inline multi-angle laser light scattering (SEC-MALLS) [87].

The composition of alginate is dependent on the specific algae species, parts of the plant, as well as growth and seasonal conditions [88, 89]. Following the biosynthesis of alginate, which is initially produced as homopolymeric M chains, the G residues are introduced into the polymer chain by alginate C-5 epimerases through the conversion of M residues [90]. Alginate epimerases have been found in brown algae and alginate-producing bacteria, primarily *Azotobacter* and *Pseudomonas* species [91]. The most thoroughly studied epimerases are the AlgE1–7 from *A. vinelandii*, which exhibit different epimerisation patterns, ranging from generating contiguous G-blocks to strictly alternating sequences [91-93]. Consequently, this allows for the enzymatic modification of alginate composition *in vitro* by utilising one or multiple epimerases to tailor alginates with specific characteristics [94, 95].

1.5.3 Ion binding and crosslinking

The predominant utilisation of alginate is attributed to its ability to form hydrogels in the presence of specific divalent cations, e.g. calcium or barium [79]. The affinity of alginate towards alkaline earth metals increases in the order $Mg^{2+} << Ca^{2+} < Sr^{2+} < Ba^{2+}$ [96]. The ion-binding selectivity is largely dictated by alginate composition, which increases with the G-block content, whereas M-blocks and MG-blocks exhibit lower selectivity [96-98]. In detail, G-blocks bind Ca^{2+}, Sr^{2+}, and Ba^{2+}, with increasing affinity; M-blocks bind Ba^{2+}; and MG-blocks bind Ca^{2+} [97, 99]. The mechanism of alginate gelation, specifically the crosslinking between alginate and calcium, has been described in an "egg box" model (**Figure 5**), initially proposed by Grant et al. [100]

and subsequently refined [101-103]. In this model, the di-axial linkages in G-blocks create cavities (junction zones) conducive for ion binding, facilitating cooperative association between consecutive pairs of G residues in opposing polymer chains [100-103]. It has also been proposed that the presence of excess calcium ions enable lateral associations of the G-block junction zones [104]. While the association of G-blocks are pivotal in alginate hydrogel formation, calcium alginate gels have been suggested to be supported by secondary junction zones with MG-blocks, including GG/MG and MG/MG junctions [105, 106].

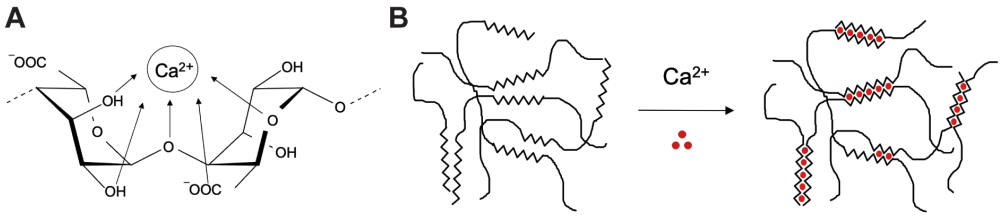

Figure 5. Ion binding and crosslinking of alginate in hydrogel formation. **A**) Calcium binding of two consecutive G residues in a G-block. **B**) Alginate crosslinking by calcium as described by the egg box model. Adapted from [97, 100].

1.5.4 Alginate hydrogel microspheres

The terms microcapsules, microbeads, and microspheres are often used interchangeably in the literature. In this thesis microcapsules refer to encapsulation systems consisting of two or more polymers which have a surface coating (e.g. polycation); microbeads denote uncoated continuous hydrogels; and microspheres serves as the collective term. Alginate hydrogel microbeads are usually prepared by dripping an alginate solution into a gelling solution (diffusion gelation), e.g. by electrostatic droplet generation [107]. In cell encapsulation, the same procedure is followed, with cells incorporated into the alginate solution prior to gelation. The hydrogel properties are largely influenced by the composition of alginate (M/G content and distribution) [97, 108, 109] and the gelling ions used [78, 99]. Alginate hydrogels are typically characterised by their mechanical properties, including elastic modulus (Young's modulus; E), which is used as a measure for gel strength. Gel strength depends on the number and length of crosslinks, increasing with the number and average length of G-blocks [94], concentration of alginate [109] and gelling ions [99, 109], and molecular weight up to

a certain point [109]. Using strontium and barium as gelling ions results in stronger gels compared to calcium [97, 99, 109, 110]. Moreover, increased gel strength is observed for calcium-crosslinked gels of epimerised alginates with extended MG-blocks [95, 105, 111].

Alginate hydrogels are prone to swelling under physiological conditions due to the presence of non-gelling ions (e.g. sodium) and chelating compounds (e.g. phosphate, citrate), which destabilise the crosslinking zones within the hydrogel network. [109, 110]. The swelling potential of alginate hydrogels is primarily dictated by the difference in concentration of mobile ions within and external to the hydrogel network [109]. As the alginate molecule carries fixed negative charges, the requirement of electroneutrality according to the Donnan equilibrium [112] results in an increased concentration of mobile ions within the gel, which leads to water influx [113]. The degree of swelling will be dependent on the integrity of the crosslinking zones in the gel, and if compromised, it may lead to increased swelling and possibly dissolution [109, 113]. The chemical composition of alginate and the type of gelling ions have a significant effect on the swelling properties of alginate hydrogels [99, 109, 114]. Utilising alginates with high G content, and employing strontium or barium ions instead of calcium ions for crosslinking, leads to the formation of more stable hydrogels [99]. Calcium-crosslinked gels of epimerised alginates containing substantial amounts of MG-blocks have also been shown to be highly stable under physiological conditions [115].

The permeability of alginate hydrogels is influenced by factors such as alginate composition [109, 115], as well as the type and concentration of gelling ions [99]. Previous studies have demonstrated the permeability of alginate hydrogel microbeads to IgG to be dependent on alginate composition and type and concentration of gelling ion [99, 115]. Traditionally, modulating the permeability of alginate microspheres has been achieved through coating with polycations such as poly-L-lysine (PLL) [116, 117], although these coatings have been shown to be highly inflammatory [118, 119].

1.5.5 Biological responses towards alginate materials

Alginate and alginate hydrogels are in general recognised as biologically inert. However, there are conflicting reports regarding the immunogenicity of different alginate compositions (M/G content). Earlier *in vitro* studies have reported that alginates with a high M content, typically around 90% (i.e. poly-M), are immunostimulatory [120-123]. High M alginate in solution has been shown to stimulate the production of proinflammatory cytokines (IL-1, TNF-α, IL-6) in human monocytes in contrast to high G alginate [120], wherein the stimulation of TNF-α by high M alginate was shown to increase with the molecular weight [122]. The immunostimulating properties of high M alginate in cell activation has further been demonstrated to involve surface receptor CD14 [121, 123] and toll-like receptors (TLR2, TLR4) [123]. Interestingly, mannuronan (100% M alginate) has been shown to *not* induce an inflammatory response in monocytes *in vitro* [124]. Antibodies against high M alginate microcapsules have been detected post-implantation in mice, but not with high G alginate microcapsules. However, in rats, no antibody responses were observed for any microcapsule type [125]. On the other hand, a transient inflammatory response, along with the presence of antibodies against high G alginate microcapsules, has been documented in a diabetic patient transplanted with encapsulated human islets [124].

With respect to foreign body reactions against implanted alginate hydrogel microspheres, previous studies have shown through different mouse models that microbeads comprising low to intermediate G alginates provoke minimal fibrosis [21, 126, 127]. In contrast, high G alginate microbeads have been widely reported to produce fibrosis in mice [21, 126], non-human primates [22], and humans [23, 24]. Alginate microcapsules with polycationic coating (e.g. poly-L-lysine, poly-L-ornithine) have been the subject of extensive research over the years, including clinical trials [25-27]. These microcapsules have been well-documented to be highly inflammatory [118, 119, 128, 129] and to produce significant cellular overgrowth [22, 118, 126, 130-133]. The inflammatory properties of alginate microspheres have been demonstrated in numerous studies using a human whole blood assay [119, 128, 129, 134], wherein poly-L-lysine-alginate microcapsules provoke significant complement and cytokine responses while the uncoated alginate microbeads overall exhibit low responses [119, 129]. In the

work of Ørning et al. it was shown that the inflammatory cytokine induction was dependent of the potential of alginate microcapsules to activate complement C3 and was further connected to monocyte/neutrophile adhesion through CD11b/CD18 [128]. Inhibiting CD11b/CD18 diminished both cell adhesion and cytokine induction. The potential of microbeads/microcapsules to induce coagulation activation has further been demonstrated [135]. Of note, dependent on the material properties, either the FXII-dependent or the monocyte TF-dependent coagulation pathway could be activated.

In recent times, strategies for producing minimally fibrotic alginate microbeads have involved various chemical modifications of alginate [28, 30]. The effects of alginate composition and microsphere formulation on inflammatory and fibrotic responses will be explored in greater detail in the general discussion of this thesis.

1.5.6 Sulfated alginate

Chemical modification of alginate enables the introduction of new functional groups, such as sulfate groups, which can alter the inherent properties of the polymer. Sulfation of alginate can be performed by using chlorosulfonic acid [136, 137] or sulfuric acid and carbodiimide chemistry [138], wherein the sulfate groups ($–SO_4^{2–}$) are chemically introduced at C2 and/or C3 by the substitution of hydroxyl groups on the M and G residues comprising the alginate [137]. The degree of substitution (DS) is typically determined by high-resolution inductively coupled plasma mass spectrometry (HR-ICP-MS) as detailed by Arlov et al. [137]. Chemical sulfation may result in some degree of depolymerisation as a consequence of acid hydrolysis [138-140]. At high DS (>0.5) the sulfate groups obstruct the gelation properties of the alginate, likely through steric hindrance and intramolecular repulsive forces that alter ion binding. Therefore, larger fractions of non-modified alginate are typically included in the hydrogel formulations to ensure stable hydrogels are formed [140]. On the other hand, sulfation increases the negative charge density of the alginate, which may promote additional electrostatic interactions with proteins [141].

The structural and functional properties of sulfated alginate have been associated with those of heparin and heparan sulfate [137, 141]. Heparin and heparan sulfate are

sulfated glycosaminoglycans (GAGs) that interact with a wide range of proteins in the regulation of different biological processes, including wound healing and immunological responses [142]. Heparin, well-recognised for its anticoagulant properties, has been a clinical staple for several decades [143]. GAGs are ubiquitously expressed, which are abundant on cell surfaces, inside the cell, and in the extracellular matrix (ECM) [144]. GAGs exhibit notable structural diversity, facilitating interactions with a plethora of biological molecules, many of which are promising for use in novel biomaterials. However, this structural variability also poses challenges for their characterisation and application [145]. Sulfated alginates could potentially serve as well-characterised functional analogues of heparin/heparan sulfate, offering structural customisability through specific enzymatic epimerisation and tuning of sulfation degree [137]. Sulfated alginate has been suggested for use in tissue engineering of cartilage [140], in delivery systems for small molecules [146], and as a coating for alginate-PLL capsules in islet transplantation [147].

In solution, sulfated alginates have been reported to exhibit anticoagulant properties *in vitro* [136, 139, 148], where the anticoagulant activity was shown to increase with polymer concentration [136, 139, 148] and sulfation degree [139]. However, the precise mechanisms underlying this anticoagulant effect remain to be elucidated [141]. Sulfated alginate has also been shown to stimulate coagulation at low doses [148]. Moreover, sulfated alginates have been shown to inhibit the formation of TCC in complement-stimulated plasma, as well as bind hepatocyte growth factor (HGF) in a manner similar to heparin [137]. When incorporated into alginate hydrogels, microbeads with sulfated alginate have demonstrated insignificant induction of TCC and moderate coagulation activation in human whole blood, in addition to a pronounced binding of factor H [134]. It was also shown to significantly reduce cytokine responses when used as a coating on proinflammatory microcapsules [134]. The binding of several heparin-binding growth factors to sulfated alginate hydrogels has also been reported [138]. Given the anti-inflammatory properties and potentially favourable protein interactions of sulfated alginate, its inclusion into alginate hydrogel microbeads may hold promise for enhancing cell encapsulation therapies, particularly in mitigating adverse host responses associated with such biomaterials.

1.6 Methods for characterising inflammatory and host responses

As previously highlighted, the biological responses towards alginate microspheres used in cell transplantation therapy are critical for the long-term therapeutic efficacy. Pericapsular fibrotic overgrowth is a significant hurdle that ultimately leads to graft failure. Hence, detailed assessment of relevant microspheres both *in vitro* and *in vivo* is essential to identify materials demonstrating low inflammatory and fibrotic responses. The human whole blood assay [149] is a clinically relevant human *ex vivo* model that serves as a valuable tool for investigating the potential of microspheres in inducing inflammatory mediators. It provides the possibility of assessing a broad panel of microspheres under the same conditions [119, 128, 150]. An inherent strength of the model is the physiological relevance provided by the use of lepirudin [*] as an anticoagulant (specific thrombin inhibitor), as opposed to other anticoagulants (e.g. EDTA, citrate, heparin) that inhibit or interfere with the complement and coagulation systems [149, 150]. This anticoagulation strategy allows for the interactions between immune cells and functional effector proteins, including the complement system, coagulation components upstream of thrombin, and the fibrinolytic system. Accordingly, the model yields readouts such as complement (e.g. TCC) and coagulation activation products (e.g. prothrombin fragment 1+2; PTF1.2), cytokines, cell-surface receptors, adsorbed proteins, and cell adhesion [128, 150, 151].

The investigation of specific proteins adsorbed to alginate microspheres can be performed using fluorescently labelled antibodies and confocal laser scanning microscopy (CLSM) [28, 29, 119, 128, 129, 134]. Utilising lepirudin-anticoagulated plasma permits the analysis of the proteolytically active protein cascades of complement and, in part, coagulation [119, 149]. CLSM represents a straightforward approach, providing high-resolution imaging that enables the detection, localisation, and quantification of target proteins *in vitro* and *in vivo* [28, 29, 128, 129]. While central for protein adsorption analyses, other methods have emerged for high-throughput analysis of a significantly broader spectrum of proteins in a single experiment. In this regard, mass spectrometry (MS)-based proteomics represents a powerful tool for in-depth protein profiling of biomaterials [48, 52]. High sensitivity

[*] Recombinant hirudin-derivative.

and resolution enable the detection and quantification of low-abundance proteins. Furthermore, the technique allows for pathway analysis (e.g. Ingenuity® Pathway Analysis) to elucidate the biological context and functional interplay between proteins in different biological processes.

Ex vivo and *in vitro* models are invaluable in the assessment of the inflammatory potentials of different alginate-based microspheres, which facilitate the identification of promising candidates for further evaluation. *In vivo* testing using animal models is needed to assess fibrotic responses. Rodent models have long served as the gold standard for evaluating alginate microspheres, yet notable variations exist among these models with respect to fibrotic tissue development [21, 130]. In general, rats and mice produce limited fibrosis compared to non-human primates and humans [22], making the differentiation of various materials challenging. However, the immunocompetent mouse strain C57BL/6J has been shown to exhibit fibrotic responses similar to larger animal models [22], thus serving as a relevant model in this context.

1.7 Methods for characterising the function of encapsulated islets

Diabetic rodent models are commonly utilised for investigating the ability of alginate microspheres to support transplanted islet function and their performance as immune barriers [12, 21]. One widely used approach involves inducing diabetes in mice through streptozotocin (STZ) administration [21, 29, 152], e.g. by intraperitoneal injection, prior to graft transplantation. STZ selectively targets and destroys the insulin-producing β-cells within the pancreas, resulting in insulin deficiency and hyperglycaemia [153]. Encapsulated islet function and efficacy can be evaluated in mice using various parameters, including blood glucose concentration, serum C-peptide concentration, and oral glucose tolerance testing (OGTT) [152, 154]. Following islet transplantation, blood glucose concentrations are consistently monitored in the recipient, e.g. using a glucometer, to assess the islets' ability to restore normoglycemia. A non-fasting blood glucose concentration of 250 mg/dL has been suggested as a suitable threshold for hyperglycaemia in mice [152, 155]. Assessing the serum concentration of C-peptide, a by-product of insulin production, provides an indicative measure of insulin secretion from the encapsulated islet graft and can be quantified

using enzyme-linked immunosorbent assay (ELISA). OGTT evaluates glucose metabolism, which can identify impaired glucose tolerance or diabetes. Mice are typically fasted to ensure stable baseline measurements and consistent changes in glucose levels during tolerance testing [156]. A standardised glucose solution is administered orally, and blood glucose levels are measured at specific time points for a duration of usually 2 h. A typical OGTT response involves a rapid rise in blood glucose after glucose intake, followed by a gradual return to normal levels [156]. To study encapsulated graft function, immunodeficient nude mice are often employed to avoid immune rejection responses that may interfere with the performance of the graft. This approach contrasts with using immunocompetent mice, such as C57BL/6J, wherein the immune barrier function of the encapsulating material is assessed in addition to graft performance. For *in vitro* assessments of islet function, islet viability can be measured pre- and post-transplantation using a live/dead assay, where live and dead encapsulated cells are distinguished by staining with specific fluorescent dyes (typically green and red, respectively) and visualised by fluorescence microscopy [157]. Glucose stimulated insulin secretion (GSIS) is commonly used to assess the glucose responsiveness of insulin-producing β-cells pre- and post-transplantation [157]. Encapsulated islets are traditionally exposed to two glucose solutions, one with relatively low concentration (typically 1–3 mM) and one with high concentration (typically 10–28 mM) of glucose [158]. The resulting insulin secretion profiles, which can be quantified using ELISA, provide insight into the functionality of the encapsulated islets.

1.8 Ethical considerations using animal models

The use of animal models adheres to ethical guidelines set by local animal ethics committees, ensuring strict compliance with the 3R principle (Replacement, Reduction, and Refinement) for animal welfare [159]. In the current work, experiments were conducted in Norway and the U.S. employing specific mouse models. In Norway, experiments followed national guidelines for the care and use of laboratory animals and were approved by the Norwegian Food Safety Authority. In the U.S., the use of animals in research is governed by federal regulations issued by the National Institutes of Health (NIH) Office of Laboratory Animal Welfare and the U.S. Department of

Agriculture (USDA). Surgical procedures and post-operative care adhered to approved protocols from the University of Illinois Chicago (UIC) Institutional Animal Care and Use Committee (IACUC) in compliance with NIH and USDA.

In general, the requirement for replacement, reduction and refinement in animal experimentation, results in fewer animals being used, preference for using non-animal methods, and in procedures that minimise pain and distress [159]. In biomaterial and diabetes research, animal experimentation is important to explore potential therapeutic interventions. To ensure the welfare of the laboratory animals, humane endpoints need to be defined and implemented. A humane endpoint is the point at which pain or distress in an experimental animal is prevented, terminated, or relieved. Humane endpoints can be considered as possible refinement alternatives for those experiments that result in unrelieved or severe animal pain and distress, including death [160]. For rodent models, specific physical indicators (e.g. bodyweight loss, hunched back, facial grimacing, reduced alertness, abnormal breathing) represent typical humane endpoints. Other important factors related to ensuring animal welfare encompass consistent welfare assessments and appropriate social housing and environmental enrichment [161].

2 Scope of the thesis

The overall aim of the current work was to provide insight into the causal factors of pericapsular fibrotic overgrowth (PFO) for alginate microspheres and develop well-characterised, biocompatible (i.e. non-fibrotic) materials with long-term efficacy in cell encapsulation therapy of type 1 diabetes.

Specific aims:

i. Assess the current and future perspectives of alginate microspheres in encapsulated pancreatic islet therapy for type 1 diabetes, highlighting key challenges, such as PFO, and advancements for long-term therapeutic efficacy.

ii. Investigate the effects of different alginates, including chemical compositions and sulfated alginate, and gelling ions, on empty alginate microbeads through the assessment of physicochemical properties, inflammatory potentials, and PFO.

iii. Characterise protein adsorption profiles of empty alginate microspheres with distinct inflammatory and PFO potentials through mass spectrometry-based proteomics and functional analysis in human whole blood, using lepirudin as an anticoagulant to enable the study of active protein cascades.

iv. Evaluate the immunoprotection and functional performance of encapsulated rat islets in pre-assessed alginate materials, exhibiting *in vivo* stability and minimal PFO, by transplantation into diabetic mice.

3 Summary of papers

This thesis comprises four papers on alginate hydrogel microspheres as an immunoisolating material in cell therapy, with an emphasis on type 1 diabetes treatment. **Paper I** provides a review of immunoprotective alginate-based microspheres in pancreatic islet transplantation. It addresses critical microsphere properties necessary for sustained graft function and outlines strategies to overcome current challenges, including pericapsular fibrotic overgrowth (PFO). In **Paper II**, we performed an *in vivo* screening study of various microbead formulations, identifying several promising candidates exhibiting minimal PFO. Specific microbeads were evaluated with respect to long-term efficacy, physicochemical and inflammatory properties, and protein deposition. **Paper III** presents a novel quantitative MS-based proteomics approach to elucidate protein adsorption profiles of alginate hydrogel microspheres, providing insight into host–material interactions relevant to PFO. Lastly, **Paper IV** examines the immunoprotection and functional performance of encapsulated rat pancreatic islets transplanted into diabetic mice.

Paper I

Current and Future Perspectives on Alginate Encapsulated Pancreatic Islet

The encapsulation of pancreatic islets within immunoprotective microspheres presents a promising alternative to conventional therapies for type 1 diabetes, potentially offering a functional cure for the disease. This strategy not only provides a semipermeable barrier that safeguards the graft from immediate immune attack, but also negates the need for immunosuppression and its associated health risks. Encapsulation in alginate hydrogel microspheres is one of the most studied approaches for the immune isolation of pancreatic islets. Several clinical trials have established the safety of transplanting human islets in alginate-based microspheres. Nevertheless, challenges persist in developing microspheres that sustain graft function in the long term. Key microsphere properties associated with these challenges include stability, permeability, and biocompatibility (i.e. absence of fibrosis). Through careful selection of alginate type (e.g. M/G content and sequential structure), gelling ions (e.g. calcium vs barium), and washing procedures, microspheres can be produced that remain stable

under physiological conditions. While the necessary permeability for microspheres to serve as an immune barrier is unclear, the primary objective appears to be preventing cell-to-cell contact between the graft and host. Traditionally, polycation coatings have been applied to control the stability and permeability of alginate microspheres; however, their proinflammatory properties are linked to PFO. While newer non-polycationic microsphere developments aim to mitigate PFO, it persists as an ongoing issue with underlying mechanisms that are not yet fully understood. PFO obstructs graft function by limiting the supply of oxygen and nutrients to the encapsulated cells. Alginate microspheres with a high G content are known to promote PFO, while microspheres with lower G content remain free of PFO yet show limited stability, restricting their immediate use for encapsulation. The latest research has shown that chemical modifications of alginate as well as an increase in microsphere size can mitigate PFO. The limited supply of insulin-producing tissue presents another significant hurdle in islet transplantation. However, advances in deriving insulin-producing cells from human stem cells offer promising potential for obtaining therapeutic cells from human sources. Collectively, recent progress in both microsphere development and stem cell technology cultivates a positive outlook for the future of encapsulated islet transplantation.

Paper II

Pericapsular fibrotic overgrowth mitigated in immunocompetent mice through microbead formulations based on sulfated or intermediate G alginates

In encapsulated cell transplantation, maintaining graft function relies on both microsphere stability *in vivo* and the mitigation of PFO. Accordingly, this study explored different alginate microbead formulations as potential immunoisolation materials, focusing on these parameters. Microbead formulations included variations of intermediate G alginate or sulfated alginate and/or high G alginate. Using an *in vitro* stability assay, large differences were observed depending on the type of alginate and gelling ions used (calcium and/or barium, or only strontium), wherein microbeads of intermediate G alginate showed the lowest stability overall. Gelation with calcium and a low concentration of barium, instead of using a high barium concentration, was

determined to be an effective trade-off between stability and biocompatibility[*] and was thus used in most microbead formulations evaluated for PFO. A screening panel of 11 microbead formulations was assessed *in vivo* (14–35 days) using an immunocompetent mouse model (C57BL/6JRj), yielding multiple promising candidates. Two candidates were chosen for long-term *in vivo* evaluation: one composed of intermediate G alginate (IntG) and the other a combination of sulfated alginate with high G alginate (1:4 ratio; HiG+SA(80/20)[†]), both gelled in calcium and barium. IntG and HiG+SA(80/20) exhibited maintained stability (13% and 5% swelling, respectively) and minimal PFO (4% and 7%, respectively) after 112 days. Of note, IntG showed high recovery rates upon explantation, while for HiG+SA(80/20) it was lower and more variable, both in the short and long term. In the short term (14 days), high G alginate (HiG) showed a notable 64% PFO, serving as a positive control. Conversely, IntG and HiG+SA(80/20) showed 1% and 7% PFO, respectively. Additionally, microbeads comprising a mixture of intermediate G alginate with smaller fractions of high G alginate displayed PFO as low as 0–1%, pointing towards compositional flexibility with respect to PFO. Neither our evaluations of material stiffness in microbeads and gel cylinders, nor the use of different gelling ions, uncovered a clear link to PFO. The protein deposition on explanted microbeads was investigated by CLSM. Minimal deposition of complement C3c was observed for all microbeads with the exception of poly-L-lysine-containing microcapsules (AP), serving as a proinflammatory control. Fibrin(ogen) deposition was positively associated with PFO, with greater deposition on fibrotic HiG microbeads compared to the minimally fibrotic IntG and HiG+SA(80/20). Lastly, the inflammatory potential of the microbeads was assessed using a human whole blood assay, including complement, coagulation, and cytokines. The responses of the microbeads were low overall. Distinctively, the microbeads containing sulfated alginate, including HiG+SA(80/20), activated coagulation and showed insignificant complement responses compared to baseline. AP microcapsules displayed significant complement and cytokine responses, coinciding with *in vivo* C3 deposition and PFO development. Conclusively, microbeads containing intermediate G alginate or sulfated

[*] In this context, referring to the potential toxicity of high barium concentrations.

[†] This microbead type is denoted as SA in **Paper III** and **IV**.

alginate, including IntG and HiG+SA(80/20), show great potential for long-term therapeutic applications of cell encapsulation.

Paper III

MS-proteomics provides insight into the host responses towards alginate microspheres

Protein adsorption to biomaterial surfaces is considered a determining factor for the host response, and thus plays a central role for the success of implanted biomaterials. This work employed LC-MS/MS-based proteomics to identify plasma proteins adsorbed to alginate hydrogel microspheres relevant for cell therapy. Microspheres previously reported (**Paper II**) to exhibit different inflammatory and fibrotic responses were examined, including high G alginate (HiG; low-inflammatory and fibrotic), high G alginate mixed with sulfated alginate (SA; low-inflammatory and anti-fibrotic), and high G alginate coated with poly-L-lysine (AP; proinflammatory and highly fibrotic). Importantly, the use of lepirudin-anticoagulated human plasma enabled the investigation of acute-phase proteins within the complement and coagulation systems, which are critical in biomaterial-mediated host responses. The biological significance of the identified acute-phase proteins was assessed through functional analysis of complement and coagulation activation in human whole blood (hWB). In support, the binding of initial complement and coagulation factors was verified by CLSM. The microspheres were incubated in pooled ($N = 7$) plasma for 24 h, and the adsorbed proteins were isolated into E- (eluted proteins) and T-fractions (residual proteins tryptically digested from the microspheres) to differentiate between weaker and stronger bound proteins, respectively. The LC-MS/MS analyses resulted in the high-confidence identification and quantification of 236 differentially adsorbed plasma proteins. Cluster analysis revealed distinct protein signatures for the microspheres, wherein numerous low-abundance plasma proteins were significantly and selectively enriched. The number of significantly enriched proteins on HiG, SA, and AP (across E-/T-fractions) compared to plasma were 106, 128, and 88, respectively. The proteins uniquely enriched on each microsphere type were predominantly hydrophilic, where most of the acidic proteins* were identified in the E-fractions and

* Net negative charge at physiological pH.

the basic proteins* in the T-fractions. The inclusion of sulfated alginate in the microbead formulation (20% sulfated alginate mixed with 80% high G alginate; namely SA) resulted in an overall increase in adsorbed proteins compared to HiG, including several uniquely enriched heparin-binding proteins with potential anti-fibrotic effects (e.g. specific matrix metalloproteinases: MMP2, MMP9). Furthermore, SA exhibited a marked enrichment of fibrinolysis-promoting factors (e.g. factor (F)XII, plasma kallikrein), potentially supporting an anti-fibrotic profile. Ingenuity® Pathway Analysis identified *the acute-phase response* and *the complement and coagulation systems* among the top enriched canonical pathways. The levels of adsorbed complement and coagulation activators and inhibitors were distinct for the different microspheres, which was reflected in the functional hWB analyses. SA induced an insignificant terminal complement response in hWB, conforming to the extensive enrichment of complement inhibitors, such as C1 inhibitor and factor H, as revealed by proteomic analysis. Additionally, SA showed a moderate coagulation response in hWB, corresponding to the highly enriched coagulation factors, such as FXII, antithrombin-III, and heparin cofactor 2. HiG exhibited low terminal complement activation in hWB, conforming to the moderate enrichment of complement inhibitors. AP displayed significant terminal complement activation in hWB, conforming to the prominent enrichment of complement activators, such as C3 and properdin, and overall low levels of inhibitors. CLSM investigations of deposited complement (C1q, C3c) and coagulation (FXII) proteins were in agreement with the proteomics analyses. In brief, HiG and SA showed an extensive surface deposition of the classical complement protein C1q as opposed to the downstream complement C3c (conversion product of C3), whereas AP showed the opposite trend. FXII was deposited on all microspheres, with the highest abundance on SA. In summary, this work presents a novel approach for proteomic profiling of alginate-based hydrogel microspheres, providing insights into host–material interactions at the protein level with potential relevance to PFO. These findings highlight MS-based proteomics as a valuable supplement to existing *in vitro* and *in vivo* methods for designing anti-inflammatory, non-fibrotic alginate microspheres for cell encapsulation therapies.

* Net positive charge at physiological pH.

Paper IV

Function of encapsulated rat islets in sulfated and intermediate G alginate in diabetic immunocompetent and immunodeficient mice

Continuing the research primarily outlined in **Paper II**, with relevance also drawn from **Paper I** and **III**, the present work investigated the *in vivo* performance of insulin-producing rat islets encapsulated in beads with either sulfated alginate (SA) or intermediate G alginate (IntG), measured against the widely-studied high G alginate beads (HiG). As a strategy to optimise PFO mitigation, the bead design for this study was scaled up to about 1 mm, which is notably larger than the conventional microbead size of around 0.5 mm. As a first step, empty beads were implanted into immunocompetent (C57BL/6J) mice for 14 and 56 days, which yielded fibrotic outcomes similar to those reported in our original study (**Paper II**). Across both time points, SA and IntG consistently showed minimal PFO with average values of 1–3% and 2%, respectively, in contrast to HiG with 13–29% PFO. Furthermore, the overall recovery rates of the beads were high upon explantation. In the subsequent step, we assessed the function of encapsulated rat islets transplanted into streptozotocin-induced diabetic C57BL/6J and immunocompromised (nude) mice. Conducted in two phases, the transplantation studies first assessed SA and HiG using both mouse models, followed by IntG and HiG. In C57BL/6J mice, SA and HiG both sustained islet-graft function for the duration of the study (120 days), exhibiting comparable outcomes overall. Throughout this period, the encapsulated islets maintained normoglycemia, and the bodyweights of the mice remained stable. At the end of the study, oral glucose tolerance testing (OGTT) demonstrated glucose-responsive islets. Additionally, measured serum C-peptide concentrations at 833±432 pmol/L and 648±117 pmol/L for SA and HiG, respectively, further indicated functional islets. Upon retrieval 120 days post-transplantation, the recovery rates of the beads were high overall. SA and HiG encapsulated islets showed low levels of PFO at 2±3% and 6±1% and high cell viabilities at 89±22% and 97±12%, respectively. For the nude mice experiments, including both the first (SA and HiG) and second phases (IntG and HiG), along with the second phase using C57BL/6J mice (IntG and HiG), the presence of precipitates in the islet-containing beads precluded optical assessments. In subsequent analyses, the precipitates were identified as hydroxyapatite ($Ca_5(PO_4)_3OH$) resulting from salts present in the culture medium. Initial hydroxyapatite formed in beads during islet

culture pre-transplantation and progressed *in vivo*. Islet function was likely affected by the precipitate, indicated by the differing outcomes of the HiG control used for both SA and IntG. In the first phase, HiG sustained graft function for the whole duration of the 120-day study in C57BL/6J mice, whereas in the second phase (with precipitates) HiG displayed reduced graft function after 50 days in the same mouse model. Moreover, lower initial islet viabilities in the second phase may have further confounded the results. Nevertheless, IntG encapsulated islets maintained normoglycemia in C57BL/6J mice for about 50 days during the 83-day study period. At the end of the study, OGTT indicated glucose responsive islets and measured C-peptide concentrations suggested limited graft function with 239±165 pmol/L and 219±124 pmol/L for IntG and HiG, respectively. In conclusion, our findings demonstrate the potential of both sulfated alginate and intermediate G alginate as immunoprotective encapsulation materials for pancreatic islet transplantation in the treatment of type 1 diabetes, as indicated by the restored glycaemic control in diabetic mice over time.

4 General discussion

This thesis explores the use of alginate hydrogel microspheres as immunoisolating materials, focusing particularly on their potential for treating type 1 diabetes. Despite extensive research, clinical success for islet transplantation using alginate microspheres has yet to be achieved, with pericapsular fibrotic overgrowth (PFO) posing as one of the primary challenges. Accordingly, the work herein has investigated the host responses following biomaterial implantation, as a means to formulate immunocompatible alginate materials that ensure long-term therapeutic efficacy. To summarise, **Paper I** highlights the advances and existing challenges of using alginate microspheres for pancreatic cell-encapsulation therapy. **Paper II** presents the impact of various chemical compositions and gelling ions on the performance of empty alginate microbeads *in vitro* and *in vivo*. **Paper III** introduces a novel MS-based methodology for detecting and quantifying plasma proteins adsorbed to alginate microspheres exhibiting different host responses. Lastly, **Paper IV** describes the functional performance of encapsulated rat islets in diabetic mice using stable, low-fibrotic alginate beads. The discussion of this thesis is organised around central themes of the research, encompassing hydrogel bead stability, permeability, mechanical properties, PFO, protein adsorption, and the use of alginate beads in cell therapy of diabetes. A key novelty of the current work is the application of chemically sulfated alginate for cell encapsulation as well as characterising alginate microspheres by MS-based proteomics to elucidate host responses.

Hydrogel beads – physicochemical properties

Stability

In cell encapsulation therapy, the integrity of the microbead is paramount, as it serves as the foundation for achieving therapeutic efficacy through a stable immune barrier (**Paper I**). Alginate hydrogels, however, are susceptible to destabilisation due to ion exchange or chelation of the gelling ions [99, 162]. Compromised microbead stability, whether through fragmentation, leakage, or dissolution, can induce immune responses that are detrimental to the encapsulated cells [151]. In the work herein, microbead

stability was assessed both *in vitro* using a saline-based assay (**Paper II**) and *in vivo* by implantation into mice (**Paper II** and **IV**). We explored various alginate formulations: high G, intermediate G, and sulfated alginates, alone or in specific combination, which were gelled with either calcium (50 mM), barium (20 mM), strontium (20 mM), or calcium with barium (50 mM, 1 mM). Using strontium or barium significantly stabilised the microbeads *in vitro*, with high barium concentrations primarily providing the most stability, as previously reported [99]. However, we selected a low concentration of barium with calcium for further evaluations *in vivo*, balancing adequate stability against potential barium toxicity [163].

In contrast to previous reports of poor *in vivo* stability for intermediate G alginate beads [126], the work herein found them generally less stable *in vitro* (**Paper II**) but not markedly different in stability from high G alginate beads *in vivo* (**Paper II** and **IV**). As opposed to the *in vitro* saline assay, the *in vivo* environment contains both destabilising (e.g. sodium, chelators) and stabilising compounds (e.g. calcium) [109]. Importantly, we included a low concentration (2 mM) of calcium in the solutions used for washing and handling the beads, in addition to using limited volumes, to ensure their stability. As a potential strategy to increase the stability of the intermediate G alginate microbeads, we incorporated smaller fractions of high G alginate with varying molecular weights or increased the polymer concentration; both of which slightly improved stability (**Paper II**).

The stability of sulfated alginate microbeads *in vitro* was generally higher than or similar to that of high G alginate microbeads, as shown in **Paper II**. This is in accordance with previous studies [140], which reported that sulfated alginate microbeads (similar formulation to this work) exhibited greater gelling ion retention compared to high G alginate microbeads, thereby likely moderating non-gelling ion influx and minimising subsequent swelling. *In vivo* stability was in general high for all alginate beads tested, gelled with either strontium or a mixture of calcium and barium, showing no notable changes over time (**Paper II** and **IV**). It should be noted that in **Paper II**, the recovery rates for empty sulfated alginate microbeads, particularly those with 40% sulfated alginate, were generally lower and more variable than for other

microbeads post-implantation, the reason for which remains elusive. However, to sum up, alginate beads containing either intermediate G or sulfated alginate, gelled with calcium and a low concentration of barium, demonstrate adequate stability for use as immunoisolation materials in cell encapsulation therapy, as indicated in **Paper IV**.

Permeability

Permeability is a critical determinant in the success of immunoisolation, governing the diffusion of nutrients, therapeutic products, and gas exchange (**Paper I**). Although not directly assessed in the current work, the functional permeability of beads consisting of either intermediate G or sulfated alginate was demonstrated through sustained blood glucose correction in diabetic immunocompetent mice (**Paper IV**). These alginate materials successfully provided immune protection for the transplanted grafts while allowing free insulin diffusion through the hydrogel network to maintain normoglycemia. The precise permeability requirements for microspheres to function as immune barriers remain unclear. The ingress of immune molecules such as inflammatory cytokines and immunoglobulins may have detrimental effects on encapsulated islets [21, 164, 165]. However, previous studies have shown that islets encapsulated in alginate microbeads can be protected from immune rejection for up to a year in allogeneic mouse models, despite the influx of cytokines (IL1-β, IFN-γ) [21]. At the least, the prevention of cell-to-cell contact between the graft and the host is essential (**Paper I**), as shown in **Paper IV** and by others [21, 22, 166].

Mechanical properties

To preserve the function of transplanted cells, the immunoisolating material must exhibit a specific level of mechanical stiffness and toughness. While not explicitly defined, this mechanical resistance is crucial for hydrogel microspheres used in cell encapsulation to withstand the stress, such as compression and shearing forces, during manipulation, transplantation, and *in vivo* application [151, 167]. In **Paper II**, we examined the stiffness of hydrogel cylinders and microbeads consisting of either high G, intermediate G or a mixture of high G and sulfated alginate. The stiffness of hydrogel cylinders and microbeads was assessed using Young's modulus and force output at defined strain, respectively, revealing consistent relative trends. At equal

polymer concentrations, high G alginate hydrogels demonstrated the greatest stiffness overall, and intermediate G alginate the lowest, as expected. This is due to the presence of more and longer G-blocks in high G alginate, responsible for the crosslinking of the hydrogel network, known to directly influence gel stiffness [94, 97, 108, 109]. Sulfated alginate hydrogels consisting of 20% chemically sulfated (DS ~ 0.8) high G alginate and 80% high G alginate, exhibited slightly lower gel stiffness than high G alginate alone. However, as the sulfated alginate constituted only a subfraction of the bead formulation, the effect on gel stiffness is minor. This corresponds to previous reports [140]. Taken together (**Paper II** and **IV**), the hydrogel beads containing intermediate G or sulfated alginate exhibited no structural damage under *in vitro* or *in vivo* conditions, underscoring their mechanical robustness and potential applicability in cell encapsulation therapy.

Pericapsular fibrotic overgrowth

As outlined in **Paper I**, PFO poses a significant challenge to the use of alginate microspheres in cell therapy. Despite their generally recognised biocompatibility, the specific design of alginate-based microspheres dictates the onset of PFO and consequently the sustained function of encapsulated cells *in vivo* [22, 151]. Although the foreign body response to biomaterials is well described [42-44], the underlying mechanisms of PFO for alginate microbeads are yet to be elucidated. Numerous studies have demonstrated the involvement of complement activation on biomaterial surfaces in promoting inflammatory cellular responses [119, 128, 129, 168-171], including fibrosis [168]. The pronounced PFO response of poly-L-lysine (PLL)-coated alginate microbeads [118, 130-132, 172] can be attributed to surface deposited complement C3 [119, 128, 129, 134], leading to leukocyte adhesion and subsequent induction of proinflammatory cytokines [119, 128, 129]. In **Paper II**, PLL-coated alginate microbeads were included as a positive proinflammatory control, showing significant complement activation in human whole blood. While prior studies have solely demonstrated C3 deposition on PLL-coated alginate microbeads *in vitro* [119, 128, 129, 134], the work herein (**Paper II**) verified this phenomenon *in vivo* following implantation in immunocompetent mice, accompanied by an extensive PFO response observed after only 2 days. In contrast, limited *in vivo* C3 deposition was observed for

fibrotic high G alginate microbeads at 14 days, and for minimally fibrotic intermediate G or sulfated alginate microbeads at both 14 and 112 days.

High G alginate

As discussed in **Paper I**, the underlying cause of PFO for high G alginate microbeads remains undetermined. Their low inflammatory potential [119, 128, 134] was further corroborated in **Paper II** and **III**, notably showing minimal induction of terminal complement complex (TCC) in human whole blood. Initially valued for their superior hydrogel stability over lower G alginate hydrogels [13, 99] and lower inflammatory cytokine induction in primary human monocytes *in vitro* [120, 122], high G alginate microbeads with encapsulated islets were tested in humans [23, 24] but without success. The fibrotic response of high G alginate beads has been well documented using specific mouse strains [21, 126], non-human primates [22] and humans [23, 24]. Therefore, it was included in the current work as a positive control for PFO using the fibrosis responsive C57BL/6J(Rj) mouse model (**Paper II** and **IV**).

Intermediate G alginate

Using beads made of intermediate G alginate offers a straightforward approach, given that this unmodified alginate is readily available and has demonstrated minimal PFO in prior studies [21, 126, 127], although stability issues have been reported [99, 126]. The current work (**Paper II** and **IV**) reaffirmed the minimal PFO response of intermediate G alginate beads, which in addition showed high *in vivo* stability through specific formulation and handling. This included using a mixture of calcium (50 mM) and barium (1 mM) or solely strontium (20 mM) for gelation, as well as incorporating a physiological concentration (2 mM) of calcium in the washing and handling solutions. Moreover, the microbeads' low inflammatory potential was shown through a minimal TCC response in human whole blood (**Paper II**). Another aspect explored was the potential enhancement of stability for intermediate G alginate microbeads by incorporating a small fraction of high G alginate of various molecular weights (**Paper II**). Intriguingly, these microbeads were essentially PFO-free, similar to those containing purely intermediate G alginate. However, microbeads with very low molecular weight high G alginate displayed a moderate increase in PFO. Importantly,

this establishes a degree of versatility in microbead formulation using unmodified alginates with different G content to achieve microbeads with minimal PFO and increased stability, a finding not previously reported.

Sulfated alginate

As presented in **Paper II** and **IV**, the inclusion of a small fraction of sulfated alginate into high G alginate beads resulted in minimal PFO. The prominent anti-fibrotic properties of sulfated alginate have also been demonstrated in mice receiving alginate-encapsulated xenotransplants of human pluripotent stem cell (hPSC)-derived hepatocytes [173], which poses even greater challenges with respect to xenogeneic immune reactions. In the work herein, the rationale for employing sulfated alginate as an immunoisolating material for cell therapy originated from its documented anti-inflammatory properties, previously assessed using complement-stimulated plasma [137] and human whole blood [134]. Incorporating sulfated alginate into alginate microspheres, either in the microbead formulation or as a second coating on PLL-containing microcapsules, significantly reduced inflammatory cytokine responses and increased the binding of complement inhibitor factor H [134], which will be addressed in the following section. Sulfated alginate microbeads exhibit a complement inert nature with insignificant induction of TCC, as well as exhibiting a moderate coagulation response [134], which was confirmed in **Paper II** and **III**.

Effect of size, stiffness, and gelling ions with regard to PFO

Exploring a different aspect, the work by Veiseh and co-workers revealed that the size of microspheres influence PFO development [29]. Increasing the size of alginate hydrogel spheres to 1.5 mm and above was shown to largely prevent PFO in C57BL/6 mice up to 180 days and in non-human primates up to 14 or 28 days. In **Paper II**, we investigated various formulations of microbeads within the 500 µm size range. This presented the materials with a greater challenge with respect to PFO. Notably, microbeads of intermediate G or sulfated alginate displayed minimal PFO up to 112 days, highlighting their potential as cell encapsulating materials. In the follow-up study (**Paper IV**), where the functional performance of encapsulated rat islets was examined, larger-sized beads of about 1000 µm were utilised to balance PFO mitigation

against potential size-dependent diffusion limitations. The effect of the size increase was evident, as our positive PFO control, consisting of high G alginate, showed significantly less PFO than its smaller-sized counterpart (**Paper II**). Consequently, high G alginate beads sustained transplanted islet function in C57BL/6J mice for the entire study duration of 120 days, paralleling the performance of the minimally fibrotic sulfated alginate beads (**Paper IV**). However, it should be noted that in the study by Veiseh et al. [29], rat islet grafts encapsulated in larger-sized (1.5 mm) high-G alginate beads failed after approximately 140 days in C57BL/6 mice, although significant PFO was not observed.

As explored in **Paper II**, material stiffness could be a potential factor in PFO development. Existing research indicates that hydrogel stiffness can influence cell behaviour [174-176], where stiffer hydrogels (gelatine-methacrylate) have been shown to promote proinflammatory M1 macrophage phenotypes *in vitro* and increased fibrosis *in vivo* [176]. To investigate this, we characterised the material stiffness of various alginate hydrogel formulations (**Paper II**), as described above. In brief, high G alginate hydrogels (prone to PFO) exhibited significantly greater stiffness than the corresponding intermediate G alginate hydrogels (minimally prone to PFO). Reducing the concentration of high G alginate hydrogels to match the stiffness to that of intermediate G alginate led to a significant *increase* in the PFO response for implanted microbeads. Conversely, increasing the concentration, and thus stiffness [109], of intermediate G alginate microbeads slightly exacerbated PFO. These observations suggest that factors other than gel stiffness are likely more crucial in the development of PFO for the alginate microbeads. This aligns with studies highlighting size and geometry [29] and chemical composition [28] as more significant determinants of PFO.

There is limited and somewhat inconsistent data concerning the role of gelling ions in PFO for alginate microspheres. The study by Duvivier-Kali et al. [21] found that high M and high G microbeads gelled with calcium (100 mM) exhibited slightly increased PFO compared to those with barium (10 mM) in BALB/c and NOD mice after 30 days. The use of calcium in the gelation of alginate hydrogels for biomedical applications has been questioned due to its role as a second messenger in immune cell signalling [177]. Immunostimulatory effects have been reported when using calcium

compared to barium for crosslinking alginate hydrogels, including increased cytokine (IL-1β) secretion from surrounding tissue after subcutaneous injection into C57BL/6J mice [177]. It should be noted that in all the referenced studies comparing calcium and barium, the concentration of calcium was significantly higher. However, the study by Tam et al. reported that PFO was independent of the type of gelling ions used, including calcium (100 mM) or barium (10 mM), for intermediate G or high G alginate microbeads implanted into C57BL/6J mice for 2 days [126]. In the work herein (**Paper II**–**IV**), the alginate beads were predominantly gelled using a mixture of calcium (50 mM) and barium (1 mM). The use of strontium (20 mM) was briefly explored in the screening study of **Paper II**, as one patent has described its use to inhibit cellular overgrowth on alginate hydrogels [178]. The type of gelling ions used did not influence PFO for intermediate G alginate microbeads. However, for microbeads with 40% sulfated alginate, a slight reduction in both PFO and inflammatory responses (TCC, cytokines) was observed when gelled in strontium. Still, the work herein demonstrates that the chemical composition of alginate seems to be the key determinant of the PFO outcome for alginate hydrogel microbeads.

Elucidating host responses through protein adsorption

The generally low complement-activating potential of high G alginate microbeads, as shown previously [119, 134] and herein (**Paper II** and **III**), consequently raises the question of other influential determinants of PFO for this material. In **Paper II**, surface deposition of fibrin(ogen) on microbeads after implantation in mice was observed to coincide with PFO. Specifically, fibrotic high G alginate microbeads displayed significantly more fibrin(ogen) than minimally fibrotic intermediate G or sulfated alginate microbeads. Considering the possible role of distinct protein deposition in PFO development, a comprehensive examination of protein adsorption profiles was performed for microbeads with different inflammatory and PFO responses, which constitutes the work of **Paper III**.

Protein adsorption to alginate microspheres has traditionally been studied using immunostaining combined with CLSM [28, 29, 119, 128, 129, 134]. While valuable for investigating specific proteins, this approach possesses inherent limitations. In

contrast, MS-based proteomics offers a broader and more sensitive quantitative assessment, capturing a wider spectrum of adsorbed proteins [48, 52]. Only a few proteomic analyses have addressed the adsorption of plasma or serum proteins to hydrogels [171, 179, 180], and alginate-based hydrogels or microspheres have yet to be explored. A significant portion of the work in this thesis was thus dedicated to developing a novel MS-based proteomics approach to characterise physiologically relevant protein adsorption profiles of alginate hydrogel microspheres (**Paper III**). A noteworthy aspect of the work in **Paper III** as well as **Paper II** (CLSM studies) is the use of lepirudin-plasma. This enables the investigation of proteolytically active acute-phase proteins of complement and coagulation (upstream of thrombin), which are pivotal in the host responses towards biomaterials [42, 46]. While the choice of medium in protein adsorption studies depends on the specific research objective, many studies utilise plasma anticoagulated with agents (e.g. heparin) that disrupt these protein cascades or serum that lacks coagulation factors.

In **Paper III**, enriched proteins conformed to the complement and coagulation inducing potentials of the materials, specifically high G, sulfated, and PLL-coated alginate microbeads. Since protein adsorption is not necessarily indicative of a biological response due to the conformational-dependent bioactivity of acute-phase effectors [46, 55], the proteomics data was interpreted alongside functional whole blood analyses of downstream complement (TCC) and coagulation (prothrombin fragment 1+2; PTF1.2) activation. The surface binding of specific factors within these cascade systems (complement C1q and C3c, and coagulation factor XII) were further verified by CLSM. Together, this multifaceted approach offers detailed insight into the host–material interactions. Indeed, the subtle differences in the low inflammatory potentials of high G alginate and sulfated alginate microbeads (**Paper II** and **III**) can be explained by the differential enrichment of complement inhibitors. As shown in **Paper III**, sulfated alginate microbeads notably enriched all the inhibitors of the complement cascade, particularly factor H, and uniquely enriched both C4-binding protein and carboxypeptidase-N (catalytic subunit). High G alginate microbeads were moderately enriched with some complement inhibitors, including C1 inhibitor and factor H. In contrast, PLL-coated alginate microbeads adsorbed minimal to no complement inhibitors, while showing the highest enrichment of complement activators like C3 and

properdin. Adsorbed complement activators and inhibitors on biomaterials have been suggested to be strong indicators for the biological outcome [50, 181, 182].

Intriguingly, the proteomics and CLSM analyses revealed an extensive enrichment of complement C1q (classical pathway) for both high G alginate and sulfated alginate microbeads, a previously unreported finding to our knowledge. However, this does not result in significant downstream complement activation, as indicated by the low TCC response in human whole blood (**Paper II** and **III**). Thus, *if* an initial complement activation occurs, which is conformation-driven, it is likely subdued. This is supported by enriched inhibitors like C1 inhibitor and low C3 levels revealed by MS-proteomics (**Paper III**), and minimal C3c deposition shown both *in vitro* (**Paper II** and **III**) and *in vivo* (**Paper II**) by CLSM analyses. Furthermore, as detailed in **Paper III**, cluster analysis of the adsorbed proteins could indicate a potential inactivation of C1 complex (C1q/Cr/Cs) based on the grouping of C1 inhibitor with the C1q-associated proteases. Still, the complement inhibitors enriched on the microbeads could be, at least in part, directly bound to the biomaterial surface, as complement inhibitors like C1 inhibitor and factor H can bind directly to polyanions such as sialic acid and sulfated GAGs, including heparin [183, 184], which has been likened to sulfated alginate [137, 141].

The host response is susceptible to influence from the coagulation system, whether directly mediated through the contact pathway or through crosstalk with the complement system [59]. In **Paper II** and **III**, sulfated alginate microbeads showed the most pronounced coagulation response among the microspheres, albeit moderate, followed by PLL-coated alginate microbeads and subsequently high G alginate microbeads. However, the proteomics analysis (**Paper III**) revealed significant enrichment of coagulation inhibitors for sulfated alginate microbeads, including antithrombin, heparin cofactor 2 and C1 inhibitor, suggesting a tight regulation of this activation. Furthermore, the limited fibrin(ogen) deposition observed *in vivo* (**Paper II**) could potentially be indicative of this regulation, considering fibrin clot formation being a downstream effect of coagulation [59]. The enrichment of intrinsic pathway proteins on sulfated alginate microbeads, including factor XII, indicate activation through the contact system. High G alginate microbeads displayed a similar coagulation profile although at lower protein abundances. Distinctively, central

intrinsic pathway proteins were not detected on PLL-coated alginate microbeads. This points towards tissue factor-dependent activation of coagulation, which is closely linked to complement activation, corroborating earlier findings [135].

As previously noted, the work in **Paper II** revealed a positive association of surface deposited fibrin(ogen) and PFO for microbeads implanted in mice. Fibrin(ogen) deposition has been demonstrated to modulate phagocytic cell recruitment in both mice [185] and humans [186]. This proinflammatory response has been shown to be mediated through the interaction with integrin receptor CD11b/CD18, also known as Mac-1 or complement receptor 3, on leukocytes [187]. In **Paper II**, the fibrin(ogen) deposition on minimally fibrotic sulfated alginate and intermediate G alginate microbeads was significantly lower than for fibrotic high G alginate microbeads after 14 days *in vivo*. While these levels remained consistent for sulfated alginate microbeads in the long term (112 days), an increase was observed for intermediate G alginate microbeads, with both maintaining minimal PFO. In **Paper III**, the proteomic profile of sulfated alginate microbeads may indicate an inherent potential for fibrinolysis, as specific pro-fibrinolytic factors (involving activation of plasminogen to plasmin) were found to be highly enriched, including factor XII and plasma kallikrein. Through its primary mechanism involving the plasmin-mediated degradation of fibrin clots during wound healing processes [188], fibrinolysis could be a key factor for the anti-fibrotic effect of sulfated alginate.

Several heparin-binding proteins, some with reported anti-fibrotic effects [189-193], were uniquely or most enriched on sulfated alginate microbeads. As detailed in **Paper III**, this included the matrix metalloproteinases MMP2 and MMP9, along with their regulators TIMP1 and TIMP2 [189, 190], which were differentially adsorbed to sulfated alginate and high G alginate microbeads. Interestingly, various proinflammatory cytokines and chemoattractants were predominantly or exclusively enriched on both high G alginate and PLL-coated alginate microbeads compared to sulfated alginate microbeads. Given the preceding observations, the proteomics data offers comprehensive detail into the proteins interacting with these materials, potentially clarifying the distinct biological responses they induce, such as the fibrotic potentials of high G alginate and sulfated alginate microbeads.

Alginate beads for immunoisolation in cell therapy of diabetes

Through detailed assessments of the physicochemical properties of alginate hydrogel microspheres and understanding their biological implications, we pave the way for enhancing their efficacy as immunoisolation materials in cell therapy. This captures the principal point of **Paper I**. In the work herein (**Paper II** and **III**), we evaluated various alginate microbead formulations, focusing on their stability, mechanical properties, and potential to induce complement and coagulation in human whole blood. Fibrotic responses and *in vivo* protein deposition were assessed in immunocompetent mice, and protein profiling was achieved through CLSM and MS-based proteomics. From our investigations, two candidate materials were selected for further evaluation as immunoisolation materials. The work of **Paper IV** demonstrates that beads with sulfated alginate or intermediate G alginate, which were stable *in vivo* and exhibited minimal PFO (**Paper II** and **IV**), supported the viability and function of encapsulated rat islets in streptozotocin (STZ)-induced diabetic C57BL/6J mice. Sulfated alginate beads sustained islet-graft function throughout the 120-day study, exhibiting maintained normoglycemia, glucose-responsive islets, and high serum C-peptide levels and cell viability at the end of the study. Intermediate G alginate-encapsulated islets sustained normoglycemia for about 50 days within an 83-day study. Notably, the results were confounded by precipitation of hydroxyapatite inside the beads, originating from the islet culture media, likely being the cause of the limited graft function observed at the end of the study. Nevertheless, our findings highlight the promise of both sulfated and intermediate G alginates as encapsulation materials for pancreatic islet transplantation to treat type 1 diabetes, demonstrated by the restored glycaemic control using a well-established mouse model.

In the animal experiments involving STZ-induced diabetes (**Paper IV**), particularly with nude mice, several animals experienced health complications resulting in a concerning number being euthanised or found deceased (nude mice: $n = 8/19$; C57BL/6J mice: $n = 2/20$). The surgical procedure and the beads themselves are unlikely causes, as evidenced by the absence of adverse effects in C57BL/6J mice ($N = 80$) following empty bead implantation. However, the higher vulnerability of immunocompromised nude mice, combined with the stress of diabetes induction and known adverse effects of STZ [194], could potentially contribute to the observed

mortality rate. Despite frequent welfare assessments and implemented humane endpoints, future studies should redefine the humane endpoints for more immediate interventions to reduce potential suffering and death. For instance, by lowering the bodyweight loss threshold (e.g. to 15%) for euthanasia and performing careful pre-transplantation assessments of STZ-treated mice to exclude compromised animals. Revision of the diabetes induction protocol may be warranted to minimise potential toxic side effects, e.g. through STZ dose adjustments [194] or using repeated low doses of STZ instead of one single high dose [195].

Renowned for their contributions to the field of cell encapsulation therapy using alginate spheres for the treatment of diabetes, Veiseh and colleagues at Massachusetts Institute of Technology (MIT) have achieved noteworthy advancements. Their development of low-fibrotic alginate formulations (such as Z1-Y15) has proven successful in pre-clinical studies of long-term immunoprotection of transplanted pancreatic islets, employing models of immunocompetent mice and non-human primates [22, 28, 29]. In parallel, the current work indicates that sulfated alginate and intermediate G alginate beads may offer similar therapeutic potential. However, additional studies involving non-human primates are essential to validate minimal PFO and ensure the long-term functionality of encapsulated islets prior to clinical translation.

Intermediate G alginate beads, representing a simple, unmodified microbead formulation, have shown minimal PFO and therapeutic efficacy in sustaining islet function, as evidenced by prolonged diabetic correction in mice herein (**Paper IV**) and corroborated by previous studies on similar alginates [21, 127]. While stability concerns have been raised [99, 126], the reasons for not advancing this type of alginate to pre-clinical assessments in diabetic non-human primates remain unclear. Sulfated alginate beads, representing a novel microbead formulation, have in the current work shown long-term glycaemic restoration in diabetic mice (**Paper IV**). Furthermore, their efficacy has been demonstrated in immunocompetent mice transplanted with encapsulated hPSC-derived hepatocytes, leading to a significant reduction in PFO under the added complexity of xenogeneic conditions [173]. While targeted at treating acute liver failure [173], these results substantiate the potent anti-fibrotic and

immunoprotective properties of sulfated alginate beads and their ability to support the function and viability of human stem cell-derived hepatocytes *in vivo*.

Recent advancements in the generation of functional islets from human stem cells hold significant promise, potentially paving the way for a new era in the field of islet transplantation [10]. With encouraging prospects, clinical trials in patients with type 1 diabetes are currently ongoing [11]. Alginate, recognised for its hydrogel-forming properties under physiological conditions and porous network facilitating nutrient and waste exchange, serves as a suitable matrix for encapsulating hPSC-derived cells during differentiation [196]. Earlier studies have demonstrated the ability of alginate microbeads to maintain long-term viability and morphological integrity of hPSC-derived pancreatic progenitors *in vitro*, albeit maturation into insulin-producing cells was not achieved [197]. A recent study found that alginate encapsulation enhanced the differentiation of hPSC-derived pancreatic progenitors *in vitro*, reshaping their proteome towards an islet-like signature, presumably through integrin-mediated intracellular signalling [196]. Alginate encapsulation has demonstrated the protection of human stem cell-derived insulin-producing cells against immune rejection in mice [198]. Accordingly, alginate beads may prove beneficial not only for immunoprotection but also for the function of pancreatic islet cells, with sulfated alginate, as well as intermediate G alginate, representing particularly promising encapsulation materials.

5 Concluding remarks

Despite considerable progress in cell encapsulation research, the optimisation of alginate microbeads remains a critical prerequisite for their clinical implementation as immunoisolation materials. Previous clinical trials with alginate-encapsulated human islets, including high G alginate microbeads without a polycation coating [23, 24], have been unsuccessful due to graft failure attributable to pericapsular fibrotic overgrowth (PFO). In the present work, we aimed to develop and examine stable, minimally fibrotic alginate microbeads, explore a novel MS-based proteomics characterisation method to elucidate host responses, and evaluate the functional properties of the beads in a diabetic mouse model.

The incorporation of sulfated alginate into high G alginate microbeads resulted in a significant mitigation of PFO in immunocompetent mice, yielding stable microbeads with minimal cellular deposition. Furthermore, these beads were demonstrated to provide long-term immune protection and sustain the function of transplanted rat islets in diabetic mice. Concurrently, alginate microbeads formulated with intermediate G alginate exhibited minimal PFO in the immunocompetent mouse model, consistent with prior findings [126, 127], and were stable *in vivo*. The beads were further shown to sustain islet function over an extended duration in diabetic mice. Bead stability was enhanced by using the gelling ions calcium with low-concentration barium or solely strontium, as opposed to calcium alone. This stability was further maintained by utilising physiological calcium concentrations in the washing and handling solutions, along with limited volume usage. A certain level of flexibility in microbead formulation was established by incorporating subfractions of high G alginate into intermediate G alginate microbeads, which yielded minimally fibrotic microbeads with slightly improved stability.

In a novel contribution to the field, the current work has demonstrated through the use of MS-based proteomics, that alginate microbeads exhibiting different inflammatory and PFO responses display distinct protein adsorption profiles. Sulfated alginate microbeads showed a prominent enrichment of complement and coagulation

inhibitors, conforming to an anti-inflammatory and minimally fibrotic profile. This bead type was also found to enrich heparin-binding and profibrinolytic proteins with potential anti-fibrotic effects. High G alginate microbeads enriched moderate levels of inhibitors, conforming to a low-inflammatory but fibrotic profile. For poly-L-lysine-coated alginate microbeads that served as a control, the abundant enrichment of complement activators in combination with low levels of inhibitors is consistent with a proinflammatory and highly fibrotic profile.

Utilising MS-based proteomics as a supplement to established *in vitro* and *in vivo* methods provide a deeper understanding of the host–material interactions, especially for biocompatibility assessments of clinically relevant biomaterials. While the PFO development for alginate beads exhibits complexity, the research presented in this thesis has given new insight on specific protein interactions with alginate microbeads. To ensure the success of clinical translation, thorough assessments of both physicochemical and biological characteristics of the materials remain imperative. In light of recent innovations in both bead design and stem cell technology, the outlook for encapsulated cell therapy is becoming more favourable. In conclusion, the work herein has shed light on potential PFO factors in alginate microspheres while also producing well-characterised, minimally fibrotic materials that show promise for cell encapsulation therapy of type 1 diabetes.

References

1. Association, A.D., *Diagnosis and Classification of Diabetes Mellitus.* Diabetes Care, 2013. **37**(Supplement_1): p. S81-S90.
2. DiMeglio, L.A., C. Evans-Molina, and R.A. Oram, *Type 1 diabetes.* Lancet, 2018. **391**(10138): p. 2449-2462.
3. Chatterjee, S., K. Khunti, and M.J. Davies, *Type 2 diabetes.* Lancet, 2017. **389**(10085): p. 2239-2251.
4. Shapiro, A.M.J., M. Pokrywczynska, and C. Ricordi, *Clinical pancreatic islet transplantation.* Nature Reviews Endocrinology, 2017. **13**(5): p. 268-277.
5. Sun, H., et al., *IDF Diabetes Atlas: Global, regional and country-level diabetes prevalence estimates for 2021 and projections for 2045.* Diabetes Research and Clinical Practice, 2022. **183**: p. 109119.
6. Bellin, M.D. and T.B. Dunn, *Transplant strategies for type 1 diabetes: whole pancreas, islet and porcine beta cell therapies.* Diabetologia, 2020. **63**(10): p. 2049-2056.
7. Shapiro, A.M.J., *State of the Art of Clinical Islet Transplantation and Novel Protocols of Immunosuppression.* Current Diabetes Reports, 2011. **11**(5): p. 345-354.
8. Administration, U.S.F.D., *FDA Approves First Cellular Therapy to Treat Patients with Type 1 Diabetes*. 2023, FDA.
9. Desai, T. and L.D. Shea, *Advances in islet encapsulation technologies.* Nature Reviews Drug Discovery, 2017. **16**(5): p. 338-350.
10. Pagliuca, F.W., et al., *Generation of functional human pancreatic β cells in vitro.* Cell, 2014. **159**(2): p. 428-39.
11. Association, A.D., *Novel Stem Cell-Derived Islet Cell Therapy Continues to Show Promise for Achieving Insulin Independence for Individuals with Type 1 Diabetes*. 2023.
12. Lim, F. and A.M. Sun, *Microencapsulated Islets as Bioartificial Endocrine Pancreas.* Science, 1980. **210**(4472): p. 908-910.
13. Qi, M., et al., *Survival of human islets in microbeads containing high guluronic acid alginate crosslinked with Ca2+ and Ba2+.* Xenotransplantation, 2012. **19**(6): p. 355-64.
14. Lanza, R.P. and W.L. Chick, *Immunoisolation: at a turning point.* Immunol Today, 1997. **18**(3): p. 135-9.
15. Sakata, N., et al., *Encapsulated islets transplantation: Past, present and future.* World J Gastrointest Pathophysiol, 2012. **3**(1): p. 19-26.

16. Ludwig, B. and S. Ludwig, *Transplantable bioartificial pancreas devices: current status and future prospects.* Langenbecks Arch Surg, 2015. **400**(5): p. 531-40.
17. Gamble, A., et al., *The journey of islet cell transplantation and future development.* Islets, 2018. **10**(2): p. 80-94.
18. Strand, B.L., *Alginate microcapsules for cell therapy: a study of functional properties of capsules made of native and enzymatically tailored alginates*, b. Norges teknisk-naturvitenskapelige universitet Institutt for, Editor. 2002, Department of Biotechnology, Faculty of Natural Science and Technology, Norwegian University of Science and Technology: Trondheim.
19. Kjesbu, J.S., *Hydrogel beads from marine polysaccharides: Investigation of bead formulations for use in cell encapsulation*, in *Department of Biotechnology and Food Science*. 2022, NTNU: Trondheim.
20. Ruiz, R. and A.D. Kirk, *Long-Term Toxicity of Immunosuppressive Therapy.* Transplantation of the Liver, 2015: p. 1354 - 1363.
21. Duvivier-Kali, V.F., et al., *Complete protection of islets against allorejection and autoimmunity by a simple barium-alginate membrane.* Diabetes, 2001. **50**(8): p. 1698-705.
22. Bochenek, M.A., et al., *Alginate encapsulation as long-term immune protection of allogeneic pancreatic islet cells transplanted into the omental bursa of macaques.* Nature biomedical engineering, 2018. **2**(11): p. 810-821.
23. Tuch, B.E., et al., *Safety and viability of microencapsulated human islets transplanted into diabetic humans.* Diabetes Care, 2009. **32**(10): p. 1887-9.
24. Jacobs-Tulleneers-Thevissen, D., et al., *Sustained function of alginate-encapsulated human islet cell implants in the peritoneal cavity of mice leading to a pilot study in a type 1 diabetic patient.* Diabetologia, 2013. **56**(7): p. 1605-1614.
25. Soon-Shiong, P., et al., *Insulin independence in a type 1 diabetic patient after encapsulated islet transplantation.* Lancet, 1994. **343**(8903): p. 950-951.
26. Calafiore, R., et al., *Microencapsulated pancreatic islet allografts into nonimmunosuppressed patients with type 1 diabetes: first two cases.* Diabetes Care, 2006. **29**(1): p. 137-138.
27. Basta, G., et al., *Long-term metabolic and immunological follow-up of nonimmunosuppressed patients with type 1 diabetes treated with microencapsulated islet allografts: four cases.* Diabetes Care, 2011. **34**(11): p. 2406-9.
28. Vegas, A.J., et al., *Combinatorial hydrogel library enables identification of materials that mitigate the foreign body response in primates.* Nature Biotechnology, 2016. **34**(3): p. 345-352.

29. Veiseh, O., et al., *Size- and shape-dependent foreign body immune response to materials implanted in rodents and non-human primates.* Nature Materials, 2015. **14**(6): p. 643-651.
30. Liu, Q., et al., *Zwitterionically modified alginates mitigate cellular overgrowth for cell encapsulation.* Nat Commun, 2019. **10**(1): p. 5262.
31. Holzapfel, B.M., et al., *How smart do biomaterials need to be? A translational science and clinical point of view.* Advanced Drug Delivery Reviews, 2013. **65**(4): p. 581-603.
32. Leeuwenburgh, S.C.G., et al., *Trends in biomaterials research: An analysis of the scientific programme of the World Biomaterials Congress 2008.* Biomaterials, 2008. **29**(21): p. 3047-3052.
33. Williams, D.F., *On the nature of biomaterials.* Biomaterials, 2009. **30**(30): p. 5897-5909.
34. Bhardwaj, A. and L.M. Pandey, *Biomaterials: Types and Applications*, in *Nanoscale Engineering of Biomaterials: Properties and Applications*, L.M. Pandey and A. Hasan, Editors. 2022, Springer Nature Singapore: Singapore. p. 89-114.
35. Williams, D.F., *On the mechanisms of biocompatibility.* Biomaterials, 2008. **29**(20): p. 2941-2953.
36. Williams, D.F., *There is no such thing as a biocompatible material.* Biomaterials, 2014. **35**(38): p. 10009-10014.
37. Ratner, B.D., *A pore way to heal and regenerate: 21st century thinking on biocompatibility.* Regen Biomater, 2016. **3**(2): p. 107-10.
38. Crawford, L., et al., *Biocompatibility Evolves: Phenomenology to Toxicology to Regeneration.* Advanced Healthcare Materials, 2021. **10**(11): p. 2002153.
39. Ratner, B.D., *Chapter 3 - The Biocompatibility of Implant Materials*, in *Host Response to Biomaterials*, S.F. Badylak, Editor. 2015, Academic Press: Oxford. p. 37-51.
40. *The Williams Dictionary of Biomaterials.* 1999: Liverpool University Press.
41. Reis, R.L., *2nd Consensus conference on definitions on biomaterials science.* Journal of Tissue Engineering and Regenerative Medicine, 2020. **14**(4): p. 561-562.
42. Anderson, J.M., A. Rodriguez, and D.T. Chang, *Foreign body reaction to biomaterials.* Seminars in Immunology, 2008. **20**(2): p. 86-100.
43. Anderson, J.M. and S. Jiang, *Implications of the Acute and Chronic Inflammatory Response and the Foreign Body Reaction to the Immune Response of Implanted Biomaterials*, in *The Immune Response to Implanted Materials and Devices: The Impact of the Immune System on the Success of an Implant*, B. Corradetti, Editor. 2017, Springer International Publishing: Cham. p. 15-36.

44. Gonzalez-Simon, A.L. and O. Eniola-Adefeso, *Host Response to Biomaterials*, in *Engineering Biomaterials for Regenerative Medicine: Novel Technologies for Clinical Applications*, S.K. Bhatia, Editor. 2012, Springer New York: New York, NY. p. 143-159.
45. Doloff, J.C., et al., *Colony stimulating factor-1 receptor is a central component of the foreign body response to biomaterial implants in rodents and non-human primates.* Nat Mater, 2017. **16**(6): p. 671-680.
46. Ekdahl, K.N., et al., *Innate immunity activation on biomaterial surfaces: a mechanistic model and coping strategies.* Adv Drug Deliv Rev, 2011. **63**(12): p. 1042-1050.
47. Hamad, O.A., et al., *Platelets, Complement, and Contact Activation: Partners in Inflammation and Thrombosis*, in *Current Topics in Innate Immunity II*, J.D. Lambris and G. Hajishengallis, Editors. 2012, Springer New York: New York, NY. p. 185-205.
48. Kim, J., *Systematic approach to characterize the dynamics of protein adsorption on the surface of biomaterials using proteomics.* Colloids Surf B Biointerfaces, 2020. **188**: p. 110756.
49. Abdallah, M.-N., et al., *Biomaterial surface proteomic signature determines interaction with epithelial cells.* Acta Biomaterialia, 2017. **54**: p. 150-163.
50. Engberg, A.E., et al., *Prediction of inflammatory responses induced by biomaterials in contact with human blood using protein fingerprint from plasma.* Biomaterials, 2015. **36**: p. 55-65.
51. Hammad, M., et al., *Identification of polymer surface adsorbed proteins implicated in pluripotent human embryonic stem cell expansion.* Biomaterials Science, 2016. **4**(9): p. 1381-1391.
52. Othman, Z., et al., *Understanding interactions between biomaterials and biological systems using proteomics.* Biomaterials, 2018. **167**: p. 191-204.
53. Vroman, L. and A.L. Adams, *Identification of rapid changes at plasma-solid interfaces.* J Biomed Mater Res, 1969. **3**(1): p. 43-67.
54. Rabe, M., D. Verdes, and S. Seeger, *Understanding protein adsorption phenomena at solid surfaces.* Advances in Colloid and Interface Science, 2011. **162**(1): p. 87-106.
55. Ricklin, D., et al., *Complement: a key system for immune surveillance and homeostasis.* Nature Immunology, 2010. **11**(9): p. 785-797.
56. Merle, N.S., et al., *Complement System Part I – Molecular Mechanisms of Activation and Regulation.* Frontiers in Immunology, 2015. **6**(262).
57. Gale, A.J., *Continuing education course #2: current understanding of hemostasis.* Toxicol Pathol, 2011. **39**(1): p. 273-280.
58. Amara, U., et al., *Molecular intercommunication between the complement and coagulation systems.* J Immunol, 2010. **185**(9): p. 5628-36.

59. Oikonomopoulou, K., et al., *Interactions between coagulation and complement--their role in inflammation.* Semin Immunopathol, 2012. **34**(1): p. 151-65.
60. Keshari, R.S., et al., *In vivo-generated thrombin and plasmin do not activate the complement system in baboons.* Blood, 2017. **130**(24): p. 2678-2681.
61. Nilsson, P.H., et al., *A Conformational Change of Complement C5 Is Required for Thrombin-Mediated Cleavage, Revealed by a Novel Ex Vivo Human Whole Blood Model Preserving Full Thrombin Activity.* J Immunol, 2021. **207**(6): p. 1641-1651.
62. Mackman, N., R.E. Tilley, and N.S. Key, *Role of the Extrinsic Pathway of Blood Coagulation in Hemostasis and Thrombosis.* Arteriosclerosis, Thrombosis, and Vascular Biology, 2007. **27**(8): p. 1687-1693.
63. Grover, S.P. and N. Mackman, *Tissue Factor.* Arteriosclerosis, Thrombosis, and Vascular Biology, 2018. **38**(4): p. 709-725.
64. Long, A.T., et al., *Contact system revisited: an interface between inflammation, coagulation, and innate immunity.* J Thromb Haemost, 2016. **14**(3): p. 427-437.
65. Weidmann, H., et al., *The plasma contact system, a protease cascade at the nexus of inflammation, coagulation and immunity.* Biochim Biophys Acta Mol Cell Res, 2017. **1864**(11 Pt B): p. 2118-2127.
66. Girard, T.J., et al., *Protein Z, protein Z-dependent protease inhibitor (serpinA10), and the acute-phase response.* Journal of thrombosis and haemostasis : JTH, 2013. **11**(2): p. 375-378.
67. Haug, A., *Composition and properties of alginates.* 1964, NTH: Trondheim.
68. Draget, K.I., et al., *Alginates*, in *Food Polysaccharides and Their Applications.* 2006, CRC Press. p. 289-334.
69. Clementi, F., *Alginate production by Azotobacter vinelandii.* Crit Rev Biotechnol, 1997. **17**(4): p. 327-61.
70. Rehm, B.H. and S. Valla, *Bacterial alginates: biosynthesis and applications.* Appl Microbiol Biotechnol, 1997. **48**(3): p. 281-8.
71. Peteiro, C., *Alginate Production from Marine Macroalgae, with Emphasis on Kelp Farming*, in *Alginates and Their Biomedical Applications*, B.H.A. Rehm and M.F. Moradali, Editors. 2018, Springer Singapore: Singapore. p. 27-66.
72. Moradali, M.F., S. Ghods, and B.H.A. Rehm, *Alginate Biosynthesis and Biotechnological Production*, in *Alginates and Their Biomedical Applications*, B.H.A. Rehm and M.F. Moradali, Editors. 2018, Springer Singapore: Singapore. p. 1-25.
73. Lee, K.Y. and D.J. Mooney, *Alginate: properties and biomedical applications.* Prog Polym Sci, 2012. **37**(1): p. 106-126.
74. Sarker, B. and A.R. Boccaccini, *Alginate Utilization in Tissue Engineering and Cell Therapy*, in *Alginates and Their Biomedical Applications*, B.H.A. Rehm and M.F. Moradali, Editors. 2018, Springer Singapore: Singapore. p. 121-155.

75. Haug, A., et al., *A Study of the Constitution of Alginic Acid by Partial Acid Hydrolysis.* Acta chemica Scandinavica, 1966. **20**: p. 183-190.
76. Atkins, E.D., W. Mackie, and E.E. Smolko, *Crystalline structures of alginic acids.* Nature, 1970. **225**(5233): p. 626-8.
77. Atkins, E.D.T., et al., *Crystalline structures of poly-D-mannuronic and poly-L-guluronic acids.* Journal of Polymer Science Part B: Polymer Letters, 1971. **9**(4): p. 311-316.
78. Smidsrød, O., R.M. Glover, and S.G. Whittington, *The relative extension of alginates having different chemical composition.* Carbohydrate Research, 1973. **27**(1): p. 107-118.
79. Skjåk-Bræk, G., I. Donati, and S. Paoletti, *Alginate Hydrogels: Properties and Applications*, in *Polysaccharide Hydrogels: Characterization and Biomedical Applications*, P. MATRICARDI and F.A.T. COVIELLO, Editors. 2015, Pan Stanford Publishing. p. 449-498.
80. Skjåk-Bræk, G., et al., *Alginates*, in *Food Polysaccharides and Their Applications*, A.M. Stephen and G.O. Phillips, Editors. 2006, CRC Press. p. 289-334.
81. Draget, K., *Handbook of hydrocolloids*, in *Alginates*, G. Philips and P. Williams, Editors. 2009, CRC Press Boca Raton, EUA. p. 807-828.
82. Grasdalen, H., B. Larsen, and O. Smisrod, *13C-n.m.r. studies of monomeric composition and sequence in alginate.* Carbohydrate Research, 1981. **89**(2): p. 179-191.
83. Grasdalen, H., *High-field, 1H-n.m.r. spectroscopy of alginate: sequential structure and linkage conformations.* Carbohydrate Research, 1983. **118**: p. 255-260.
84. Aarstad, O.A., et al., *Alginate Sequencing: An Analysis of Block Distribution in Alginates Using Specific Alginate Degrading Enzymes.* Biomacromolecules, 2012. **13**(1): p. 106-116.
85. Andersen, T., et al., *Alginates as biomaterials in tissue engineering*, in *Carbohydrate Chemistry*, A. Pilar Rauter and T. Lindhorst, Editors. 2011, The Royal Society of Chemistry. p. 0.
86. Draget, K.I., O. Smidsrød, and G. Skjåk-Bræk, *Alginates from algae*, in *Polysaccharides and polyamides in the food industry: properties, production, and patents*. 2005. p. 1-30.
87. Vold, I.M.N., K.A. Kristiansen, and B.E. Christensen, *A Study of the Chain Stiffness and Extension of Alginates, in Vitro Epimerized Alginates, and Periodate-Oxidized Alginates Using Size-Exclusion Chromatography Combined with Light Scattering and Viscosity Detectors.* Biomacromolecules, 2006. **7**(7): p. 2136-2146.

88. Haug, A., B. Larsen, and O. Smidsrød, *Uronic acid sequence in alginate from different sources.* Carbohydrate Research, 1974. **32**(2): p. 217-225.
89. Indergaard, M. and G. Skjåk-Bræk, *Characteristics of alginate from Laminaria digitata cultivated in a high-phosphate environment.* Hydrobiologia, 1987. **151**(1): p. 541-549.
90. Haug, A. and B. Larsen, *Biosynthesis of alginate. Epimerisation of D-mannuronic to L-guluronic acid residues in the polymer chain.* Biochim Biophys Acta, 1969. **192**(3): p. 557-9.
91. Petersen, A.B., et al., *Mannuronate C-5 epimerases and their use in alginate modification.* Essays Biochem, 2023. **67**(3): p. 615-627.
92. Ertesvåg, H., et al., *Cloning and expression of an Azotobacter vinelandii mannuronan C-5-epimerase gene.* J Bacteriol, 1994. **176**(10): p. 2846-53.
93. Svanem, B.I., et al., *Cloning and expression of three new Aazotobacter vinelandii genes closely related to a previously described gene family encoding mannuronan C-5-epimerases.* J Bacteriol, 1999. **181**(1): p. 68-77.
94. Skjåk-Bræk, G., O. Smidsrød, and B. Larsen, *Tailoring of alginates by enzymatic modification in vitro.* International Journal of Biological Macromolecules, 1986. **8**(6): p. 330-336.
95. Mørch, Ý.A., et al., *Mechanical properties of C-5 epimerized alginates.* Biomacromolecules, 2008. **9**(9): p. 2360-8.
96. Haug, A., et al., *Selectivity of Some Anionic Polymers for Divalent Metal Ions.* Acta Chemica Scandinavica, 1970. **24**: p. 843-854.
97. Smidsrød, O., *Molecular basis for some physical properties of alginates in the gel state.* Faraday Discussions of the Chemical Society, 1974. **57**(0): p. 263-274.
98. Smidsrød, O.A., et al., *Dependence upon Uronic Acid Composition of Some Ion-Exchange Properties of Alginates.* Acta Chemica Scandinavica, 1968. **22**: p. 1989-1997.
99. Mørch, Ý.A., I. Donati, and B.L. Strand, *Effect of Ca2+, Ba2+, and Sr2+ on Alginate Microbeads.* Biomacromolecules, 2006. **7**(5): p. 1471-1480.
100. Grant, G.T., et al., *Biological interactions between polysaccharides and divalent cations: The egg-box model.* FEBS Letters, 1973. **32**(1): p. 195-198.
101. Braccini, I. and S. Pérez, *Molecular Basis of Ca2+-Induced Gelation in Alginates and Pectins: The Egg-Box Model Revisited.* Biomacromolecules, 2001. **2**(4): p. 1089-1096.
102. Sikorski, P., et al., *Evidence for Egg-Box-Compatible Interactions in Calcium−Alginate Gels from Fiber X-ray Diffraction.* Biomacromolecules, 2007. **8**(7): p. 2098-2103.
103. Borgogna, M., et al., *On the Initial Binding of Alginate by Calcium Ions. The Tilted Egg-Box Hypothesis.* The Journal of Physical Chemistry B, 2013. **117**(24): p. 7277-7282.

104. Stokke, B.T., et al., *Small-Angle X-ray Scattering and Rheological Characterization of Alginate Gels. 1. Ca−Alginate Gels.* Macromolecules, 2000. **33**(5): p. 1853-1863.
105. Donati, I., et al., *New hypothesis on the role of alternating sequences in calcium-alginate gels.* Biomacromolecules, 2005. **6**(2): p. 1031-40.
106. Donati, I., et al., *Effect of elongation of alternating sequences on swelling behavior and large deformation properties of natural alginate gels.* J Phys Chem B, 2009. **113**(39): p. 12916-22.
107. Strand, B.L., et al., *Alginate-polylysine-alginate microcapsules: effect of size reduction on capsule properties.* J Microencapsul, 2002. **19**(5): p. 615-630.
108. Draget, K.I., K. Østgaard, and O. Smidsrød, *Homogeneous alginate gels: A technical approach.* Carbohydrate Polymers, 1990. **14**(2): p. 159-178.
109. Martinsen, A., G. Skjåk-Bræk, and O. Smidsrød, *Alginate as immobilization material: I. Correlation between chemical and physical properties of alginate gel beads.* Biotechnol Bioeng, 1989. **33**(1): p. 79-89.
110. Smidsrød, O. and G. Skjåk-Bræk, *Alginate as immobilization matrix for cells.* Trends in Biotechnology, 1990. **8**: p. 71-78.
111. Draget, K.I., et al., *Ionic and acid gel formation of epimerised alginates; the effect of AlgE4.* International Journal of Biological Macromolecules, 2000. **27**(2): p. 117-122.
112. Manning, G.S., *Limiting Laws and Counterion Condensation in Polyelectrolyte Solutions I. Colligative Properties.* The Journal of Chemical Physics, 1969. **51**(3): p. 924-933.
113. Moe, S.T., et al., *Swelling of covalently crosslinked alginate gels: influence of ionic solutes and nonpolar solvents.* Macromolecules, 1993. **26**(14): p. 3589-3597.
114. Darrabie, M.D., W.F. Kendall, and E.C. Opara, *Effect of alginate composition and gelling cation on micro-bead swelling.* J Microencapsul, 2006. **23**(1): p. 29-37.
115. Mørch, Ý.A., et al., *Molecular Engineering as an Approach to Design New Functional Properties of Alginate.* Biomacromolecules, 2007. **8**(9): p. 2809-2814.
116. Kulseng, B., et al., *Alginate polylysine microcapsules as immune barrier: permeability of cytokines and immunoglobulins over the capsule membrane.* Cell Transplant, 1997. **6**(4): p. 387-394.
117. Strand, B.L., et al., *Microcapsules made by enzymatically tailored alginate.* Journal of Biomedical Materials Research Part A, 2003. **64A**(3): p. 540-550.
118. Strand, B.L., et al., *Poly-L-Lysine Induces Fibrosis on Alginate Microcapsules via the Induction of Cytokines.* Cell Transplantation, 2001. **10**(3): p. 263-275.

119. Rokstad, A.M., et al., *Alginate microbeads are complement compatible, in contrast to polycation containing microcapsules, as revealed in a human whole blood model.* Acta Biomaterialia, 2011. **7**(6): p. 2566-2578.
120. Otterlei, M., et al., *Induction of cytokine production from human monocytes stimulated with alginate.* J Immunother (1991), 1991. **10**(4): p. 286-91.
121. Espevik, T., et al., *The involvement of CD14 in stimulation of cytokine production by uronic acid polymers.* European Journal of Immunology, 1993. **23**(1): p. 255-261.
122. Otterlei, M., et al., *Similar mechanisms of action of defined polysaccharides and lipopolysaccharides: characterization of binding and tumor necrosis factor alpha induction.* Infect Immun, 1993. **61**(5): p. 1917-25.
123. Flo, T.H., et al., *Involvement of toll-like receptor (TLR) 2 and TLR4 in cell activation by mannuronic acid polymers.* J Biol Chem, 2002. **277**(38): p. 35489-95.
124. Espevik, T., et al., *Mechanisms of the host immune response to alginate microcapsules.* The Bioartificial Pancreas and Other Biohybrid Therapies, 2009: p. 279-290.
125. Kulseng, B., et al., *Transplantation of alginate microcapsules: generation of antibodies against alginates and encapsulated porcine islet-like cell clusters.* Transplantation, 1999. **67**(7): p. 978-84.
126. Tam, S.K., et al., *Factors influencing alginate gel biocompatibility.* Journal of Biomedical Materials Research Part A, 2011. **98A**(1): p. 40-52.
127. Safley, S.A., et al., *Microencapsulated islet allografts in diabetic NOD mice and nonhuman primates.* Eur Rev Med Pharmacol Sci, 2020. **24**(16): p. 8551-8565.
128. Ørning, P., et al., *Alginate microsphere compositions dictate different mechanisms of complement activation with consequences for cytokine release and leukocyte activation.* Journal of Controlled Release, 2016. **229**: p. 58-69.
129. Rokstad, A.M., et al., *The induction of cytokines by polycation containing microspheres by a complement dependent mechanism.* Biomaterials, 2013. **34**(3): p. 621-630.
130. King, A., S. Sandler, and A. Andersson, *The effect of host factors and capsule composition on the cellular overgrowth on implanted alginate capsules.* Journal of Biomedical Materials Research, 2001. **57**(3): p. 374-383.
131. King, A., et al., *Improvement of the biocompatibility of alginate/poly-L-lysine/alginate microcapsules by the use of epimerized alginate as a coating.* Journal of Biomedical Materials Research Part A, 2003. **64A**(3): p. 533-539.
132. Vandenbossche, G.M., et al., *Host reaction against empty alginate-polylysine microcapsules. Influence of preparation procedure.* J Pharm Pharmacol, 1993. **45**(2): p. 115-20.

133. Safley, S.A., et al., *Biocompatibility and immune acceptance of adult porcine islets transplanted intraperitoneally in diabetic NOD mice in calcium alginate poly-L-lysine microcapsules versus barium alginate microcapsules without poly-L-lysine.* J Diabetes Sci Technol, 2008. **2**(5): p. 760-7.
134. Arlov, Ø., G. Skjåk-Bræk, and A.M. Rokstad, *Sulfated alginate microspheres associate with factor H and dampen the inflammatory cytokine response.* Acta Biomaterialia, 2016. **42**: p. 180-188.
135. Gravastrand, C., et al., *Alginate microbeads are coagulation compatible, while alginate microcapsules activate coagulation secondary to complement or directly through FXII.* Acta Biomaterialia, 2017. **58**: p. 158-167.
136. Ronghua, H., D. Yumin, and Y. Jianhong, *Preparation and in vitro anticoagulant activities of alginate sulfate and its quaterized derivatives.* Carbohydrate Polymers, 2003. **52**(1): p. 19-24.
137. Arlov, Ø., et al., *Heparin-Like Properties of Sulfated Alginates with Defined Sequences and Sulfation Degrees.* Biomacromolecules, 2014. **15**(7): p. 2744-2750.
138. Freeman, I., A. Kedem, and S. Cohen, *The effect of sulfation of alginate hydrogels on the specific binding and controlled release of heparin-binding proteins.* Biomaterials, 2008. **29**(22): p. 3260-8.
139. Ma, L., et al., *Anticoagulant sodium alginate sulfates and their mussel-inspired heparin-mimetic coatings.* Journal of Materials Chemistry B, 2016. **4**(19): p. 3203-3215.
140. Arlov, Ø., et al., *Biomimetic sulphated alginate hydrogels suppress IL-1β-induced inflammatory responses in human chondrocytes.* Eur Cell Mater, 2017. **33**: p. 76-89.
141. Arlov, Ø. and G. Skjåk-Bræk, *Sulfated Alginates as Heparin Analogues: A Review of Chemical and Functional Properties.* Molecules, 2017. **22**(5): p. 778.
142. Ori, A., M.C. Wilkinson, and D.G. Fernig, *A systems biology approach for the investigation of the heparin/heparan sulfate interactome.* J Biol Chem, 2011. **286**(22): p. 19892-19904.
143. Wardrop, D. and D. Keeling, *The story of the discovery of heparin and warfarin.* British Journal of Haematology, 2008. **141**(6): p. 757-763.
144. Merry, C.L., et al., *Proteoglycans and sulfated glycosaminoglycans.* Essentials of Glycobiology [Internet]. 4th edition, 2022.
145. Arlov, Ø., et al., *Engineered Sulfated Polysaccharides for Biomedical Applications.* Advanced Functional Materials, 2021. **31**(19): p. 2010732.
146. Nazemi, Z., et al., *Effect of chemical composition and sulfated modification of alginate in the development of delivery systems based on electrostatic interactions for small molecule drugs.* Materials Letters, 2020. **263**: p. 127235.

147. Samsonchi, Z., et al., *Transplantation of Islet-Containing microcapsules modified with constitutional isomers of sulfated alginate in diabetic mice to mitigate fibrosis for Long-term glycemic control.* Chemical Engineering Journal, 2022. **432**: p. 134298.
148. Kopplin, G., et al., *Structural Characterization of Fucoidan from Laminaria hyperborea: Assessment of Coagulation and Inflammatory Properties and Their Structure-Function Relationship.* ACS Appl Bio Mater, 2018. **1**(6): p. 1880-1892.
149. Mollnes, T.E., et al., *Essential role of the C5a receptor in E coli–induced oxidative burst and phagocytosis revealed by a novel lepirudin-based human whole blood model of inflammation.* Blood, 2002. **100**(5): p. 1869-1877.
150. Rokstad, M.A., et al., *Biocompatibility and Biotolerability Assessment of Microspheres Using a Whole Blood Model.* Micro and Nanosystems, 2013. **5**(3): p. 177-185.
151. Rokstad, A.M.A., et al., *Advances in biocompatibility and physico-chemical characterization of microspheres for cell encapsulation.* Advanced Drug Delivery Reviews, 2014. **67-68**: p. 111-130.
152. King, A.J., *The use of animal models in diabetes research.* Br J Pharmacol, 2012. **166**(3): p. 877-94.
153. Lenzen, S., *The mechanisms of alloxan- and streptozotocin-induced diabetes.* Diabetologia, 2008. **51**(2): p. 216-226.
154. McGuinness, O.P., et al., *NIH experiment in centralized mouse phenotyping: the Vanderbilt experience and recommendations for evaluating glucose homeostasis in the mouse.* Am J Physiol Endocrinol Metab, 2009. **297**(4): p. E849-55.
155. Leiter, E.H., *Selecting the "right" mouse model for metabolic syndrome and type 2 diabetes research.* Methods Mol Biol, 2009. **560**: p. 1-17.
156. Benedé-Ubieto, R., et al., *Guidelines and Considerations for Metabolic Tolerance Tests in Mice.* Diabetes Metab Syndr Obes, 2020. **13**: p. 439-450.
157. Carter, J.D., et al., *A practical guide to rodent islet isolation and assessment.* Biol Proced Online, 2009. **11**: p. 3-31.
158. Slepchenko, K.G., K.L. Corbin, and C.S. Nunemaker, *Comparing methods to normalize insulin secretion shows the process may not be needed.* Journal of Endocrinology, 2019. **241**(2): p. 149-159.
159. Fenwick, N., G. Griffin, and C. Gauthier, *The welfare of animals used in science: how the "Three Rs" ethic guides improvements.* Can Vet J, 2009. **50**(5): p. 523-30.
160. Council, N.R., *Guide for the Care and Use of Laboratory Animals: Eighth Edition.* 2011, Washington, DC: The National Academies Press. 246.

161. Turner, P.V., D.S. Pang, and J.L. Lofgren, *A Review of Pain Assessment Methods in Laboratory Rodents.* Comp Med, 2019. **69**(6): p. 451-467.
162. Thu, B., et al., *Alginate polycation microcapsules: II. Some functional properties.* Biomaterials, 1996. **17**(11): p. 1069-1079.
163. Mørch, Ý.A., et al., *Binding and leakage of barium in alginate microbeads.* J Biomed Mater Res A, 2012. **100**(11): p. 2939-47.
164. King, A., A. Andersson, and S. Sandler, *Cytokine-induced functional suppression of microencapsulated rat pancreatic islets in vitro.* Transplantation, 2000. **70**(2): p. 380-3.
165. de Vos, P., et al., *Alginate-based microcapsules for immunoisolation of pancreatic islets.* Biomaterials, 2006. **27**(32): p. 5603-17.
166. Omer, A., et al., *Survival and maturation of microencapsulated porcine neonatal pancreatic cell clusters transplanted into immunocompetent diabetic mice.* Diabetes, 2003. **52**(1): p. 69-75.
167. Schmidt, J.J., J. Rowley, and H.J. Kong, *Hydrogels used for cell-based drug delivery.* J Biomed Mater Res A, 2008. **87**(4): p. 1113-22.
168. Vaithilingam, V., et al., *In Vitro and In Vivo Biocompatibility Evaluation of Polyallylamine and Macromolecular Heparin Conjugates Modified Alginate Microbeads.* Scientific Reports, 2017. **7**(1): p. 11695.
169. McNally, A.K. and J.M. Anderson, *Complement C3 participation in monocyte adhesion to different surfaces.* Proc Natl Acad Sci U S A, 1994. **91**(21): p. 10119-23.
170. Kourtzelis, I., et al., *Inhibition of biomaterial-induced complement activation attenuates the inflammatory host response to implantation.* FASEB journal : official publication of the Federation of American Societies for Experimental Biology, 2013. **27**(7): p. 2768-2776.
171. Wang, X., et al., *Application of MS-based proteomics to study serum protein adsorption/absorption and complement C3 activation on poly(ethylene glycol) hydrogels.* Journal of biomaterials science. Polymer edition, 2011. **22**(10): p. 1343-1362.
172. Tam, S.K., et al., *Biocompatibility and physicochemical characteristics of alginate–polycation microcapsules.* Acta Biomaterialia, 2011. **7**(4): p. 1683-1692.
173. Syanda, A.M., et al., *Sulfated Alginate Reduces Pericapsular Fibrotic Overgrowth on Encapsulated cGMP-Compliant hPSC-Hepatocytes in Mice.* Frontiers in Bioengineering and Biotechnology, 2022. **9**.
174. Lee, K.Y. and D.J. Mooney, *Hydrogels for tissue engineering.* Chem Rev, 2001. **101**(7): p. 1869-79.
175. Discher, D.E., D.J. Mooney, and P.W. Zandstra, *Growth factors, matrices, and forces combine and control stem cells.* Science, 2009. **324**(5935): p. 1673-7.

176. Zhuang, Z., et al., *Control of Matrix Stiffness Using Methacrylate-Gelatin Hydrogels for a Macrophage-Mediated Inflammatory Response.* ACS Biomater Sci Eng, 2020. **6**(5): p. 3091-3102.
177. Chan, G. and D.J. Mooney, *Ca2+ released from calcium alginate gels can promote inflammatory responses in vitro and in vivo.* Acta Biomaterialia, 2013. **9**(12): p. 9281-9291.
178. Melvik, J.E. and M. Dornish, *Use of alginate matrices to control cell growth*, F.B. AS, Editor. 2005, United States Patent. p. 1-12.
179. Swartzlander, M.D., et al., *Linking the foreign body response and protein adsorption to PEG-based hydrogels using proteomics.* Biomaterials, 2015. **41**: p. 26-36.
180. Yamada, Y., G. Fichman, and J.P. Schneider, *Serum Protein Adsorption Modulates the Toxicity of Highly Positively Charged Hydrogel Surfaces.* ACS Appl Mater Interfaces, 2021. **13**(7): p. 8006-8014.
181. Nilsson, B., et al., *The role of complement in biomaterial-induced inflammation.* Mol Immunol, 2007. **44**(1-3): p. 82-94.
182. Romero-Gavilan, F., et al., *Proteomic analysis of silica hybrid sol-gel coatings: a potential tool for predicting the biocompatibility of implants in vivo.* Biofouling, 2017. **33**(8): p. 676-689.
183. Ricklin, D., et al., *Complement component C3 - The "Swiss Army Knife" of innate immunity and host defense.* Immunol Rev, 2016. **274**(1): p. 33-58.
184. Rajabi, M., et al., *Potentiation of C1-esterase inhibitor by heparin and interactions with C1s protease as assessed by surface plasmon resonance.* Biochimica et Biophysica Acta (BBA) - General Subjects, 2012. **1820**(1): p. 56-63.
185. Tang, L. and J.W. Eaton, *Fibrin(ogen) mediates acute inflammatory responses to biomaterials.* J Exp Med, 1993. **178**(6): p. 2147-56.
186. Zdolsek, J., J.W. Eaton, and L. Tang, *Histamine release and fibrinogen adsorption mediate acute inflammatory responses to biomaterial implants in humans.* J Transl Med, 2007. **5**: p. 31.
187. Tang, L., et al., *Molecular determinants of acute inflammatory responses to biomaterials.* J Clin Invest, 1996. **97**(5): p. 1329-34.
188. Lin, H., et al., *Therapeutics targeting the fibrinolytic system.* Experimental & Molecular Medicine, 2020. **52**(3): p. 367-379.
189. Giannandrea, M. and W.C. Parks, *Diverse functions of matrix metalloproteinases during fibrosis.* Disease models & mechanisms, 2014. **7**(2): p. 193-203.
190. Leong, E., M. Bezuhly, and J.S. Marshall, *Distinct Metalloproteinase Expression and Functions in Systemic Sclerosis and Fibrosis: What We Know*

and the Potential for Intervention. Frontiers in Physiology, 2021. **12**(1426): p. 727451.

191. Cui, H., et al., *Monocyte-derived alveolar macrophage apolipoprotein E participates in pulmonary fibrosis resolution.* JCI Insight, 2020. **5**(5): p. e134539.
192. Wang, T., et al., *Reduced beta 2 glycoprotein I improves diabetic nephropathy via inhibiting TGF-β1-p38 MAPK pathway.* Int J Clin Exp Pathol, 2015. **8**(3): p. 2321-2333.
193. Pilling, D. and R.H. Gomer, *The Development of Serum Amyloid P as a Possible Therapeutic.* Frontiers in immunology, 2018. **9**: p. 2328-2328.
194. Graham, M.L., et al., *The streptozotocin-induced diabetic nude mouse model: differences between animals from different sources.* Comp Med, 2011. **61**(4): p. 356-60.
195. Furman, B.L., *Streptozotocin-Induced Diabetic Models in Mice and Rats.* Current Protocols, 2021. **1**(4): p. e78.
196. Legøy, T.A., et al., *Encapsulation boosts islet-cell signature in differentiating human induced pluripotent stem cells via integrin signalling.* Sci Rep, 2020. **10**(1): p. 414.
197. Formo, K., et al., *Culture of hESC-derived pancreatic progenitors in alginate-based scaffolds.* J Biomed Mater Res A, 2015. **103**(12): p. 3717-26.
198. Vegas, A.J., et al., *Long-term glycemic control using polymer-encapsulated human stem cell–derived beta cells in immune-competent mice.* Nature Medicine, 2016. **22**(3): p. 306-311.

Paper I

STEM CELLS TRANSLATIONAL MEDICINE®

PERSPECTIVES

Current and Future Perspectives on Alginate Encapsulated Pancreatic Islet

BERIT L. STRAND, ABBA E. CORON, GUDMUND SKJAK-BRAEK

NOBIPOL, Department of Biotechnology, NTNU Norwegian University of Science and Technology, Trondheim, Norway

Key Words. Diabetes • Capsules • Encapsulation • Islets • Stem Cells • Alginate

ABSTRACT

Transplantation of pancreatic islets in immune protective capsules holds the promise as a functional cure for type 1 diabetes, also about 40 years after the first proof of principal study. The concept is simple in using semipermeable capsules that allow the ingress of oxygen and nutrients, but limit the access of the immune system. Encapsulated human islets have been evaluated in four small clinical trials where the procedure has been evaluated as safe, but lacking long-term efficacy. Host reactions toward the biomaterials used in the capsules may be one parameter limiting the long-term function of the graft in humans. The present article briefly discusses important capsule properties such as stability, permeability and biocompatibility, as well as possible strategies to overcome current challenges. Also, recent progress in capsule development as well as the production of insulin-producing cells from human stem cells that gives promising perspectives for the transplantation of encapsulated insulin-producing tissue is briefly discussed. STEM CELLS TRANSLATIONAL MEDICINE *2017;6:1053–1058*

SIGNIFICANCE STATEMENT

Transplantation of pancreatic islets in immune protective capsules holds the promise as a functional cure for type 1 diabetes. The present article discusses briefly important capsules properties such as stability, permeability, and biocompatibility, and possible strategies to overcome current challenges. Recent progress in capsule development as well as the production of insulin producing cells from human stem cells gives promising perspectives for the transplantation of encapsulated insulin producing tissue.

DIABETES, ISLET TRANSPLANTATION, AND THE PRINCIPLE OF ENCAPSULATION FOR IMMUNE PROTECTION

Diabetes is one of the leading causes of both morbidity and mortality worldwide and the number of diabetics are rapidly increasing [1]. Type 1 diabetes, accounting for about 10% of the incidents of diabetes, is an autoimmune disease where the immune system attacks the body's own beta cells that produce the insulin needed to regulate the blood glucose. The disease is normally treated by daily insulin injections, however poor regulation of the blood glucose is associated with secondary complications such as cardiovascular disease, nephropathy, and neuropathy [1]. Newer ways of distributing insulin exist, including infusions and injections; where continuous glucose monitoring allows tighter control over the blood glucose. However, an appealing alternative to controlling the blood glucose is via the transplantation of insulin-producing cells. Pancreas transplantation from deceased donors is one alternative, however this requires major surgery followed by associated risks. Pancreatic islets, cell clusters containing the endocrine function of the pancreas, can be isolated from the pancreas through enzymatic digestion [2, 3]. In the future, stem cells may offer an unlimited source of insulin-producing cells. This is a field of rapid development, where exciting progress is made in the development of insulin-producing cells both in vivo and in vitro [4–6].

Today, pancreatic islets are transplanted with a limited surgical procedure via injection into the portal vein to the liver. Although being successful in reducing the need for external insulin and also in reducing the incidents of hyper- and hypo-glycemic events, the transplantation of insulin-producing cells requires the need for immune suppression to avoid graft rejection [7]. The use of immune suppression is associated with increased risk of infections and cancer. However, islet transplantation is still considered a better alternative for patients with severely unstable blood glucose and in particular those previously transplanted with, for example, a kidney. Encapsulation of the pancreatic islets offers an alternative to immune suppression where the capsules act as semipermeable membranes that hinder the immune attack of the transplanted cells (Fig. 1). Importantly, the capsules must allow for the diffusion of oxygen and nutrients to the encapsulated cells and also permit the diffusion of insulin out to the surrounding environment.

Correspondence: Berit L. Strand, Ph.D., Department of Biotechnology, NTNU, Sem Saelandsvei 6/8, N-7491 Trondheim, Norway. Telephone: +47 73594069; Fax: +47 73591283; e-mail: berit.l.strand@ntnu.no
Received March 6, 2016; accepted for publication December 1, 2016; published Online First on February 2, 2017. © AlphaMed Press 1066-5099/2016/$30.00/0 doi: 10.1002/sctm.16-0116

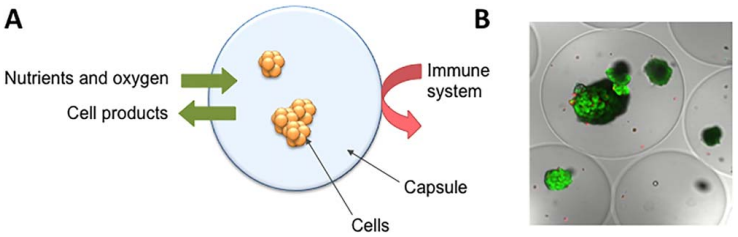

Figure 1. Immune isolation by encapsulation. Concept illustration of cells in capsule where nutrients and oxygen can diffuse into the capsule and cell products (e.g. insulin) can diffuse out, but effectors of the immune system is excluded **(A)** and picture of encapsulated human islets **(B)** stained by calcein and ethidium homodimer to visualize living and dead cells, respectively. The photomicrograph is a cross-section obtained using confocal microscopy. Bead diameter is approximately 500 μm. Picture is printed from [8].

The immune protection of pancreatic islets by using capsules was first demonstrated in rats by Lim and Sun [9]. Capsules are advantageous over larger devices in that they provide rapid diffusion of nutrients as well as oxygen. In addition, the use of capsules reduces the risk of graft failure due to the distribution of cells in numerous devices, limiting the mechanical failure to only the affected device containing a limited portion of the transplanted graft. Also, the ease of transplantation by laparoscopy is attractive [10]. The capsules are normally injected into the peritoneal cavity, where the encapsulated cells get the access to nutrients and oxygen from the surrounding fluids.

Capsules for Immune Protection

Many different variations of capsules and capsule materials have been suggested for the immune isolation of pancreatic islets as reviewed in [11]. Of polymers, agarose, chitosan, gelatin, polyethylene glycol, methacrylic acid, 2-hydroxyethyl methacrylate have been used, however the vast majority is based on alginate [11]. Alginate is a structural polysaccharide found in seaweed that is nontoxic, exhibiting a low immunogenic profile [12]. It has the unique property of forming a gel at physiological conditions with divalent ions, such as calcium. The encapsulation is performed by dripping a mixture of alginate and islets into a solution of divalent ions, where the droplet is immediately fixed at the surface. The gelation proceeds throughout the droplet, resulting in a gel bead with entrapped islets that are kept viable and functional. In the original encapsulation procedure, the gel bead was further coated with a layer of polycation [9]. Poly-L-lysine (PLL) [9, 13], poly-L-ornithine (PLO) [14] and poly-methylene co-guanidine [15] form stable complexes with alginate at the surface of the gel beads. The inner core of the gel beads can further be liquefied by using chelating compounds (e.g., citrate or EDTA), leaving the outer shell as the capsule structure. Both capsule stability and permeability can to a great extent be controlled by the polycation exposure [13, 16–18]. Alginate-PLL based capsules were the first to be tested in clinical trials of encapsulated human islets in 1994 [19] and alginate-PLO based capsules have been tested more recently [20, 21] (Table 1). However, the pro-inflammatory properties of polycations have been linked to a fibrotic response toward the capsules upon transplantation, also after the addition of a second coating layer of alginate [22]. The attachment of host cells on the surface of the capsules is believed to limit the diffusion of oxygen and nutrients to the encapsulated islets and lead to nonfunctioning grafts [23, 24]. Hence, newer capsule developments are based on using the alginate solely without the polycation layer. Progress in newer capsule designs has led to two additional encapsulated human islet transplantations to diabetic recipients (Table 1) [25, 26]. Although the studies conclude with a safe procedure, the efficacy of the transplanted graft has been limited. Hence, challenges still remain in making capsules that support graft function.

Table 1. Overview of capsules used in encapsulated human islet transplantations to diabetic recipients

Capsule composition	Number of patients	References
Alginate-poly-L-lysine-alginate	1	[19]
Alginate-poly-L-ornithine-alginate	4	[20, 21]
Barium-alginate	4	[25]
Calcium/Barium-alginate	1	[26]

Important Capsule Properties

The challenges of supporting graft function may be linked to some capsule properties that are believed to be of major importance. This includes (a) stability, as the capsules need to protect the graft over a prolonged period of time, (b) permeability to allow the diffusion of nutrients and oxygen and limit the access of the immune system and (c) biocompatibility, that in this setting is mostly connected to avoiding a fibrotic response (Fig. 2). A thorough review on capsule properties is given in [27].

Stable alginate beads without a polycation layer can be made by careful selection of alginate and gelling ion. Alginate is composed of β-D-Mannuronic acid (M) and its C5 epimer α-L-Guluronic acid (G) that is 1->4 linked via glycosidic linkages. The M and G monomers are found in M-blocks, G-blocks, and MG-blocks of various lengths. The sequential arrangement of M and G, together with the molecular weight, determines to a great extent the properties of the alginate, and consequently the properties of the gel beads [28]. Originally, alginate beads were made by gelation with calcium ions. Calcium is historically known to cross-link G-blocks in the alginate, however, recent results show that also MG-blocks participate in the cross-linking with calcium [29]. Hence, alginates with a high content of G, situated in either G-blocks or MG-blocks, form relatively stable beads with calcium. However, upon

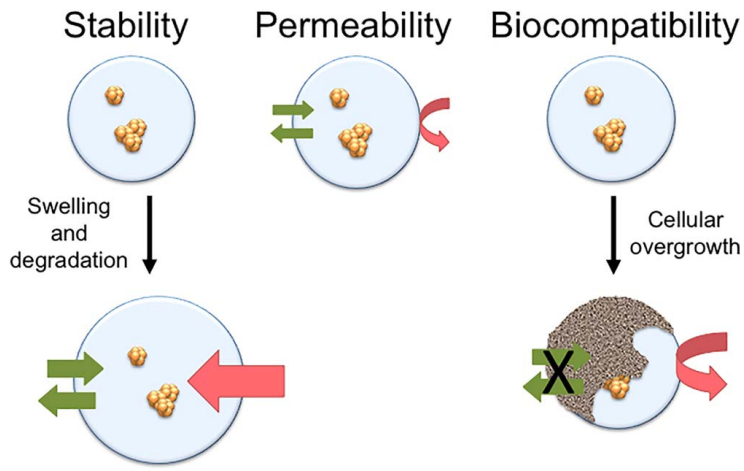

Figure 2. Important capsule properties are stability, permeability and biocompatibility. These properties are interconnected as the capsule permeability will increase with capsule destabilization through swelling and this may lead to loss of immune protection. The attachment of cells on the capsule surface leads to limited access of nutrients and oxygen for the encapsulated cells.

the removal of polycation followed a need to increase the stability of the alginate beads. Alginate beads are vulnerable toward destabilization by the depletion of calcium ions at physiological conditions due to chelating compounds such as phosphates, and also by the exchange with sodium ions. More stable calcium-alginate beads can be made by enzymatic modification of the alginate to contain solely G- and MG-blocks [30]. Though, more commonly used is the addition of barium ions to the gelling solution that also may result in more stable beads. Barium ions bind strongly to the G-blocks in the alginate and to some extent to the M-blocks [31], and incorporate shorter G-blocks in the cross-links upon gelation compared to calcium [32]. In fact, the addition of 1 mM barium ions to a solution of 50 mM calcium ions has a great impact on the stability of alginate beads made of alginate with a high content of G-blocks [31]. Such Ca/Ba-alginate beads have been shown to protect human islets in a diabetic mouse model for up to 220 days [33]. When transplanted to a diabetic patient, positive c-peptide was detected until 3 months post-transplantation [26]. Also, higher barium ion concentrations (e.g., 10 mM and 20 mM) have been used for encapsulation, without the use of calcium [24, 25, 34]. Using higher barium concentration poses the risk of leakage of potential toxic barium ions to the recipients. The accumulation of barium in blood and femur bone in mice has been linked to increased barium concentrations in implanted alginate beads [35]. Hence, care should be made for clinical transplantation regarding the selection of alginate and gelling ions, as well as washing procedures.

Polycation containing capsules were shown to limit the ingress of the antibodies as well as the larger cytokines (e.g., TNF-α) and the permeability can be tuned based on the polycation type and exposure time [17]. However, for the permeability of small cytokines, nitric oxide, and free radicals, both from the islets as well as from the host, it is challenging to limit the diffusion through the capsules by pore size as the absolute request of the capsules is to allow the diffusion of glucose and insulin, as well as some of the larger proteins, like transferrin [14]. Alginate beads, without the polycation, are more open structures that do not exclude the cytokines or complement factors. It is not known what permeability is needed for the capsules to function as an immune barrier, but it may seem like the most important function of immune isolation lies in the avoidance of cell-to-cell contact between the graft and the host, as there are now several reports of the function of both allo- and xeno grafts in alginate beads without a polycation coating in mouse models [33, 34, 36, 37]. Alginate beads of different permeability toward antibodies (e.g., IgG) can be made with the selection of alginate composition and gelling ions [30, 31], and barium gelled alginate beads are shown to protect transplanted allograft in mice despite antibody response of IgG and IgM [38].

In small animal models, for example, mice and rats, the alginate beads are in general shown to promote minimal fibrotic overgrowth. However, there may still be a problem connected to the fibrosis of alginate beads in larger animal models such as monkeys and humans. Although not promoting any detectable inflammatory responses in human blood [39, 40], the two clinical transplantations of human islets in Ba-alginate and Ca/Ba-alginate beads [25, 26] may indicate a continued problem of fibrosis, even when omitting the polycation. Fibrosis is also seen in one immune competent mouse strain (C57Bl6 mice), which is consequently used for the evaluation of capsule biocompatibility where also differences between alginate beads can be observed [41–43]. In this strain of mice, alginate beads with a high G content have been shown to promote fibrosis, whereas for alginate beads with a lower G content fibrosis was not observed, regardless of the gelling ions used [43]. However, the low stability of the beads consisting of alginate with a low G content limits the immediate use of these alginates for encapsulation. This challenge may be met by enzymatically tailored alginates that can be made very stable with a low G content [30]. Very recently, a positive effect on fibrosis has been shown by using chemically modified alginate in the

alginate beads in a mixture with nonmodified alginate [44]. Positive effects on limiting fibrosis were seen with structurally diverse chemical substituents. As the alginates were substituted on the carboxylic groups, the removal of charge upon substitution is one general effect, resulting in a lower charge density of the alginate. However, the differences in responses for the varying substituents clearly show that the type of molecule matters for the response. Very recent results also show a dependency of size, as larger alginate beads of about 1.5 mm in diameter had a significantly lower fibrotic response than the conventional size of about 0.5 mm in diameter [24]. Less fibrosis on larger capsules was shown both in C57Bl6 mice and in monkeys. Although no negative effect on islet function was reported as a result of increasing capsule size, questions remain regarding a possible limited oxygen supply for the encapsulated islets in general as well as with increasing capsule size.

The Inner Life of the Capsule—Oxygen Supply and Microenvironment

Although no difference has been detected on the transcriptome of microencapsulated islets versus nonencapsulated islets [45], concerns have been raised regarding the islets' access to oxygen and nutrients. The oxygen concentration in alginate microcapsules has been estimated to be constant up to about 200 μm into the capsule [46]. Hence, the ideal capsule size for maximum oxygen access would be less than 400 μm. The spherical shape and large surface to volume ratio, makes microcapsules attractive for the access of oxygen and nutrients compared to larger devices and devices of other geometries. Islets in their natural habitat are highly vascularized. Hence, lack of vascularization and potential hypoxia is also an issue without capsules, however with capsules the potential ingrowth of blood vessels into the islets is physically hindered by the capsule. For short-term (acute) hypoxia in vitro, no difference on viability or function was seen for encapsulated versus nonencapsulated human islets [47]. However, culture of encapsulated islets under low oxygen conditions shows loss of viable tissue and necrotic cores [48]. To counteract the lowering of oxygen tension, perfluorocarbon emulsion [48]and CaO_2 [49] have been suggested as coencapsulated sources of oxygen. Although the need for increased oxygen supply is debated for microencapsulated pancreatic islets, indeed, positive effects have been seen on islet viability in a clinical transplantation of a macrodevice, where oxygen was infused to the encapsulated islets on a daily basis [50]. Also, pretreatment of the transplantation site to induce vascularization has been shown to increase the function of the graft without capsules [51], and strategies for increased vascularization to the graft are being pursued [52, 53].

A bottleneck in islet transplantation has been the access to enough insulin-producing tissue, where also porcine islets have been suggested as a potential source [54]. Recent break-through in stem cell differentiation toward insulin-producing cells as well as induced pluripotent stem cells (iPSC), gives promising perspectives of obtaining cells from human sources. Functional beta cells have been produced in vitro from human embryonic stem cells (hESC) [5, 6], and very recently from iPSCs from diabetic patients [55]. With cells form human sources, and potentially from the patients' own cells, it is assumed that the host immune response toward the graft will be largely eliminated. However, as type 1 diabetes is an ongoing autoimmune disease, capsules may still be needed to avoid the destruction of the new beta cells from the immune system. For the encapsulation of stem cell derived tissue, there is no obvious reason to change the design criteria of the capsules, except for a possible change in criteria for capsule permeability. ViaCyte is currently in Phase 1/2 clinical trial to test the safety and efficacy of their macroencapsulated pancreatic progenitors derived from hESCs. The ViaCyte team has shown the development of pancreatic islet like tissue in their macrodevice in mice [4], where micro vessels were formed around and partly into the device. This is one of the first embryonic stem cell derived therapies to be tested in the clinic. For the recently shown full differentiation in vitro [5, 6], the differentiation protocols are complex with respect to culture conditions as clusters and suspensions and varying glucose and oxygen levels have been used in addition to various growth factors [5, 6]. A positive effect of encapsulation has been shown for the development of neonatal porcine islets into mature islets upon culture in serum-containing media [56]. This may be partly due to the hindering of aggregation of clusters upon culture, as has also been shown for human pancreatic progenitors when cultured in alginate beads [57]. hESC have been differentiated to definitive endoderm in alginate capsules [58]. For pancreatic progenitors, no effect on differentiation was seen when extracellular matrix (ECM) components (proteins and peptides) were added to the capsule composition [57]. Although no effect was seen in the previous study, the design of the capsule microenvironment to mimic the natural microenvironment has drawn recent attention [59]and positive effects have been shown on beta cell lines [60] as well as on human islets [61]. The use of heparan sulfate in the differentiation protocol of pancreatic islets [5]is interesting in this perspective as this is a natural component of the ECM. Sulfated alginate mimics the structure of heparan sulfate and the function related to the binding of growth factors [62, 63] may be an interesting alternative to chemical modification of alginate capsules, both related to the microenvironment for the encapsulated cells as well as for the reduction of fibrosis [64].

Conclusion

In conclusion, transplantation of human islets in alginate-based capsules have been clinically evaluated in four small trials and are in general recognized as safe. However, limited graft function has been connected to the observed fibrosis on the capsules limiting the access of oxygen and nutrients to the encapsulated islets. Although the problem of fibrosis has been reduced as a function of avoiding the polycation in the capsules, fibrosis seems to still be a problem. The mechanisms of fibrosis on alginate beads are still not elucidated. However, very recent positive findings regarding increased size of capsules and chemical modifications of the alginate where reduced fibrosis is seen also in monkeys, make an optimistic view of the future of encapsulated islet transplantation. Importantly, the very recent developments of insulin-producing cells from stem cells, gives the transplantation of encapsulated insulin-producing tissue a very promising outlook both long-term and in the near future. As type 1 diabetes is an autoimmune disease, the capsules may still be needed regardless of cell source for a protection of the graft from the destruction from the recipient's own immune system.

Acknowledgment

We acknowledg e financial support from the MARPOL project 221576, the Norwegian Research Council and NTNU, EC-FP7 project BetaCellTherapy and The Chicago Diabetes Project.

Author Contributions

B.L.S. and G.S.-B.: conception and design, financial support, manuscript writing, final approval of manuscript; A.E.C: manuscript writing, final approval of manuscript.

Disclosure of Potential Conflicts of Interest

The authors indicate no potential conflicts of interest.

References

1 IDF diabetes atlas - Seventh Edition. International Diabetes Federation, 2015. Brussels, Belgium (Retrieved from: http://www.diabetesatlas.org/)

2 Lacy PE, Kostianovsky M. Method for the isolation of intact islets of Langerhans from the rat pancreas. Diabetes 1967;16:35–39.

3 Shapiro AM, Lakey JR, Ryan EA et al. Islet transplantation in seven patients with type 1 diabetes mellitus using a glucocorticoid-free immunosuppressive regimen. N Engl J Med 2000;343:230–238.

4 D'Amour KA, Bang AG, Eliazer S et al. Production of pancreatic hormone-expressing endocrine cells from human embryonic stem cells. Nat Biotechnol 2006;24:1392–1401.

5 Pagliuca FW, Millman JR, Gurtler M et al. Generation of functional human pancreatic beta cells in vitro. Cell 2014;159:428–439.

6 Rezania A, Bruin JE, Arora P et al. Reversal of diabetes with insulin-producing cells derived in vitro from human pluripotent stem cells. Nat Biotechnol 2014;32:1121–1133.

7 Barton FB, Rickels MR, Alejandro R et al. Improvement in outcomes of clinical islet transplantation: 1999-2010. Diabetes Care 2012;35:1436–1445.

8 Andersen T, Strand BL, Formo K et al. Alginate as biomaterials in tissue engineering. In: Pilar Rauter A, Lindhorst TK, eds. Carbohydrate Chemistry: Chemical and Biological Approaches – Glycosciences for human health and disease. RSC Publishing, 2012:227–258.

9 Lim F, Sun AM. Microencapsulated islets as bioartificial endocrine pancreas. Science 1980;210:908–910.

10 Qi M, Lacik I, Kollarikova G et al. A recommended laparoscopic procedure for implantation of microcapsules in the peritoneal cavity of non-human primates. J Surg Res 2011;168:e117–123.

11 de Vos P, Lazarjani HA, Poncelet D et al. Polymers in cell encapsulation from an enveloped cell perspective. Adv Drug Deliv Rev 2014;67–68:15–34.

12 Smidsrod O, Skjak-Braek G. Alginate as immobilization matrix for cells. Trends Biotechnol 1990;8:71–78.

13 Thu B, Bruheim P, Espevik T et al. Alginate polycation microcapsules. I. Interaction between alginate and polycation. Biomaterials 1996;17:1031–1040.

14 Calafiore R, Basta G, Sarchielli P et al. A rapid qualitative method to assess in vitro immunobarrier competence of pancreatic islets containing alginate/polyaminoacidic microcapsules. Acta Diabetol 1996;33:150–153.

15 Wang T, Lacik I, Brissova M et al. An encapsulation system for the immunoisolation of pancreatic islets. Nat Biotechnol 1997;15:358–362.

16 Thu B, Bruheim P, Espevik T et al. Alginate polycation microcapsules. II. Some functional properties. Biomaterials 1996;17:1069–1079.

17 Kulseng B, Thu B, Espevik T et al. Alginate polylysine microcapsules as immune barrier: Permeability of cytokines and immunoglobulins over the capsule membrane. Cell Transplant 1997;6:387–394.

18 Thanos CG, Calafiore R, Basta G et al. Formulating the alginate-polyornithine biocapsule for prolonged stability: Evaluation of composition and manufacturing technique. J Biomed Mater Res Part A 2007;83A:216–224.

19 Soon-Shiong P, Heintz RE, Merideth N et al. Insulin independence in a type 1 diabetic patient after encapsulated islet transplantation. Lancet 1994;343:950–951.

20 Basta G, Montanucci P, Luca G et al. Long-term metabolic and immunological follow-up of nonimmunosuppressed patients with type 1 diabetes treated with microencapsulated islet allografts: Four cases. Diabetes Care 2011;34:2406–2409.

21 Calafiore R, Basta G, Luca G et al. Microencapsulated pancreatic islet allografts into nonimmunosuppressed patients with type 1 diabetes: First two cases. Diabetes Care 2006;29:137–138.

22 Strand BL, Ryan TL, In't Veld P et al. Poly-L-lysine induces fibrosis on alginate microcapsules via the induction of cytokines. Cell Transplant 2001;10:263–275.

23 Kobayashi T, Harb G, Rayat GR. Prolonged survival of microencapsulated neonatal porcine islets in mice treated with a combination of anti-CD154 and anti-LFA-1 monoclonal antibodies. Transplantation 2005;80:821–827.

24 Veiseh O, Doloff JC, Ma M et al. Size- and shape-dependent foreign body immune response to materials implanted in rodents and non-human primates. Nat Mater 2015;14:643–651.

25 Tuch BE, Keogh GW, Williams LJ et al. Safety and viability of microencapsulated human islets transplanted into diabetic humans. Diabetes Care 2009;32:1887–1889.

26 Jacobs-Tulleneers-Thevissen D, Chintinne M, Ling Z et al. Sustained function of alginate-encapsulated human islet cell implants in the peritoneal cavity of mice leading to a pilot study in a type 1 diabetic patient. Diabetologia 2013;56:1605–1614.

27 Rokstad AM, Lacik I, de Vos P et al. Advances in biocompatibility and physicochemical characterization of microspheres for cell encapsulation. Adv Drug Deliv Rev 2014;67–68C:111–130.

28 Martinsen A, Skjak-Braek G, Smidrsod O. Alginate as immobilization material: I. Correlation between chemical and physical properties of alginate gel beads. Biotechnol Bioeng 1989;33:79–89.

29 Donati I, Holtan S, Morch YA et al. New hypothesis on the role of alternating sequences in calcium-alginate gels. Biomacromolecules 2005;6:1031–1040.

30 Morch YA, Donati I, Strand BL et al. Molecular engineering as an approach to design new functional properties of alginate. Biomacromolecules 2007;8:2809–2814.

31 Morch YA, Donati I, Strand BL et al. Effect of Ca2+, Ba2+, and Sr2+ on alginate microbeads. Biomacromolecules 2006;7:1471–1480.

32 Stokke BT, Smidrsod O, Zanetti F et al. Distribution of uronate residues in alginate chains in relation to alginate gelling properties-2: Enrichment of beta-D-mannuronic acid and depletion of alfa-L-guluronic acid in sol fraction. Carbohydr Polym 1993; 21:39–46.

33 Qi M, Morch Y, Lacik I et al. Survival of human islets in microbeads containing high guluronic acid alginate crosslinked with Ca(2+) and Ba(2+). Xenotransplantation 2012;19:355–364.

34 Duvivier-Kali VF, Omer A, Parent RJ et al. Complete protection of islets against allorejection and autoimmunity by a simple barium-alginate membrane. Diabetes 2001;50:1698–1705.

35 Morch YA, Qi M, Gundersen PO et al. Binding and leakage of barium in alginate microbeads. J Biomed Mater Res A 2012;100:2939–2947.

36 Duvivier-Kali VF, Omer A, Lopez-Avalos MD et al. Survival of microencapsulated adult pig islets transplanted into diabetic B6AF1 mice in spite of antibody production. Diabetes 2002;51:1991–2000.

37 Lanza RP, Kuhtreiber WM, Ecker D et al. Xenotransplantation of porcine and bovine islets without immunosuppression using uncoated alginate microspheres. Transplantation 1995;59:1377–1384.

38 Duvivier-Kali VF, Omer A, Lopez-Avalos MD et al. Survival of microencapsulated adult pig islets in mice in spite of an antibody response. Am J Transplant 2004;4:1991–2000.

39 Rokstad AM, Brekke OL, Steinkjer B et al. Alginate microbeads are complement compatible, in contrast to polycation containing microcapsules, as revealed in a human whole blood model. Acta Biomater 2011;7:2566–2578.

40 Rokstad AM, Brekke OL, Steinkjer B et al. The induction of cytokines by polycation containing microspheres by a complement dependent mechanism. Biomaterials 2013;34: 621–630.

41 King A, Sandler S, Andersson A. The effect of host factors and capsule composition on the cellular overgrowth on implanted alginate capsules. J Biomed Mater Res 2001;57: 374–383.

42 Tam SK, Bilodeau S, Dusseault J et al. Biocompatibility and physicochemical characteristics of alginate-polycation microcapsules. Acta Biomater 2011;7:1683–1692.

43 Tam SK, Dusseault J, Bilodeau S et al. Factors influencing alginate gel biocompatibility. J Biomed Mater Res Part A 2011;98A:40–52.

44 Vegas AJ, Veiseh O, Doloff JC, Ma M, Tam HH, Bratlie KA-Ohoo, et al. Combinatorial hydrogel library enables identification of materials that mitigate the foreign body response in primates. Nat Biotech 2016;34: 345–352.

45 Vaithilingam V, Quayum N, Joglekar MV et al. Effect of alginate encapsulation on the cellular transcriptome of human islets. Biomaterials 2011;32:8416–8425.

46 Johnson AS, Fisher RJ, Weir GC et al. Oxygen consumption and diffusion in assemblages of respiring spheres: Performance enhancement of a bioartificial pancreas. Chem Eng Sci 2009;64:4470–4487.

47 Hals IK, Rokstad AM, Strand BL et al. Alginate microencapsulation of human islets does not increase susceptibility to acute hypoxia. J Diabetes Res 2013;2013:9.

48 Johnson AS, O'Sullivan E, D'Aoust LN et al. Quantitative assessment of islets of Langerhans encapsulated in alginate. Tissue Eng Part C 2011;17:435–449.

49 Coronel MM, Stabler CL. Engineering a local microenvironment for pancreatic islet replacement. Curr Opin Biotechnol 2013;24: 900–908.

50 Ludwig B, Rotem A, Schmid J et al. Improvement of islet function in a bioartificial pancreas by enhanced oxygen supply and growth hormone releasing hormone agonist. PNAS 2012;109:5022–5027.

51 Pepper AR, Gala-Lopez B, Pawlick R et al. A prevascularized subcutaneous device-less site for islet and cellular transplantation. Nat Biotechnol 2015;33:518–523.

52 Phelps EA, Headen DM, Taylor WR et al. Vasculogenic bio-synthetic hydrogel for enhancement of pancreatic islet engraftment and function in type 1 diabetes. Biomaterials 2013;34:4602–4611.

53 Gupta R, Sefton MV. Application of an endothelialized modular construct for islet transplantation in syngeneic and allogeneic immunosuppressed rat models. Tissue Eng Part A 2011;17:2005–2015.

54 Korbutt GS, Elliott JF, Ao Z et al. Large scale isolation, growth, and function of porcine neonatal islet cells. J Clin Invest 1996;97: 2119–2129.

55 Millman JR, Xie C, Van Dervort A et al. Generation of stem cell-derived beta-cells from patients with type 1 diabetes. Nat Commun 2016;7:8.

56 Binette TM, Dufour JM, Korbutt GS. In vitro maturation of neonatal porcine islets: A novel model for the study of islet development and xenotransplantation. Ann N Y Acad Sci 2001;944:47–61.

57 Formo K, Cho CH-H, Vallier L et al. Culture of hESC-derived pancreatic progenitors in alginate-based scaffolds. J Biomed Mater Res Part A 2015;103:3717–3726.

58 Chayosumrit M, Tuch B, Sidhu K. Alginate microcapsule for propagation and directed differentiation of hESCs to definitive endoderm. Biomaterials 2010;31:505–514.

59 Stendahl JC, Kaufman DB, Stupp SI. Extracellular matrix in pancreatic islets: relevance to scaffold design and transplantation. Cell Transplant 2009;18:1–12.

60 Weber LM, Hayda KN, Anseth KS. Cell-matrix interactions improve beta-cell survival and insulin secretion in three-dimensional culture. Tissue Eng Part A 2008;14:1959–1968.

61 Daoud J, Petropavlovskaia M, Rosenberg L et al. The effect of extracellular matrix components on the preservation of human islet function in vitro. Biomaterials 2010;31:1676–1682.

62 Arlov O, Aachmann FL, Feyzi E et al. The impact of chain length and flexibility in the interaction between sulfated alginates and HGF and FGF-2. Biomacromolecules 2015; 16:3417–3424.

63 Arlov O, Aachmann FL, Sundan A et al. Heparin-like properties of sulfated alginates with defined sequences and sulfation degrees. Biomacromolecules 2014;15:2744–2750.

64 Chen X, Shao W, Chen JB et al. Allotransplantation of sulphate glucomannan-alginate barium (SGA)-microencapsulated rat islets for the treatment of diabetes mellitus. Immunol Invest 2009;38:561–571.

Paper II

Acta Biomaterialia 137 (2022) 172–185

Contents lists available at ScienceDirect

Acta Biomaterialia

journal homepage: www.elsevier.com/locate/actbio

Full length article

Pericapsular fibrotic overgrowth mitigated in immunocompetent mice through microbead formulations based on sulfated or intermediate G alginates

Abba E. Coron[a,b,1], Joachim S. Kjesbu[a,1], Fredrikke Kjærnsmo[a,b], José Oberholzer[c], Anne Mari A. Rokstad[b,d,2], Berit L. Strand[a,2,*]

[a] NOBIPOL, Department of Biotechnology and Food Science, Norwegian University of Science and Technology, N-7491 Trondheim, Norway.
[b] Centre of Molecular Inflammation Research, Department of Clinical and Molecular Research, Norwegian University of Science and Technology, Trondheim, Norway.
[c] Charles O. Strickler Transplant Center. Division of Transplantation, Department of Surgery, University of Virginia, VA 22903, USA.
[d] Centre for Obesity, Clinic of Surgery, St. Olav's University Hospital, NO-7006 Trondheim, Norway.

ARTICLE INFO

Article history:
Received 3 June 2021
Revised 1 October 2021
Accepted 4 October 2021
Available online 8 October 2021

Keywords:
Alginate
Microbeads
Fibrosis
Biocompatibility
Fibrinogen

ABSTRACT

Cell encapsulation in alginate microbeads is a promising approach to provide immune isolation in cell therapy without immunosuppression. However, the efficacy is hampered by pericapsular fibrotic overgrowth (PFO), causing encapsulated cells to lose function. Stability of the microbeads is important to maintain immune isolation in the long-term. Here, we report alginate microbeads with minimal PFO in immunocompetent C57BL/6JRj mice. Microbead formulations included either alginate with an intermediate (47 %) guluronate (G) content (IntG) or sulfated alginate (SA), gelled in Ca^{2+}/Ba^{2+} or Sr^{2+}. A screening panel of eleven microbead formulations were evaluated for PFO, yielding multiple promising microbeads. Two candidate formulations were evaluated for 112 days *in vivo*, exhibiting maintained stability and minimal PFO. Microbeads investigated in a human whole blood assay revealed low cytokine and complement responses, while SA microbeads activated coagulation. Protein deposition on microbeads explanted from mice investigated by confocal laser scanning microscopy (CLSM) showed minimal deposition of complement C3. Fibrinogen was positively associated with PFO, with a high deposition on microbeads of high G (68 %) alginate compared to IntG and SA microbeads. Overall, stable microbeads containing IntG or SA may serve in long-term therapeutic applications of cell encapsulation.

Statement of significance

Alginate-based hydrogels in the format of micrometer size beads is a promising approach for the immunoisolation of cells in cell therapy. Clinical trials in type 1 diabetes have so far had limited success due to fibrotic responses that hinder the diffusion of nutrients and oxygen to the encapsulated cells, resulting in graft failure. In this study, minimal fibrotic response towards micrometer size alginate beads was achieved by chemical modification of alginate with sulfate groups. Also, the use of alginate with intermediate guluronic acid content resulted in minimally fibrotic microbeads. Fibrinogen deposition was revealed to be a good indicator of fibrosis. This study points to both new microsphere developments and novel insight in the mechanisms behind the fibrotic responses.

1. Introduction

Cell therapy may provide a functional cure for conditions such as type 1 diabetes or acute liver failure. Encapsulation is a strategy to circumvent or mitigate the need for immunosuppressive treatment by isolating the graft from the host immune system. In order to provide long-term efficacy and mitigate the loss of function of grafted cells, the microspheres are required to be stable in the *in*

* Corresponding author.
E-mail address: berit.l.strand@ntnu.no (B.L. Strand).
[1] Abba E. Coron and Joachim S. Kjesbu contributed equally as co-first authors.
[2] Anne Mari A. Rokstad and Berit L. Strand contributed equally as co-last authors.

https://doi.org/10.1016/j.actbio.2021.10.004
1742-7061/

vivo conditions and to be tolerated by the host immune system with respect to pericapsular fibrotic overgrowth (PFO) [1,2].

Alginate is the most commonly used material for cell encapsulation. It is a kelp-derived linear polysaccharide, which consists of (1,4)-linked β-D-mannuronic (M) acid and α-L-guluronic acid (G) residues, found in blocks of various lengths and amounts as G-, M- and MG-blocks. Alginates form ionically crosslinked hydrogels under physiological conditions and are generally well tolerated without provoking harmful reactions in the host. Transplantation of alginate microencapsulated cells is considered safe, but the functional performance has been hampered by PFO [3,4], causing loss of function in encapsulated cells by depriving them of nutrients and oxygen. In brief, the establishment of PFO follows the same sequence as in wound healing processes, beginning with protein adherence to the biomaterial surface followed by population of immune cells (neutrophiles, monocytes/macrophages and lymphocytes) [2,5,6]. At later stages fibroblasts are recruited, and the result of the process is a fibrous cap enclosing the microspheres. Accordingly, mitigating PFO is key to the use of microspheres in cell therapy. Advances to mitigate PFO has included size increase of microspheres [7] and chemical modifications of alginate [8–10]. While these findings hold promise for the future of alginate as a cell-encapsulation material, there is a need to explore several strategies to expand our understanding, and in the end create robust and persistently PFO-free materials.

The association between PFO and alginate microsphere composition have been thoroughly described in animal models [9,11–13]. Microsphere composition affects the inflammatory potential as demonstrated through a human whole blood model [14–16], where complement reactivity has been linked to PFO [17]. Microspheres with a polycation layer, e.g., poly-L-lysine, are known as microcapsules and have been shown to induce PFO in mice [13]. Furthermore, poly-L-lysine microcapsules (AP) are complement reactive and produce a cytokine response in human blood [16,18]. In contrast, alginate microspheres without a polycation layer, known as alginate microbeads, are less complement reactive with lower inflammatory cytokine responses [16,18]. Alginates with a high content of G, crosslinked with Ca^{2+} and small amounts of Ba^{2+}, form stable microbeads [19–21]. However, these microbeads induce PFO in C57BL/6J mice, non-human primates, and humans [4,9]. Using alginate with a lower content of G reduces PFO significantly [11], but also the microbead stability [11,19]. Thus, one challenge is to maintain stability while reducing PFO. Here we explore the potential of alginate materials, both unmodified or modified by sulfation. The use of sulfated alginate in alginate microbeads has previously shown reduced inflammatory potential, when compared to unmodified alginate in a human whole blood model [22]. The current study examines different approaches to meet both stability and immune tolerability requirements needed for a functional device. As smaller alginate microbeads have been shown to be more prone to fibrosis [7], we chose beads in a size range of approximately 400-500 µm as a strategy to challenge our materials. For microbead stability, crosslinking was performed either with Ca^{2+}/Ba^{2+} or Sr^{2+}. Additionally, alginates with a high G content were mixed into intermediate G formulations to explore if we could increase stability while preserving a low-fibrotic material. The PFO response and protein adsorption on retrieved materials from a C57BL/6JRj mouse model, stability *in vitro* and *in vivo*, and the inflammatory outcome in a human whole blood model was further examined. The current work is the first to document the use of sulfated alginate in microbeads aimed at cell encapsulation with a minimal fibrotic response *in vivo*. Our study also shows that sufficiently stable microbeads can be produced from alginate with an intermediate G content, contrary to what has been shown previously [11]; crosslinking with calcium and a low concentration of barium as opposed to higher barium concentrations [23] reduces exposure to toxic barium ions [21]. Furthermore, our low-fibrotic microbeads elicited low inflammatory responses in human whole blood. Additionally, we document a possible link between the deposition of fibrinogen *in vivo* and PFO on alginate microbeads that is dependent on the composition of the microbeads. In conclusion, alginate microbeads based on formulations with sulfated or intermediate G alginate are promising for use in long-term cell encapsulation for therapeutic purposes.

2. Materials and methods

2.1. Chemicals and reagents

2.1.1. Alginates

Ultra-pure (UP) alginates were acquired from Novamatrix (Sandvika, Norway), including low viscosity high G (LVG), medium viscosity high G (MVG), low viscosity high M (LVM) and very low viscosity high G (VLVG) alginates. Low molecular weight high G alginate (GLVSU) was obtained from Protan (Drammen, Norway). Chemical compositions determined by ^{1}H-NMR [24,25] and weight average molecular weights (Mw) measured by SEC MALLS [26] of the alginates are included in Table 1. Chemical modification of UP-MVG-alginate by sulfation was performed as previously described [27], using 2.91 % (v/v) chlorosulfonic acid (99 %, Sigma-Aldrich, St. Louis, MO, USA) in formamide (Merck, Whitehouse Station, NJ, USA) for 2.5 h at 60°C, resulting in the substitution of hydroxyl- by sulfate groups. The degree of substitution for sulfated alginates was estimated to 0.76 and 0.83 [27] with Mw 149 and 162 kDa [28], respectively. Sulfated alginate was purified using a Millistak+® CR40 activated carbon filter provided by Millipore (Billerica, MA, USA).

2.2. Preparation of alginate microspheres

All solutions for animal experiments and the human whole blood assay were made with sterile endotoxin and pyrogen free water provided by Fresenius Kabi AG (Bad Homburg, Germany). Alginates were dissolved in 0.3 M mannitol (VWR International BVBA, Leuven, Belgium) to concentrations of 0.7 %, 1.8 % or 2.8 % (w/v). Microspheres of approximately 350-550 µm were produced using an in-house built electrostatic droplet generator operated at 6-8 kV. Alginate solutions were supplied to the droplet generator using a 10 mL syringe fitted in a syringe pump (Cole-Parmer Instrument Company LLC., Vernon Hills, IL, USA), with flow rates between 5-10 mL/h. The alginate solutions were extruded through a 0.35 mm nozzle. Alginate droplets were collected in a bath containing gelling solution either with 50 mM $CaCl_2$ (Sigma-Aldrich, St. Louis, MO, USA) with 1 mM $BaCl_2$ (Merck KGaA, Darmstadt, Germany) or 20 mM $SrCl_2$ (Merck KGaA, Darmstadt, Germany). To produce AP microcapsules, alginate microbeads were gelled in 50 mM $CaCl_2$ prior to incubation (10 min) in 0.1 % poly-L-lysine (Mw = 15-30 kDa, Sigma-Aldrich, St. Louis, MO, USA) dissolved in 0.9 % NaCl (VWR International BVBA, Leuven, Belgium). All gelling solutions contained 150 mM mannitol and 10 mM HEPES (PanReac AppliChem GmbH, Darmstadt, Germany) and were adjusted to pH 7.3-7.4. Alginate microspheres were gelled for 5 min, timed after production ceased. For microspheres to be implanted in mice and analyzed in the human whole blood assay, each batch of microspheres was rinsed twice in 40 mL washing solution (WS) containing 0.9 % NaCl, 2 mM $CaCl_2$ and 10 mM HEPES at pH 7.3-7.4. AP microcapsules were washed exclusively in 0.9 % NaCl after gelation. Microspheres were aliquoted into samples of approximately 0.5 mL microspheres and 0.5 mL WS and were stored at 4 °C. For animal experiments, each aliquot of microspheres was washed twice with 1.0 mL and left in 0.5 mL WS. Diameters (n = 30) of microspheres were determined pre-implantation, and post-explantation, from all mice, by microscopy: Nikon Eclipse TS100 with objective CFI Plan

Table 1
Chemical compositions given as fractions of G (F_G) and M (F_M), duplets (F_{GG}, F_{MM}, $F_{MG/GM}$) and triplets ($F_{GGM/MGG}$, F_{MGM}, F_{GGG}), and estimates of G-block length ($N_{G>1}$) and weight average molecular weights (Mw) of alginates.

Alginate	F_G	F_M	F_{GG}	F_{MM}	$F_{MG/GM}$	$F_{GGM/MGG}$	F_{MGM}	F_{GGG}	$N_{G>1}$	Mw (kDa)
UP-LVG	0.68	0.32	0.57	0.21	0.11	0.04	0.07	0.53	16	237
UP-MVG	0.66	0.34	0.55	0.22	0.12	0.05	0.09	0.50	13	235
UP-LVM	0.47	0.53	0.29	0.34	0.06	0.06	0.14	0.23	5	235
GLVSU	0.67	0.33	0.55	0.22	0.11	0.04	0.08	0.51	15	67
UP-VLVG	0.69	0.31	0.57	0.19	0.12	0.05	0.08	0.51	11	32

Table 2
Microsphere compositions and alginate concentrations, including measured endotoxin levels for alginate solutions. A selection of microbeads was produced as mixtures of different alginates to a total concentration of 1.8 % (w/v). Concentration of ions for crosslinking: Ca^{2+}/Ba^{2+} (50 mM, 1 mM), Sr^{2+} (20 mM), and Ca^{2+} (50 mM).*Positive control for PFO.**Selected candidate microbeads for further PFO studies, including long-term.***Positive control for protein deposition (C3c), as well as TCC and cytokine induction (whole blood assay).

Microsphere	Material(s)	Concentration(s) % (w/v)	Ions	EU/g alginate
HiG*	UP-LVG	1.80	Ca^{2+}/Ba^{2+}	6.6-14.2
IntG**	UP-LVM	1.80	Ca^{2+}/Ba^{2+}	4.3-13.6
HiG+SA (80/20)**	UP-LVG / UP-MVG-sulfated	1.44 / 0.36	Ca^{2+}/Ba^{2+}	15.4-26.9
IntG-Sr	UP-LVM	1.80	Sr^{2+}	13.6
IntG (2.8%)	UP-LVM	2.80	Ca^{2+}/Ba^{2+}	25.5
IntG+HiG	UP-LVM / UP-LVG	1.15 / 0.65	Ca^{2+}/Ba^{2+}	3.4
IntG+L-HiG	UP-LVM / GLVSU	1.15 / 0.65	Ca^{2+}/Ba^{2+}	165.1
IntG+VL-HiG	UP-LVM / UP-VLVG	1.15 / 0.65	Ca^{2+}/Ba^{2+}	NA
HiG+SA (60/40)	UP-LVG / UP-MVG-sulfated	1.08 / 0.72	Ca^{2+}/Ba^{2+}	17.2
HiG+SA (60/40)-Sr	UP-LVG / UP-MVG-sulfated	1.08 / 0.72	Sr^{2+}	17.2
HiG (0.7%)	UP-LVG	0.70	Ca^{2+}/Ba^{2+}	8.6
AP***	UP-LVG / Poly-L-lysine	1.80 / 0.1	Ca^{2+}	6.6-14.2 / NA

Fluor 4×/0.13 Phl DL (Nikon, Tokyo, Japan, software NIS Elements v. 4.51, build 1145) and Zeiss LSM 800 with objective EC Plan-Neofluar 2.5×/0.085 M27 (Carl Zeiss MicroImaging GmbH, Göttingen, Germany, software ImageJ v. 2.1.0/1.53c, National Institutes of Health, New York, USA). For the whole blood assay, each aliquot of microspheres (0.5 mL) was washed twice in 1.0 mL 0.9 % NaCl, thereafter added NaCl to a total volume of 10.2 mL and aliquoted as 0.5 mL samples containing each 0.05 mL microspheres. Immediately thereafter, 0.4 mL of the saline solution was retracted resulting in a total volume of 0.1 mL for each sample. Endotoxin concentrations of alginate solutions used to produce microspheres were measured using Limulus Amebocyte Lysate (LAL) QCL-1000 (Lonza Group AG, Basel, Switzerland, 50 647U, lot no: 0000561043) and Pierce™ chromogenic endotoxin quant kit (Thermo Scientific, Meridian R.D, Rockford, USA, A39552, lot no: 0H60kO4800). Types and concentrations of alginate, and endotoxin levels in the alginate solutions made to produce microspheres are given in Table 2.

2.3. Physicochemical properties of alginate hydrogels

2.3.1. In vitro stability assay of microbeads

Size stability of alginate microbeads was assessed in a saline treatment assay [29]. After removal of gelling solution, 0.5 mL of microbeads were exposed to six consecutive treatments (1 h) in 3.0 mL 0.9 % (w/v) NaCl solution, with three parallels. Microsphere diameters (n = 30) were determined by microscopy (Nikon Eclipse TS100).

2.3.2. Gel strength of alginate gel cylinders and compression of alginate microbeads

Alginate gel cylinders were prepared using an internal gelation protocol [30]. Alginate gel cylinders were prepared with alginate concentrations of 0.7 % (w/v) for HiG (0.7 %) and 1.8 % (w/v) for all other alginate gel cylinders. 15 mM $CaCO_3$ (Specialty Minerals Inc., Adams, MA, USA) and 30 mM glucono-δ-lactone (GDL, Sigma-Aldrich, St. Louis, MO, USA) was used for internal gelation for 20 h. Gel cylinders were saturated in 50 mM $CaCl_2$ with 1 mM $BaCl_2$, 150 mM mannitol and 10 mM HEPES (pH 7.3-7.4) for 24 h.

Alginate gel cylinders were uniaxially compressed on a Stable Micro Systems TA.XTplusC texture analyzer (Godalming, Surrey, UK) with Exponent Connect software v. 7.0.3.0 (Hamilton, MA, USA), using a P/35 cylindrical probe and a 500 g load cell. Force-deformation curves were recorded using a trigger force of 0.1 g, at a compression speed of 0.1 mm/s at a temperature of 22 °C. From the force-deformation curves, the initial slope (≈ 1-4 % strain) was used to calculate Young's modulus (E). Correction for syneresis was performed as previously described [31,32].

Microbeads were compressed using a previously described approach [33]. The same instrument, operating parameters and conditions as for the cylinders were applied, except for the use of a P/5 cylindrical probe and continuous compression measurement (button trigger). The force output (g) was obtained at 70 % strain, which was calculated from the mean diameter of microbeads. In order to correct for the effect of size discrepancy between microsphere types the force output was normalized. The mean volume of microbeads was calculated and divided by the volume of a sphere of 500 µm and multiplied by the recorded force output.

2.4. Animals

Inbred immunocompetent mice of strain C57BL/6JRj were acquired from Janvier Labs (Saint Berthevin Cedex, France). All mice were female, aged 10 weeks at the onset of the experiment with body weights from 17.1 g-22.4 g. Mice were housed separately and provided with nesting materials. Health inspections were conducted twice a week for the duration of the experiment.

2.5. Surgical procedure, implantation and explantation

Mice were anesthetized using 1.5-3.0 % isoflurane (Baxter International Inc., Deerfield, IL, USA). The lower abdomen was shaved

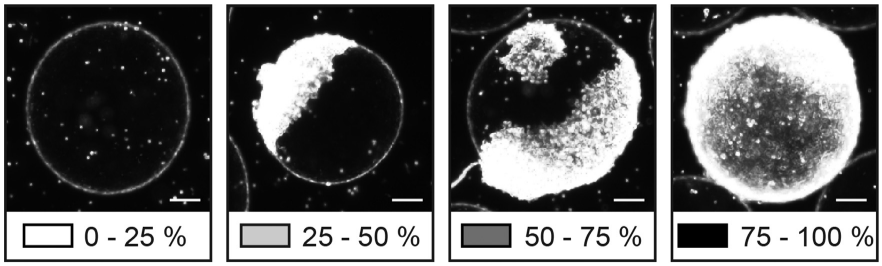

Fig. 1. Representative phase-contrast images of explanted alginate microspheres with assigned pericapsular fibrotic overgrowth (PFO) scores. Scale bar, 100 µm.

and disinfected with 70 % ethanol. An incision was made in the skin and a 16 GA catheter was inserted intraperitoneally (I.P.) in the lower abdomen. Microspheres suspended in WS were injected with a 1 mL syringe. After injection, the syringe was refilled with WS, to a total injected volume of 1 mL to ensure the injection of leftover microspheres in the catheter. After implantation, the volume of microspheres remaining in the syringe and catheter was quantified. The peritoneal membrane and abdominal skin were sealed with one suture and one to three sutures, respectively. Mice were locally analgized with sub-cutaneous injections of 50 µL (0.5 mg/mL) bupivacaine (AstraZeneca plc, Cambridge, UK).

Upon explantation, mice were anesthetized as described previously and euthanized by cervical dislocation. Skin covering the peritoneal cavity was removed and 5 mL WS was injected into the peritoneal cavity. Mice were gently shaken, and the frontal section of the peritoneum was excised over a petri dish filled with 15 mL WS. After thorough rinsing, the remainder of non-attached microspheres were manually recovered.

2.6. Initial volume and recovery of alginate microspheres

Prior to implantation, each sample was transferred to a 1 mL syringe for assessment of the initial volume of microspheres (after sedimentation). Following explantation, microsphere volumes were recorded (1 mL syringes) and their diameters measured by microscopy as previously described. Recovery estimates were made accounting for the mean volume change caused by changes in the diameter of the alginate microspheres.

2.7. Quantification of PFO

Quantification of PFO was performed using brightfield and phase contrasted image microscopy on a Zeiss LSM 800 with an EC Plan-Neofluar 2.5×/0.085 M27 objective. Overgrowth coverage on microspheres was estimated and grouped in intervals of 0-25 %, 25-50 %, 50-75 % and 75-100 %. Representative example images are given in Fig. 1.

2.8. Protein adsorption on explanted alginate microspheres

Alginate microspheres retrieved from C57BL/6JRj mice after 2, 14 and 112 days were washed and stained for selected proteins prior to confocal scanning microscopy (CLSM). In detail, the explantation solution (20 mL WS) was removed, alginate microspheres were resuspended in 0.5 mL WS, aliquoted to approximately 50 µL microspheres/tube and finally 0.2 mL WS was added to each tube prior to storage (4 °C, 0-8 days). Alginate microspheres were subsequently washed (2 × 0.5 mL WS) and stained using 125 µg/mL FITC-conjugated (F/P ≈ 1.5) polyclonal goat anti-mouse C3c and fibrinogen (Nordic-MU-bio, Susteren, Netherlands). As a control for non-specific antibody binding, FITC-conjugated (F/P ≈ 2.8) goat anti-chicken IgY (GeneTex, Irvine, CA, USA) was used at a concentration of 67 µg/mL, giving comparable FITC-signals. The staining procedure (1 h) was performed at room temperature under mild rotation. For visualization of cell adsorption DRAQ5™ (BioLegend Europe BV, London, UK, 1:1000) was added to the microspheres with 15 min of the staining process remaining. After staining, microspheres were washed (2 × 0.5 mL WS) and kept in 0.2 mL WS. Microspheres were analyzed by CLSM (Zeiss LSM 800), equipped with a C-Apochromat 10×/0.45W objective. CLSM images were obtained using three separate channels simultaneously for visualization of the microspheres (ESID), adsorbed FITC-labelled antibodies (Diode laser 488 nm, with detection wavelength 410-617 nm), and adsorbing cells using DRAQ5™ (Diode laser 640 nm, with detection wavelength 650-700 nm). Images were captured by optical cross-sections (pinhole = 30 µm) through the equator of the microspheres and 3D images were constructed from sections through the entire microsphere using z-stacks and ImageJ software v. 2.1.0/1.53c (National Institutes of Health, New York, USA). CLSM settings were identical for all captured images. Assessment of protein deposition was based on explanted microspheres that were not overgrown with host cells.

2.9. Inflammatory properties evaluated in human whole blood

2.9.1. Human whole blood model

The human whole blood model first described by Mollnes et al. (2002) [34], was used following the modifications for microspheres as described by Rokstad et al. (2011) [18]. Briefly, microspheres (50 μL) suspended in 0.9 % NaCl (50 μL, B. Braun, Melsungen, Germany) and the control samples had PBS with $CaCl_2$ and $MgCl_2$ (100 µL, Sigma Aldrich, St. Louis, MO, USA) added. Subsequently, whole blood (500 μL) from healthy donors (N = 5) anticoagulated with lepirudin (Refludan, Celgene Europe Ltd., Switzerland, 50 μg/mL) was added to the samples. Incubation was performed for 4 h in low activating polypropylene vials under continuous rotation at 37 °C. Positive controls comprised *Escherichia coli* (1×10^7 particles/mL in 0.9 % NaCl, heat-inactivated strain LE392, American Type Culture Collection, Manassas, VA, USA), Zymosan (10 μg/vial in 0.9% NaCl, Sigma Aldrich, St. Louis, MO, USA, Z4250), and BD vacutainer glass (Belliver Industrial Estate, Plymouth, UK) with 0.9 % NaCl (100 μL). Saline control (0.9 % NaCl, 100 μL) served as a negative control providing the background activation. Baseline (0.9 % NaCl, 100 μL) was equal to the saline control but inactivated by EDTA (10 mM final concentration) immediately upon blood addition. After incubation, EDTA (10 mM final concentration) was added to each sample, followed by centrifugation (3000 rpm,

15 min, 4 °C) and harvesting of plasma. Plasma was stored at -20 °C for further analysis of activation of complement (terminal complement complex), coagulation (prothrombin fragment F1+2) and cytokines.

2.9.2. Complement activation

Complement activation was assessed through the level of soluble terminal complement complex (sTCC) using the enzyme-linked immunosorbent assay (ELISA) kit for the Human Terminal Complement Complex (Hycult Biotech, Uden, Netherlands). The assay was performed in accordance with the provided protocol, using the following dilution factors for the plasma harvested from the given samples: Baseline (1:50), saline control and microspheres (1:100), *E. coli* and glass (1:200), and zymosan (1:400). Absorbance was measured at 450 nm with a spectrophotometer (POLARstar Omega, BMG Labtech, Ortenberg, Germany).

2.9.3. Coagulation activation

Activation of coagulation was determined by the level of prothrombin fragment F1+2 (PTF1.2), a cleavage product formed upon activation of prothrombin to thrombin. PTF1.2 was measured by ELISA kit Enzygnost® F1+2, monoclonal (Siemens Healthcare Diagnostics, Marburg, Germany). Analysis was performed following the producer's protocol, except increasing the dilution of plasma for the respective samples: Baseline (1:10), saline control (1:10/20), microspheres (1:20/50/100/1000), *E. coli* (1:1000), glass (1:100/1000), and zymosan (1:500). Absorbance was measured at 450 nm, with a reference wavelength of 650 nm.

2.9.4. Cytokine induction

Plasma samples were analyzed using the multiplex assay Bioplex™ Pro Human Cytokine Assay (Bio-Rad Laboratories, Inc.) for selected cytokines: interleukin-1β (IL-1β), interleukin-6 (IL-6), interleukin-8 (IL-8), interleukin-10 (IL-10), tumor necrosis factor-α (TNF-α), and monocyte chemoattractant protein 1 (MCP-1). Analyses were performed in accordance with the provided protocol, using half of the recommended amount of magnetic beads coated with capture antibodies. Analyte concentrations were quantified using a Bio-Plex 200 Reader (Bio-Rad Laboratories Inc.).

2.10. Statistical methods

Statistical differences in fibrinogen deposition between alginate microbeads were determined by Brown-Forsythe and Welch ANOVA with Dunnett's multiple comparison test, on the account of unequal standard deviations. The data were assumed to not be normally distributed due to low sample numbers (n = 9-18) and were therefore log-transformed prior to analysis. Differences were considered significant at $p < 0.05$.

In the whole blood assay, repeated measures one-way ANOVA with Dunnett's multiple comparison test was performed to define statistical differences between the baseline, saline control and HiG, to other investigated microspheres. The data were log-transformed prior to analysis due to low sample numbers (N = 5). Statistical significance was set to $p < 0.05$.

2.11. Ethics

The use of human whole blood for basal experiments was approved by the Regional Ethic Committee at the Norwegian University of Science and Technology under the approval 2009/2245. Animal experiments were in accordance with national guidelines for the care and use of laboratory animals and approved by the Norwegian Food Safety Authority.

3. Results

3.1. Formation of stable alginate microbeads by the selection of gelling ions

Here, we explored strategies to stabilize alginate microbeads by using gelling ions Ba^{2+} and Sr^{2+} that crosslink strongly to G-blocks, alone or in combination with Ca^{2+} [19]. Investigated gelling ions included Ca^{2+} (50 mM), Ca^{2+}/Ba^{2+} (50 mM, 1 mM), Sr^{2+} (20 mM) and Ba^{2+} (20 mM). All microbeads were stabilized to a greater degree when using Sr^{2+} or Ba^{2+} as gelling ion compared to Ca^{2+} alone, as illustrated by the reduced diameter increase after six consecutive saline treatments (Fig. 2B). In addition, using a low concentration of Ba^{2+} (1 mM) in the gelling solution in combination with Ca^{2+} (50 mM) stabilized the microbeads to approximately the same extent as Ba^{2+} alone. As expected, the effect of changing the gelling ions was more pronounced for alginate with a high content of G (HiG), where an increase in diameter of 28 % or less was recorded for Sr-, Ba- and Ca/Ba-microbeads compared to 97 % increase for Ca-microbeads. However, microbeads containing sulfated alginate (HiG+SA (80/20)), as well as the microbeads with a lower G content (IntG), were also stabilized by the change in gelling ions, and particularly by Ba^{2+}. The diameter increase for IntG gelled with Ba^{2+} or Ca^{2+}/Ba^{2+} was 53 % and 46 %, respectively, after six saline treatments, compared to 80 % for Sr^{2+} and 110 % for Ca^{2+}. The microbeads HiG+SA (80/20) showed the highest stability with 73 % increase in diameter with Ca^{2+} as gelling ion, 19 % increase for Ca/Ba-microbeads, 32 % for Sr-microbeads and 9 % for Ba-microbeads. The initial sizes of the microbeads were predominantly in the size range between 400-450 µm. IntG Ca-microbeads were smaller with a size of 354 ± 12 µm and HiG+SA (80/20) Ba-microbeads were larger with a size of 487 ± 16 µm (Fig. 2A). A detailed overview of the recorded microbead diameters from the stability assay can be found in supplementary Fig. S1.

Material stiffness has been shown as a contributing factor to PFO in other hydrogel systems [35]. Therefore, we characterized a selection of materials for their compression resistance to investigate this relationship. As an approximate indicator of hydrogel stiffness, we measured the force output resulting from uniaxial compression of individual microspheres to 70 % strain. The measurement of material stiffness can be challenging for microspheres due to equipment sensitivity and the change in contact area upon compression. Therefore, we also determined the Young's moduli of gel cylinders with the same polymer composition, made by internal gelation with subsequent saturation in Ca^{2+}/Ba^{2} (50 mM, 1 mM). Although their modes of production were slightly different, the trends in the data for cylinders and microbeads correlated well (Fig. 2C). As expected, the Young's modulus (E) of gel cylinders correlated positively with the G-content of the alginates. The Young's modulus of HiG (40.1 ± 2.4 kPa) was four times higher than IntG (11.2 ± 0.9 kPa) (Fig. 2C, left). Since HiG alginate microbeads are stiffer than IntG and lead to fibrosis in C57BL6/J mice, monkeys and humans [3,9], it was of interest to investigate if softer HiG alginate microbeads would lead to a different fibrotic outcome. As a reduction in alginate concentration is known to reduce gel stiffness [31,32], gels of HiG alginate with similar mechanical properties to IntG gels were made by reducing the alginate concentration to 0.7 % (w/v) with E equal to 7.3 ± 0.9 kPa. Substituting 20 % dry weight of HiG alginate with sulfated alginate (HiG+SA (80/20)) reduced the Young's modulus considerably (22.6 ± 1.5 kPa) compared to HiG. Compression measurements were also performed on microbeads corresponding to the composition of the cylinders (Fig. 2C, right). The force (g) from the microbeads at 70 % strain displayed a trend similar to that of the cylinders. HiG microbeads yielded the highest force (2.0 ± 0.9 g), followed by HiG+SA (80/20)

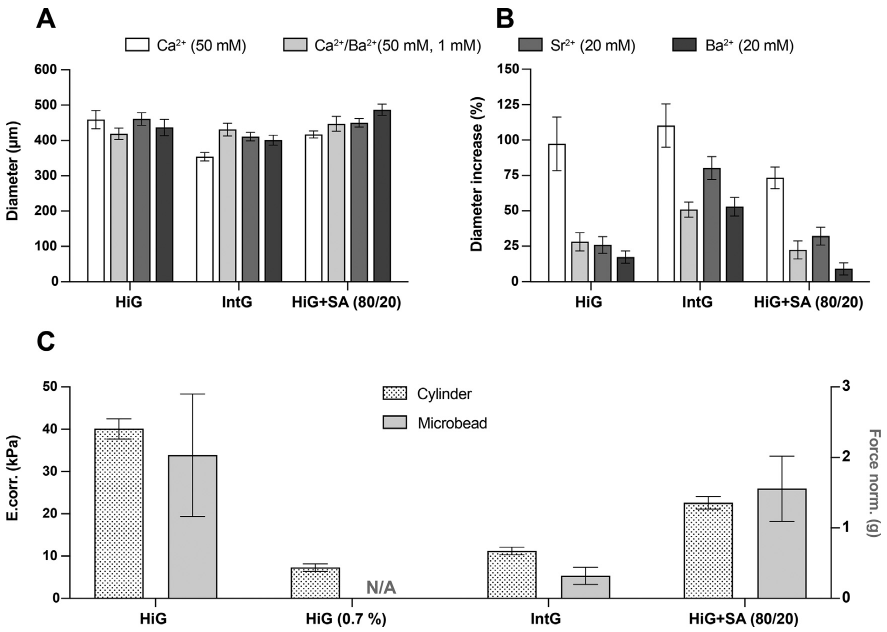

Fig. 2. Size and size stability of microbeads produced with different gelling ions, and Young's modulus (kPa) and force output (g) at 70 % strain of alginate gel cylinders and microbeads, respectively. (**A**) Initial diameters of microbeads HiG, IntG and HiG+SA (80/20). (**B**) Relative diameter increase for microbeads HiG, IntG and HiG+SA (80/20) after six consecutive saline treatments. (**C**) Gel strength measured for gel cylinders given as Young's modulus (E.corr, left) and for microbeads force (g) at 70 % strain, normalized for microbead diameter (Force norm., right). All measurements are given as the mean ± SD. Compression studies were performed on alginate gel cylinders (N = 12)/microbeads (N = 31-38) HiG, HiG (0.7 %), IntG and HiG+SA (80/20) saturated/gelled in Ca^{2+}/Ba^{2+} (50 mM, 1 mM).

(1.6 ± 0.5 g) and IntG (0.3 ± 0.1 g). The 0.7 % HiG microbead was not possible to measure, as it was too soft to give measurements above noise.

3.2. Evaluation of microbead formulations in mice reveals microbeads of intermediate G and sulfated alginate largely free of PFO

3.2.1. Short-term screening study of alginate microbeads shows several candidates largely free of PFO

Alginate microbeads of various formulations were screened for PFO after implantation in C57BL/6JRj mice after 14-35 days (Fig. 3). The panel of microbeads investigated included eleven alginate formulations with optimized stability using Ca^{2+}/Ba^{2+} or Sr^{2+} as gelling ions (Table 2). Microbeads consisted of intermediate G (IntG), sulfated (SA), and/or high G alginate (HiG). Microbeads comparable to the HiG microbead in this study have previously been found to produce PFO [9]. The HiG microbead was therefore included as a control.

Explanted microbeads containing either entirely or 64 % IntG or fractions (20 or 40 %) of SA exhibited a substantial reduction in PFO compared to microbeads of HiG alginate. PFO grading above 25 % (Fig. 1) is summed up as a total PFO score (%) in the following section. PFO was 54-68 % for HiG-category microbeads, 0-19 % for IntG-category microbeads and 1-7 % for SA-category microbeads (Fig. 3A). Surprisingly, reducing the concentration of HiG alginate from 1.8 % to 0.7 % (w/v) gave similar total PFO but a 2.5-fold increase in the high grade (75-100 % cell coverage) PFO category. For microbeads containing IntG, inclusion of 36 % of either high-Mw (IntG+HiG) or low-Mw HiG (IntG-L-HiG) gave minimal PFO (0-1 % PFO), similar to the pure IntG microbeads (2 % PFO). Intriguingly, higher endotoxin levels in IntG+L-HiG did not result in PFO. Contrastingly, higher PFO was seen for IntG with very low-Mw HiG (IntG+VL-HiG) with 19 % PFO. IntG microbeads with a higher alginate concentration (IntG (2.8 %)) produced more PFO (8 %) compared to the 1.8 % IntG microbeads. For the SA-containing microbeads, increasing the percentage of SA relative to HiG from 20 % to 40 % increased PFO from 1 % (HiG+SA (80/20)) to 7 % (HiG+SA (60/40)). By using Sr^{2+} as gelling ion, the PFO was reduced to 2 % for the higher content of sulfated alginate (HiG-SA (60/40)-Sr). No effect of Sr^{2+} as gelling ion was seen on the PFO of IntG microbeads, relative to Ca^{2+}/Ba^{2+}. Overall, lower recovery rates were seen for microbeads containing SA, regardless of the high size stability. Changing the gelling ions (Ca^{2+}/Ba^{2+} vs. Sr^{2+}) had minimal effect on recovery rates (Fig. 3B) and size stability *in vivo* (Fig. 3C) for alginate microbeads containing either IntG or SA alginate. Based on these observations, two candidate microbeads with minimal PFO, namely IntG and HiG+SA (80/20), were chosen for further evaluation.

3.2.2. Long term evaluation of candidate microbeads, IntG and HiG+SA (80/20), shows limited PFO

Two microsphere designs that predominantly were free of PFO, were chosen for extended evaluations. The number of animals was increased for a 14-day evaluation and a long-term evaluation for 112 days was included (Fig. 4). After 14 days *in vivo*, microbead types containing intermediate G, IntG, or sulfated alginate, HiG+SA (80/20), remained largely free of PFO with 99 and 93 % within the minimal PFO score (0-25 %), respectively (Fig. 4A). Comparably low PFO was found in the 112-day groups for the same microbeads (Fig. 4A). Only a marginal increase in PFO was found on IntG with 96 % of microbeads within 0-25 % PFO, whereas no increase in PFO was found on HiG+SA (80/20). The recovery of HiG+SA (80/20) mi-

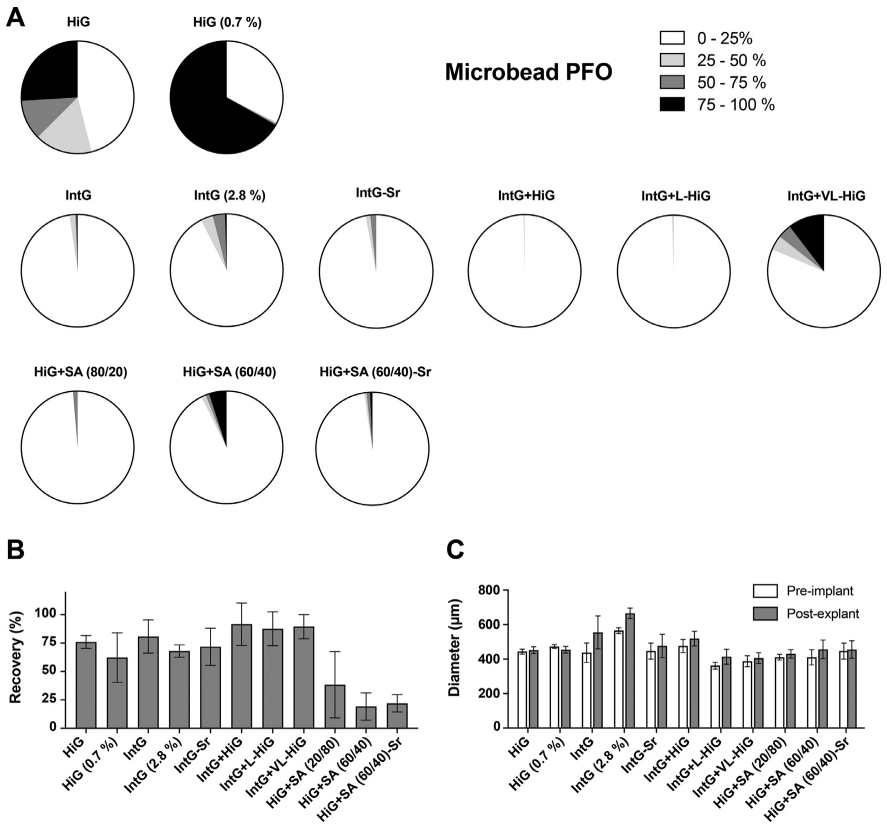

Fig. 3. *In vivo* screening of alginate microbeads explanted from C57BL/6JRj mice after 14-35 days. Microbeads were gelled in Ca^{2+}/Ba^{2+} (50 mM, 1 mM), or in Sr^{2+} (20 mM) which are denoted by -Sr. (**A**) Pie charts depict the average degree of PFO for each microsphere formulation. The pie sections represent the average percentage of microbeads assessed in each category, where the white pie sections depict minimal cell coverage on microbeads (< 25 % PFO) and gray to black pie sections depict a pronounced cell coverage on the categorized microbeads (> 25 % PFO). (**B**) Recovered volume of microbeads, given as the mean ± SD. (**C**) Diameter of microbeads (n = 30) pre-implant and post-explant, given as mean ± SD. Number of mice (N) and retrieval time in days (d) for each microsphere formulation: [HiG: N=2, 19d], [HiG (0.7%): N=5, 14d], [IntG: N=2, 19d; N=1, 35d], [IntG (2.8%): N=2, 19d], [IntG-Sr: N=2, 19d; N=1, 35d], [IntG+HiG: N=3, 14d], [IntG+L-HiG: N=6-8, 14d], [IntG+VL-HiG: N=5, 14d], [HiG+SA (80/20): N=2, 19d; N=1, 35d], [HiG+SA (60/40): N=2, 19d; N=1, 35d] and [HiG+SA (60/40)-Sr: N=2, 19d; N=1, 35d].

crobeads was lower than for IntG (Fig. 4B). For IntG microbeads, a recovery of 81 ± 18 % after 14 days and 85 ± 3 % after 112 days was recorded. HiG+SA (80/20) had variable recovery rates with 57 ± 27 % at 14 days and 62 ± 38 % at 112 days. Recovery may reflect both microbead stability and residual microbeads left in the animal. Hence, the mean diameters of explanted microbeads were measured and compared to initial size (Fig. 4C). IntG microbeads increased in size with 16 ± 2 % after 14 days and 13 ± 1 % after 112 days. HiG+SA (80/20) microbeads showed a size increase of 8 ± 1 % after 14 days and 5 ± 3 % after 112 days *in vivo*.

3.3. Fibrinogen deposition on explanted alginate microspheres coincides with PFO

To further evaluate explanted microspheres, fibrinogen and complement C3c deposition was assessed by CLSM on alginate microspheres retrieved from C57BL/6JRj mice after 14 and 112 days (Fig. 5). The *in vivo* fibrinogen and C3c depositions were quantified on microspheres free of cellular overgrowth to avoid additional contribution from adhering cells. Microbeads IntG, HiG+SA (80/20), HiG and HiG (0.7 %) retrieved at 14 days showed adsorption of fibrinogen, with lower amounts of C3c deposition (Fig. 5A). Overall, the greatest accumulation of fibrinogen was found on the HiG (0.7 %) microbead and secondly HiG. Lower fibrinogen depositions were observed for IntG and HiG+SA (80/20), albeit with larger variations for the IntG microbead. After 112 days, deposition of fibrinogen remained low for HiG+SA (80/20), while an increase was seen for IntG (Fig. 5B). Poly-L-lysine coated alginate microcapsules (AP) were retrieved after 2 days *in vivo* to avoid complete cell coverage. Distinctively, AP microcapsules exhibited a clear deposition of C3c (Fig. 5C).

The adsorption patterns differed between microsphere types. Fibrinogen was distributed more evenly on the surface of HiG+SA (80/20) as compared to IntG, which showed a spotted pattern (Fig. 5D). Similar adsorption patterns were observed for C3c deposition on the microbeads, overall, with low levels of C3c adsorption (Fig. 5E, 5A). Quantification of fibrinogen on microspheres retrieved after 14 days revealed statistically lower deposition for IntG ($p < 0.0001$-0.001) and HiG+SA (80/20) ($p < 0.0001$) compared to HiG and HiG (0.7 %) (Fig. 5F). Quantification of complement C3c

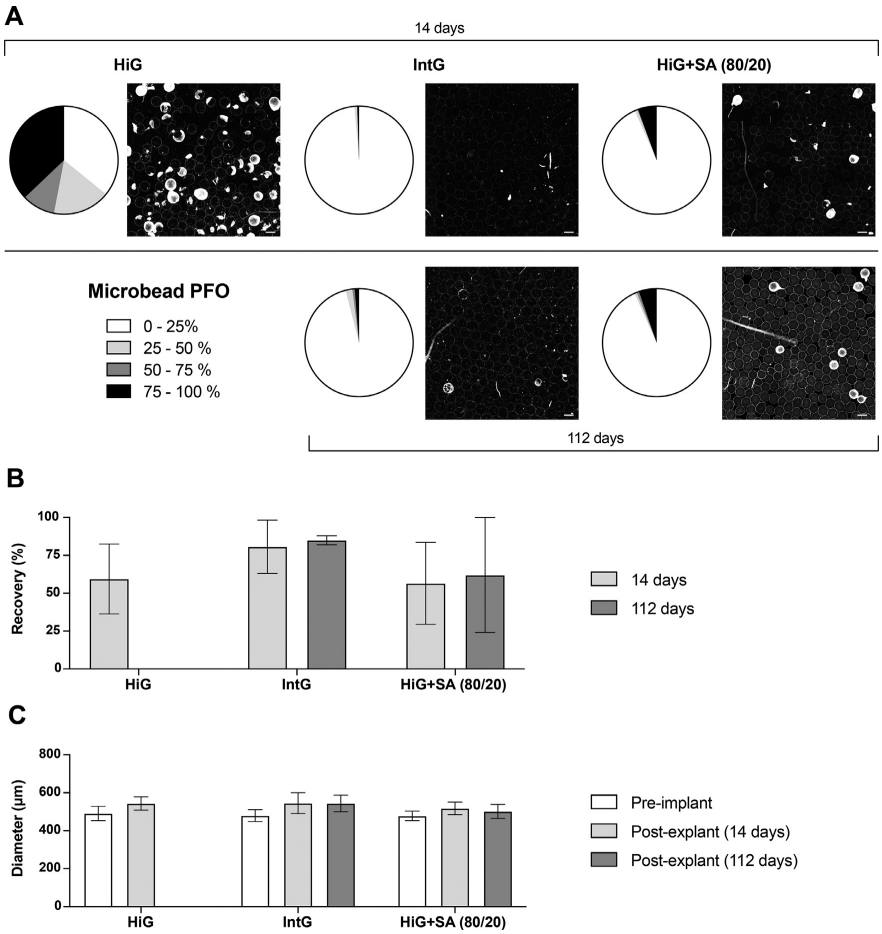

Fig. 4. Alginate microbeads IntG and HiG+SA (80/20) with HiG as a positive PFO control, gelled in Ca^{2+}/Ba^{2+}(50 mM, 1 mM), explanted from C57BL/6JRj mice after 14 days and 112 days. (**A**) Pie charts depict the average degree of PFO for each microsphere formulation. The pie sections represent the average percentage of microbeads assessed in each category, where the white pie sections depict minimal cell coverage on microbeads (< 25 % PFO) and gray to black pie sections depict a pronounced cell coverage on categorized microbeads (> 25 % PFO). Representative phase contrasted images following explant are shown. Scale bar, 500 µm. (**B**) Percent volume of implanted microbeads recovered, given as the mean ± SD. (**C**) Diameters of microbeads (n = 30) pre-implant and post explant, given as the mean ± SD. Number of mice and retrieval time in days (d) for each microsphere design: [IntG: N=7, 14d; N=3, 112d], [HiG+SA (80/20): N=13*, 14d; N=3, 112d] and [HiG: N=6, 14d].*In Fig. 4C: [HiG+SA (80/20): N=7, 14d].

(Fig. 5G) revealed low adsorption to microbeads, compared to the AP microcapsule.

3.4. Alginate microbeads show low inflammatory properties in human whole blood

Alginate microbeads IntG, HiG+SA (80/20) and HiG were evaluated for acute inflammatory responses in a human whole blood assay (Fig. 6), together with a broader panel of microbeads shown in supplementary Fig. S2. The AP microcapsule was included as a positive control for TCC and cytokine induction (Fig. 6A, C, D) [18]. IntG, HiG+SA (80/20) and HiG displayed minimal activation of complement, measured by the soluble terminal complement complex (TCC, Fig. 6A and S2 for controls). HiG+SA (80/20) reduced TCC induction to be non-significant from baseline, contrasting HiG and IntG ($p < 0.01$) and the saline control ($p < 0.001$). The TCC levels for the microbeads were lower than the saline control, albeit not significantly different. In contrast, the TCC response for AP microcapsules was significantly elevated above baseline ($p < 0.001$), saline control and HiG ($p < 0.01$). Coagulation activation was measured by the level of prothrombin fragment 1+2 (PTF1.2) (Fig. 6B). All microspheres gave significantly ($p < 0.001$-0.05) elevated responses compared to the baseline. HiG+SA (80/20) induced a marked PTF1.2 response, significantly ($p < 0.01$) elevated above the saline control and HiG. HiG, IntG and HiG+SA (80/20) induced overall low cytokine responses. The proinflammatory cytokines (IL-1β, IL-6, IL-8 and TNF-α, Fig. 6C) and the anti-inflammatory cytokine IL-10 (Fig. 6D) induced modest responses, with no significant difference from the saline control. However, all microspheres were significantly ($p < 0.001$-0.05) elevated above

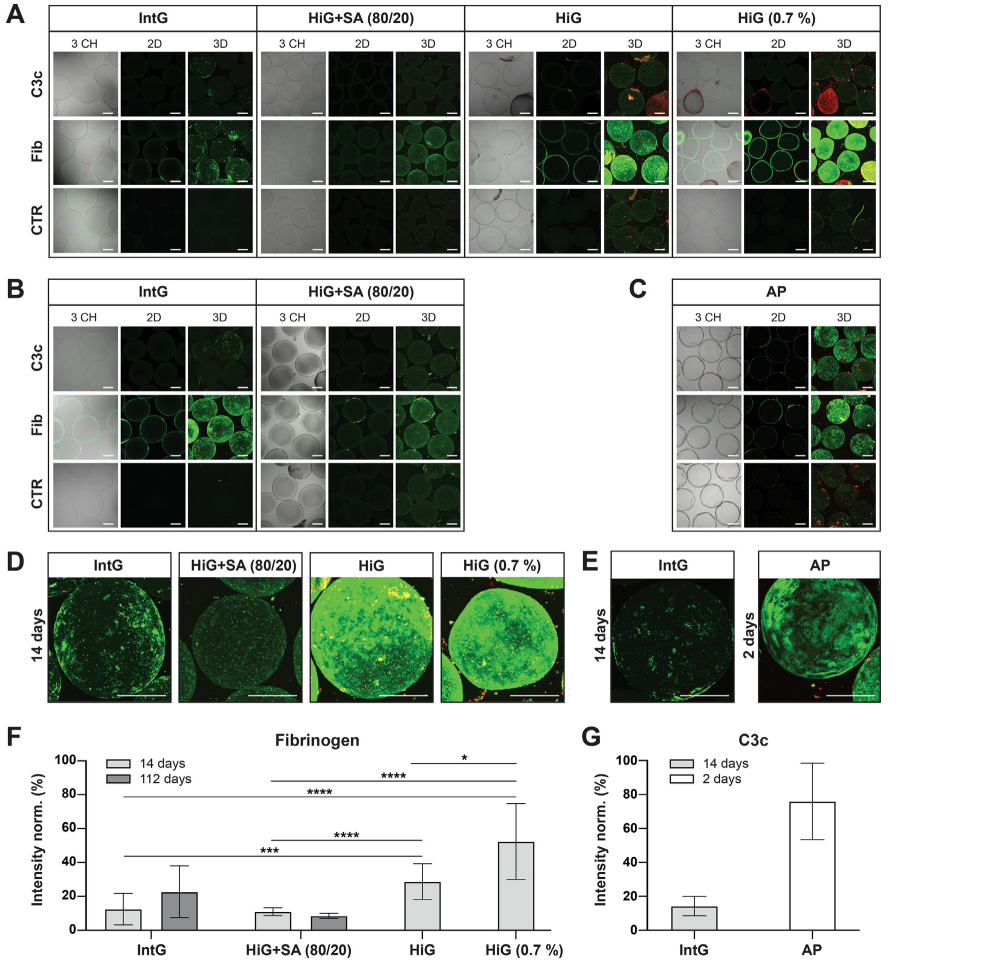

Fig. 5. Representative CLSM images and intensity quantifications of antibody-FITC incubated microspheres retrieved from C57BL/6JRj mice. Gelation was performed in Ca^{2+}/Ba^{2+} (50 mM, 1 mM) for microbeads and Ca^{2+} (50 mM) for microcapsules (AP). Deposition of complement C3c and fibrinogen (Fib), including a control (CTR) for non-specific antibody binding. Microsphere retrieval after (**A**) 14 days for IntG (N = 5 mice), HiG+SA (80/20) (N = 6 mice), HiG (N = 5 mice) and HiG (0.7 %) (N = 3 mice), (**B**) 112 days for IntG (N = 3 mice) and HiG+SA (80/20) (N = 3 mice), and (**C**) 2 days for AP (N = 2 mice). Close up 3D-images of (D) fibrinogen (after 14 days) and (**E**) C3c deposition (after 14 and 2 days) on explanted microspheres. Scale bar, 200 µm. Relative protein depositions between microspheres were estimated by quantification of fluorescence intensity, shown as normalized intensity, for (**F**) fibrinogen (after 14 and 112 days) and (**G**) C3c (after 14 and 2 days). Quantified controls (not shown) exhibited minimal binding. Significant values are given as $p < 0.05$ (*), $p < 0.01$ (**), $p < 0.001$ (***), $p < 0.0001$ (****) between microspheres. Data are expressed as the mean value of 6-18 microspheres ± SD. Images were captured using three separate channels (CH) for detection of transmitted light, FITC (proteins = green) and DRAQ5 (cells = red), shown in 2D and 3D (z-stacks).

baseline. HiG gave a consistently higher, although non-significant, response for the proinflammatory cytokines compared to IntG and HiG+SA (80/20). As for IL-10, HiG+SA (80/20) was slightly, yet not significantly elevated above HiG and IntG. Overall, AP induced a significant ($p < 0.0001$-0.01) cytokine response above baseline, where induction of TNF-α was significantly ($p < 0.05$) elevated above HiG. The monocyte chemoattractant (MCP-1) showed no significant differences between the baseline, saline control and microspheres (Fig. 6E). Positive controls (*E. coli*, zymosan and glass) and microbeads from the screening study that were included in the whole blood assay are outlined in Fig. S2.

4. Discussion

Mitigating PFO on the surface of the material is key to the successful application of alginate encapsulated cells in therapy [1,2,9]. Herein we have shown two types of microbeads based on intermediate G alginate (IntG) or sulfated alginate (HiG+SA (80/20)) with minimal PFO in a mouse (C57BL/6JRj) model, where more than 93 % of the microbeads were free of PFO after 112 days. These microbeads were selected from a panel of alginate microbeads of various compositions and gelling ions, several of which were low in PFO. The microbead IntG represents a simple approach, utilizing an alginate with an intermediate fraction of G (47 %). The microbead

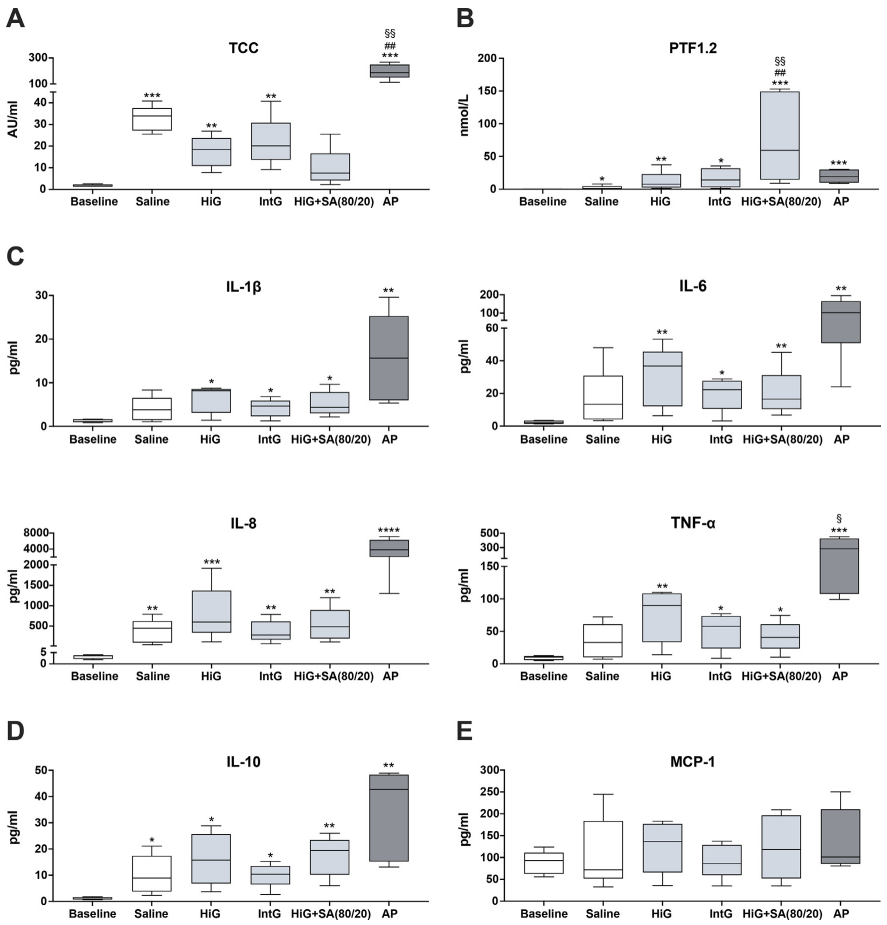

Fig. 6. Inflammatory responses to microspheres incubated (4 h) in lepirudin-anticoagulated human whole blood. Gelation was performed in Ca^{2+}/ Ba^{2+} (50 mM, 1 mM) for microbeads and Ca^{2+} (50 mM) for microcapsules (AP). (**A**) Activation of complement determined by soluble terminal complement complex (TCC), (**B**) coagulation indicated by prothrombin fragment 1+2 (PTF1.2); positive control (glass) median value = 225 nmol/L, (**C**) proinflammatory cytokines IL-1β, IL-6, IL-8, and TNF-α, (D) anti-inflammatory cytokine IL-10, and (**E**) monocyte chemoattractant MCP-1; positive control (*E. coli*) median value = 370 pg/mL. The AP microcapsule was included as a control for TCC (**A**) and cytokine responses (**C**, D). Data are expressed in box plots with values from five donors. Significant difference compared to baseline (*), saline control (#) and HiG (§), where one symbol = $p < 0.05$, two symbols = $p < 0.01$, three symbols = $p < 0.001$, and four symbols = $p < 0.0001$. Positive controls (*E. coli*, zymosan and glass) are included in supplementary Fig. S2.

HiG+SA (80/20) involves modification of alginate by sulfation and producing microbeads from a mixture of sulfated and unmodified high G alginate. In the following we discuss these promising microbeads in the context of existing literature, focusing on PFO and key parameters such as stability and low inflammatory potential.

The current work has shown that microbeads of intermediate G alginate were essentially PFO-free (96 % clean after 112 days) in immunocompetent mice, and additionally, stable *in vivo*. Intermediate G alginate microbeads have also been shown by others to produce low PFO responses [11,23]. However, problems related to stability have been described [11,19]. Swelling and destabilization of alginate hydrogels is linked to osmotic swelling and the exchange of gelling ions with non-gelling ions [19,21,36,37]. The intermediate G alginate used in this study had a high content of M- and G-blocks relative to MG-blocks (Table 1). The sufficient size stability can be explained by the binding of gelling ions to different block structures of alginate, where G-blocks bind Sr^{2+}, Ca^{2+} and Ba^{2+}, M-blocks bind Ba^{2+} and MG-blocks bind Ca^{2+} [19]. Hence, the stabilization of the microbeads with Ba^{2+} is expected, although contrasting previously reported intermediate-G alginate microbeads with higher levels of MG-blocks [21]. In the current study, no evident ruptures or fragmented microbeads were found among explanted microbeads containing intermediate G alginate gelled in Ca^{2+}/Ba^{2+}, and the size did not increase over time (14 vs. 112 days). Microbeads of intermediate G alginate with low MG content were stabilized by Sr^{2+} or Ba^{2+} compared to gelation in Ca^{2+} alone, as shown by the *in vitro* stability assay. In general, gelation utilizing a high concentration of Ba^{2+} (20 mM) produced the most stable microbeads. However, the microbead stability after

gelation in Ca^{2+} with a lower concentration of Ba^{2+} (1 mM) was found to be close to that of microbeads gelled in a high concentration of Ba^{2+}. The use of 20 mM Ba^{2+} in the gelation of alginate microbeads has been shown to exceed the tolerable intake of barium in an *in vivo* mouse model [21]. Microbeads gelled in Ca^{2+} with a low concentration of Ba^{2+} (1 mM) thus represents a good compromise between stability and biocompatibility. The stiffness of alginate hydrogels is correlated with G-content and concentration of both alginate and gelling ions, due to the formation of G-block junction zones [32]. In other hydrogel systems, stiffer materials have been shown to induce macrophages towards a proinflammatory phenotype and to result in a thicker fibrotic layer *in vivo* compared to softer hydrogels [35]. Although these hydrogels were within a comparable range of stiffness (5-40 kPa), differences in chemical characteristics and mouse strains (BALB/c and C57BL/6J) can influence fibrotic outcome [12]. In other studies, gel stiffness has been shown to affect cell adhesion to hydrogel surfaces [38] and the differentiation of stem cells [39]. In short, stiffness could be discussed as a potential factor in the development of PFO. By our estimates using uniaxial compression of microbeads and gel cylinders, the low concentration high G alginate microbead (HiG (0.7 %)) had a gel stiffness comparable to intermediate G microbeads (IntG), and hence lower than HiG (1.8%) microbeads. However, HiG (0.7%) microbeads still produced severe PFO. On the other hand, increasing the alginate concentration of intermediate G alginate from 1.8 % to 2.8 % (w/v) in the microbeads, and consequently increasing the gel stiffness [31,32], produced more PFO. Hence, these observations suggest that variables aside from gel stiffness may be more important causative factors of PFO on the current alginate microbeads. One such factor could be fibrinogen deposition which is discussed in a later section. It has been hypothesized that swelling could confer positive outcomes in mitigating PFO [11]. We observed that mixing a fraction of high G alginate in the IntG-formulation (e.g., IntG+HiG) yielded swelling comparable to high G alginate (HiG) microbeads, but with PFO comparable to that of the IntG microbead type. This indicates that swelling by itself does not explain the reduced PFO. Taken together, these findings thus do not support the differences in gel-stiffness or swelling as key factors in the development of PFO on alginate microbeads. A previous study on microbeads of high G and intermediate G alginate microbeads gelled in calcium or barium ions showed fibrosis to be independent of gelling ions, but dependent on the alginate used [11]. However, calcium ions leaking from alginate gels have been shown to activate dendritic cells *in vitro* and induce cytokine production *in vivo* when implanted in mice [40]. Furthermore, strontium alginate gels have been suggested to provide PFO free hydrogels [41]. In the current study 50 mM Ca^{2+} and 1 mM Ba^{2+} was used as gelling ions, with extensive washing after gel formation. Hence, limited amounts of calcium ions are expected to leak out from the gel. Limited leakage of barium ions has previously been shown from similar microbeads of high G alginate [21]. Using strontium as gelling ion showed limited effect on fibrosis compared to calcium/barium in the current study. However, an overall lower induction of complement activity and cytokine production was seen for the microbeads with sulfated alginate gelled in strontium (Fig. S2).

Microbeads containing sulfated alginate were stabilized by ionic crosslinking with Sr^{2+}or Ba^{2+}, compared to only Ca^{2+}, as shown by the *in vitro* stability studies. While these microbeads showed promisingly low PFO, the recovery rate was surprisingly low both with Sr^{2+} or Ca^{2+}/Ba^{2+} as gelling ions. This was not due to PFO or adherence to the peritoneal cavity, nor could the *in vitro* stability assay explain the findings. One may speculate that the biological activity of sulfated alginates [42] could impose a different *in vivo* stability than what is observed *in vitro*. Hence, the *in vivo* stability of sulfated alginates needs to be further evaluated. Studies, for instance with encapsulated islets would reveal if this observation was relevant to the function of implanted encapsulated cells.

Intermediate G microbeads showed low levels of inflammatory cytokines and complement activation in human whole blood, further underlining their clinical potential. This is similar to what has previously been reported for high G alginate microbeads [16,18]. In contrast, microcapsules containing poly-L-lysine (AP) induce complement activation with C3c deposition on the surface and subsequent induction of cytokines by leukocytes [13,16,18]. Here we show that *in vitro* complement activation also coincided with the *in vivo* deposition of C3c after intraperitoneal implantation of AP microcapsules. The deposition of activated C3 has previously been shown to promote leukocyte adhesion [14] and is likely connected to the substantial PFO response on the AP microcapsules found at day 2 (data not shown). This corresponds with previous findings of PFO induced by Poly-L-lysine on microcapsules [12,13]. The PFO response of alginate microbeads seems to appear later, and thus could be induced by other pathways than complement. This is in correspondence with the whole blood findings of the current work, and also previously concluded by Doloff et al. [6]. However, the sulfated alginate microbeads displayed low PFO in conjunction with the lowest complement activation of microbeads. Previously, sulfated alginate in solution has been shown to reduce complement activation [27], whereas sulfated alginate microbeads bind complement factor H [22]. Of note, factor H inhibits complement activation by preventing the action of the opsonin C3b, firstly, by acting as a cofactor to factor I (enzymatic factor C3b inactivator), and secondly, by exerting an inhibitory effect on C3 convertases which catalyze the formation of activated C3b [43,44]. The binding of factor H to sulfated alginate microbeads could thus be an important inherent property contributing to the low complement activating potential. Thus, we cannot fully exclude the involvement of complement in PFO in the present study. On the other hand, the introduction of sulfate groups could potentially interact with other pathways as discussed below.

Sulfation of alginate results in substitution of hydroxyl groups with sulfate groups on C2 and/or C3 [27]. Due to the presence of sulfate groups on 1,4-linked uronic acid polysaccharides, the structure-function properties of sulfated alginate have been compared to those of heparin [27,42], and promote interactions with various proteins [22,45]. Heparin is known for its anticoagulatory effects, and, importantly, its ability to bind Mac-1 (leukocyte integrin) as well as L and P selectins [46–48]. Hypothetically, sulfated alginate might similarly hamper several modes of cellular adhesion that may be involved in PFO. Heparin also interacts with several proteins of both the complement and coagulation cascades [48]. Thus, sulfated alginates could possibly interfere with proteins of both the coagulation cascade and complement system, as discussed above for factor H [22]. This is further supported by the sulfated alginate microbeads' unique ability to potentiate coagulation activation in the human whole blood assay in this study. Although the mechanisms are not fully understood [42], sulfated alginate has been shown to inhibit coagulation in high doses and stimulate coagulation in low doses [49]. Thus, the current finding could be dependent on the concentration of sulfated alginate. Arlov & Skjåk-Bræk postulate that there may be interactions of sulfated alginate with coagulation cascade proteases or sequestration of coagulate precursors such as fibrinogen [42].

The adsorption of fibrinogen to alginate microspheres, *in vivo*, was investigated by CLSM. Protein adsorption to biomaterial surfaces is regarded as a deciding factor for the activation of inflammatory protein cascades, cell adhesion and, accordingly, the *in vivo* outcome [5]. Interestingly, in the current work, the deposition of fibrinogen coincided with the degree of PFO. Intermediate G and sulfated alginate microbeads displayed both minimal PFO and low fibrinogen deposition, in contrast to microbeads composed of high

G alginate. Furthermore, we observed a greater deposition of fibrinogen on the low concentration high G alginate microbeads (HiG (0.7%)) compared to higher concentration high G microbeads (HiG). This may indicate other factors than the chemical composition of the alginate as contributors to the PFO observed in this study. It has been shown that physical properties such as surface structure can affect fibrosis [50]. Here, a lower concentration of alginate could contribute to a rougher surface structure [51] and possibly increased fibrosis. However, further studies are needed to investigate this aspect. The promising intermediate G and sulfated alginate microbeads differed in their fibrinogen adsorption patterns. Intermediate G microbeads showed an uneven (spotted) and more variable distribution of adsorbed fibrinogen that increased with time. Sulfated alginate microbeads consistently exhibited a low-grade evenly distributed fibrinogen layer and remained unchanged over time. The hypothesized sequestration of fibrinogen by sulfated alginate proposed by Arlov & Skjåk-Bræk [42] may explain the low levels of detected fibrinogen on these microbeads. This sequestration may mask epitopes for cell adhesion on fibrinogen, and accordingly be relevant to the development of PFO. A limitation with our study was the use of a polyclonal antibody against fibrinogen that could bind several epitopes, and not exclusively those involved in cell adhesion.

Adsorption of fibrinogen has been described as a critical determinant of subsequent inflammatory cell responses following biomaterial implantation, where the accumulation of fibrinogen directs the recruitment of phagocytic cells (i.e., monocyte/macrophages and neutrophils) to implant surfaces both in mice [52] and humans [53]. Numerous recognition sites for cell receptors have been identified, and the pro-inflammatory function has largely been ascribed to its interaction with distinct integrin receptors [54]. Notably, fibrinogen mediates cell adhesion to biomaterials through the integrin receptor Mac-1 [55], expressed on leukocytes, macrophages and monocytes. It has been proposed that mitigating fibrinogen adsorption to implant surfaces may enhance the biocompatibility [53]. In accordance with previous studies, this study corroborates the link between deposition of fibrinogen and cell adhesion to implanted biomaterials.

Several types of microbeads based on intermediate G alginate or sulfated alginate gelled either with Ca^{2+}/Ba^{2+} or Sr^{2+} were largely free of PFO in this study, indicating a level of flexibility within the microbead formulations. In recent studies, chemical modifications of alginate by grafting with triazole-containing molecules [9] or with zwitterions based on sulfobetaine and carboxybetaine [10] has resulted in microbeads that mitigate PFO in C57BL/6J mice and monkeys or mice, dogs and pigs, respectively. Safley and collaborators had a positive outcome with respect to PFO in monkeys using microspheres of intermediate G [23]. In this study, alginates with a high content of G resulted in PFO, whereas intermediate G alginate resulted in microbeads with minimal PFO. Interestingly, intermediate-G alginate microbeads with a smaller fraction (36 %) of alginate with a high G content also resulted in microbeads with minimal PFO after 14 days. No clear link between PFO and the estimated gel stiffness of the materials was found in the current study, in contrast to what has been shown for other hydrogel systems [35]. Alginate composition and hydrogel stiffness can be tailored using epimerized alginates [56]. This may clarify the intricate relationship between alginate structure and PFO, and accordingly enable tailoring of microbeads with low PFO responses. In addition, our observations of the positive association between fibrinogen deposition and PFO on alginate microbeads may reveal mechanistic insight to the still underdetermined causes of the PFO response. The use of intermediate G alginate constitutes a straightforward approach to produce fibrosis free microbeads compared to chemically or enzymatically modified alginates. However, as alginates are a group of linear yet heterogeneous polysaccharides with respect to composition and molecular weight, fractions of soluble high M alginate may induce inflammatory responses [57,58]. For sulfated alginate, the biological activities such as the effects on coagulation should be elucidated for the clinical use of this material. Future studies will include *in vivo* function of cells encapsulated in the microbeads with limited PFO, which will further investigate the therapeutic efficacy of the microbeads.

Conclusion

This study has shown that microbeads with intermediate G- or sulfated alginate yield minimal PFO in immunocompetent mice and demonstrated their potential as long-term implantable biomaterials. Stable alginate microbeads were produced by ionic crosslinking with calcium together with barium in low concentration. The microbeads elicited low responses in human whole blood with respect to complement and inflammatory cytokines. Distinctively, the microbeads with sulfated alginate activated coagulation. Fibrinogen deposition on microspheres explanted from mice was positively associated with PFO. Microbeads with high G alginate showed both high degrees of PFO and fibrinogen deposition. Microbeads with intermediate G- or sulfated alginate displayed low PFO in conjunction with low fibrinogen deposition. An overall low deposition of complement C3 was found on all alginate microbeads, whereas a positive association with PFO and complement response was seen for microcapsules containing poly-L-lysine. Our study points to the importance of protein deposition at the biomaterial-host interface which is believed to govern the fate of the biomaterial. In-depth studies to identify and quantify proteins adherent to the microsphere surface could provide further insight into the mechanisms leading to PFO.

Declaration of Competing Interest

The authors declare that they have no known competing financial interests or personal relationships that could have appeared to influence the work reported in this paper.

CRediT authorship contribution statement

Abba E. Coron: Conceptualization, Methodology, Validation, Formal analysis, Investigation, Resources, Writing – original draft, Writing – review & editing, Visualization. **Joachim S. Kjesbu:** Conceptualization, Methodology, Validation, Investigation, Resources, Writing – original draft, Writing – review & editing, Visualization. **Fredrikke Kjærnsmo:** Investigation, Formal analysis. **José Oberholzer:** Conceptualization, Methodology, Writing – review & editing, Funding acquisition. **Anne Mari A. Rokstad:** Conceptualization, Methodology, Validation, Investigation, Resources, Writing – review & editing, Supervision, Project administration, Funding acquisition. **Berit L. Strand:** Conceptualization, Methodology, Validation, Writing – review & editing, Supervision, Project administration, Funding acquisition.

Acknowledgements

We thank professor emeritus Gudmund Skjåk-Bræk, NTNU, for support on the development of sulfated alginate as well as on previous work on alginate microspheres. Wenche I. Strand is credited for performing, in large part, characterization of alginates using ^{1}H-NMR as well as purification of alginates. Ann-Sissel T. Ulset is acknowledged for performing SEC-MALLS analysis on alginates. Their work was performed at the Department of Biotechnology and Food Science, at the Norwegian University of Science and Technology. Liv Ryan is acknowledged for conducting the multiplex analysis at CEMIR, Department of Clinical and Molecular Medicine, at

the Norwegian University of Science and Technology. Øystein Arlov at the SINTEF research institute is credited for providing insight into the sulfation of alginate.

Funding

This work was supported by the Norwegian University of Science and Technology (NTNU), Faculty for Natural Science, The Liaison Committee for Education, Research, and Innovation in Central Norway (Regional Health Authority, Samarbeidsorganet) under grant 46056819, NTNU Health and the Chicago Diabetes Project (www.chicagodiabetesproject.org).

Data availability

The raw/processed data required to reproduce these findings cannot be shared at this time due to technical or time limitations.

Supplementary materials

Supplementary material associated with this article can be found, in the online version, at doi:10.1016/j.actbio.2021.10.004.

References

[1] B.L. Strand, A.E. Coron, G. Skjåk-Bræk, Current and future perspectives on alginate encapsulated pancreatic islet, Stem Cells Transl. Med. 6 (4) (2017) 1053–1058.
[2] A.M.A. Rokstad, I. Lacík, P. de Vos, B.L. Strand, Advances in biocompatibility and physico-chemical characterization of microspheres for cell encapsulation, Adv. Drug. Deliv. Rev. 67-68 (2014) 111–130.
[3] B.E. Tuch, G.W. Keogh, L.J. Williams, W. Wu, J.L. Foster, V. Vaithilingam, R. Philips, Safety and viability of microencapsulated human islets transplanted into diabetic humans, Diabetes Care 32 (10) (2009) 1887–1889.
[4] D. Jacobs-Tulleneers-Thevissen, M. Chintinne, Z. Ling, P. Gillard, L. Schoonjans, G. Delvaux, B.L. Strand, F. Gorus, B. Keymeulen, D. Pipeleers, Sustained function of alginate-encapsulated human islet cell implants in the peritoneal cavity of mice leading to a pilot study in a type 1 diabetic patient, Diabetologia 56 (7) (2013) 1605–1614.
[5] J.M. Anderson, A. Rodriguez, D.T. Chang, Foreign body reaction to biomaterials, Semin. Immunol. 20 (2) (2008) 86–100.
[6] J.C. Doloff, O. Veiseh, A.J. Vegas, H.H. Tam, S. Farah, M. Ma, J. Li, A. Bader, A. Chiu, A. Sadraei, S. Aresta-Dasilva, M. Griffin, S. Jhunjhunwala, M. Webber, S. Siebert, K. Tang, M. Chen, E. Langan, N. Dholokia, R. Thakrar, M. Qi, J. Oberholzer, D.L. Greiner, R. Langer, D.G. Anderson, Colony stimulating factor-1 receptor is a central component of the foreign body response to biomaterial implants in rodents and non-human primates, Nat. Mater. 16 (6) (2017) 671–680.
[7] O. Veiseh, J.C. Doloff, M. Ma, A.J. Vegas, H.H. Tam, A.R. Bader, J. Li, E. Langan, J. Wyckoff, W.S. Loo, S. Jhunjhunwala, A. Chiu, S. Siebert, K. Tang, J. Hollister-Lock, S. Aresta-Dasilva, M. Bochenek, J. Mendoza-Elias, Y. Wang, M. Qi, D.M. Lavin, M. Chen, N. Dholakia, R. Thakrar, I. Lacik, G.C. Weir, J. Oberholzer, D.L. Greiner, R. Langer, D.G. Anderson, Size and shape-dependent foreign body immune response to materials implanted in rodents and non-human primates, Nat. Mater. 14 (6) (2015) 643–651.
[8] A.J. Vegas, O. Veiseh, J.C. Doloff, M. Ma, H.H. Tam, K. Bratlie, J. Li, A.R. Bader, E. Langan, K. Olejnik, P. Fenton, J.W. Kang, J. Hollister-Locke, M.A. Bochenek, A. Chiu, S. Siebert, K. Tang, S. Jhunjhunwala, S. Aresta-Dasilva, N. Dholakia, R. Thakrar, T. Vietti, M. Chen, J. Cohen, K. Siniakowicz, M. Qi, J. McGarrigle, A.C. Graham, S. Lyle, D.M. Harlan, D.L. Greiner, J. Oberholzer, G.C. Weir, R. Langer, D.G. Anderson, Combinatorial hydrogel library enables identification of materials that mitigate the foreign body response in primates, Nat. Biotechnol. 34 (3) (2016) 345–352.
[9] M.A. Bochenek, O. Veiseh, A.J. Vegas, J.J. McGarrigle, M. Qi, E. Marchese, M. Omami, J.C. Doloff, J. Mendoza-Elias, M. Nourmohammadzadeh, A. Khan, C.C. Yeh, Y. Xing, D. Isa, S. Ghani, J. Li, C. Landry, A.R. Bader, K. Olejnik, M. Chen, J. Hollister-Lock, Y. Wang, D.L. Greiner, G.C. Weir, B.L. Strand, A.M.A. Rokstad, I. Lacik, R. Langer, D.G. Anderson, J. Oberholzer, Alginate encapsulation as long-term immune protection of allogeneic pancreatic islet cells transplanted into the omental bursa of macaques, Nat. Biomed. Eng. 2 (11) (2018) 810–821.
[10] Q. Liu, A. Chiu, L.H. Wang, D. An, M. Zhong, A.M. Smink, B.J. de Haan, P. de Vos, K. Keane, A. Vegge, E.Y. Chen, W. Song, W.F. Liu, J. Flanders, C. Rescan, L.G. Grunnet, X. Wang, M. Ma, Zwitterionically modified alginates mitigate cellular overgrowth for cell encapsulation, Nat. Commun. 10 (1) (2019) 5262.
[11] S.K. Tam, J. Dusseault, S. Bilodeau, G. Langlois, J.P. Halle, L. Yahia, Factors influencing alginate gel biocompatibility, J. Biomed. Mater. Res. A 98 (1) (2011) 40–52.
[12] A. King, S. Sandler, A. Andersson, The effect of host factors and capsule composition on the cellular overgrowth on implanted alginate capsules, J. Biomed. Mater. Res. 57 (3) (2001) 374–383.
[13] B.L. Strand, T.L. Ryan, P. In't Veld, B. Kulseng, A.M. Rokstad, G. Skjåk-Bræk, T. Espevik, Poly-L-Lysine induces fibrosis on alginate microcapsules via the induction of cytokines, Cell Transplant 10 (3) (2001) 263–275.
[14] P. Ørning, K.S. Hoem, A.E. Coron, G. Skjåk-Bræk, T.E. Mollnes, O.-L. Brekke, T. Espevik, A.M. Rokstad, Alginate microsphere compositions dictate different mechanisms of complement activation with consequences for cytokine release and leukocyte activation, J. Control. Release 229 (2016) 58–69.
[15] C. Gravastrand, S. Hamad, H. Fure, B. Steinkjer, L. Ryan, J. Oberholzer, J. Lambris, I. Lacík, T. Mollnes, T. Espevik, O.-L. Brekke, A.M. Rokstad, Alginate microbeads are coagulation compatible, while alginate microcapsules activate coagulation secondary to complement or directly through FXII, Acta Biomater. 58 (2017) 158–167.
[16] A.M. Rokstad, O.L. Brekke, B. Steinkjer, L. Ryan, G. Kollárikovà, B.L. Strand, G. Skjåk-Bræk, J.D. Lambris, I. Lacík, T.E. Mollnes, T. Espevik, The induction of cytokines by polycation containing microspheres by a complement dependent mechanism, Biomaterials 34 (3) (2013) 621–630.
[17] V. Vaithilingam, B. Steinkjer, L. Ryan, R. Larsson, B. Tuch, J. Oberholzer, A.M. Rokstad, Vitro and in vivo biocompatibility evaluation of polyallylamine and macromolecular heparin conjugates modified alginate microbeads, Sci. Rep. (2017) 7.
[18] A.M. Rokstad, O.-L. Brekke, B. Steinkjer, L. Ryan, G. Kollárikovà, B.L. Strand, G. Skjåk-Bræk, I. Lacík, T. Espevik, T.E. Mollnes, Alginate microbeads are complement compatible, in contrast to polycation containing microcapsules, as revealed in a human whole blood model, Acta Biomater. 7 (6) (2011) 2566–2578.
[19] Y.A. Mørch, I. Donati, B.L. Strand, G. Skjak-Bræk, Effect of Ca2+, Ba2+, and Sr2+ on alginate microbeads, Biomacromolecules 7 (5) (2006) 1471–1480.
[20] M. Qi, B.L. Strand, Y. Mørch, I. Lacík, Y. Wang, P. Salehi, B. Barbaro, A. Gangemi, J. Kuechle, T. Romagnoli, M.A. Hansen, L.A. Rodriguez, E. Benedetti, D. Hunkeler, G. Skjåk-Bræk, J. Oberholzer, Encapsulation of human islets in novel inhomogeneous alginate-Ca2+/Ba2+ microbeads: in vitro and in vivo function. artificial cells, Blood Substitutes, Biotechnol. 36 (5) (2008) 403–420.
[21] Y.A. Mørch, M. Qi, P.O. Gundersen, K. Formo, I. Lacik, G. Skjåk-Bræk, J. Oberholzer, B.L. Strand, Binding and leakage of barium in alginate microbeads, J. Biomed. Mater. Res. A 100 (11) (2012) 2939–2947.
[22] Ø. Arlov, G. Skjåk-Bræk, A.M. Rokstad, Sulfated alginate microspheres associate with factor H and dampen the inflammatory cytokine response, Acta Biomater. 42 (2016) 180–188.
[23] S.A. Safley, N.S. Kenyon, D.M. Berman, G.F. Barber, H. Cui, S. Duncanson, T. De Toni, M. Willman, P. De Vos, A.A. Tomei, A. Sambanis, N.M. Kenyon, C. Ricordi, C.J. Weber, Microencapsulated islet allografts in diabetic NOD mice and nonhuman primates, Eur. Rev. Med. Pharmacol. Sci. 24 (16) (2020) 8551–8565.
[24] H. Grasdalen, B. Larsen, O. Smidsrød, A p.m.r. study of the composition and sequence of uronate residues in alginates, Carbohydr. Res. 68 (1) (1979) 23–31.
[25] H. Grasdalen, High-field, 1H-n.m.r. spectroscopy of alginate: sequential structure and linkage conformations, Carbohydr. Res. 118 (1983) 255–260.
[26] I.M.N. Vold, K.A. Kristiansen, B.E. Christensen, A study of the chain stiffness and extension of alginates, in vitro epimerized alginates, and periodate-oxidized alginates using size-exclusion chromatography combined with light scattering and viscosity detectors, Biomacromolecules 7 (7) (2006) 2136–2146.
[27] Ø. Arlov, F.L. Aachmann, A. Sundan, T. Espevik, G. Skjåk-Bræk, Heparin-like properties of sulfated alginates with defined sequences and sulfation degrees, Biomacromolecules 15 (7) (2014) 2744–2750.
[28] Ø. Arlov, F.L. Aachmann, E. Feyzi, A. Sundan, G. Skjåk-Bræk, The impact of chain length and flexibility in the interaction between sulfated alginates and HGF and FGF-2, Biomacromolecules 16 (11) (2015) 3417–3424.
[29] B.L. Strand, Y.A. Mørch, K.R. Syvertsen, T. Espevik, G. Skjåk-Bræk, Microcapsules made by enzymatically tailored alginate, J. Biomed. Mater. Res. A 64 (3) (2003) 540–550.
[30] K. Ingar Draget, K. Østgaard, O. Smidsrød, Homogeneous alginate gels: a technical approach, Carbohydr. Polym. 14 (2) (1990) 159–178.
[31] Arne O.H. Smidsrød, Bjørn Lian, Properties of poly(1,4-hexuronates) in the gel state. I. evaluation of a method for the determination of stiffness, Acta Chemica. Scandinavia 26 (1972) 79–88.
[32] A. Martinsen, G. Skjåk-Bræk, O. Smidsrød, Alginate as immobilization material: I. correlation between chemical and physical properties of alginate gel beads, Biotechnol. Bioeng. 33 (1) (1989) 79–89.
[33] V. Vaithilingam, G. Kollarikova, M. Qi, I. Lacik, J. Oberholzer, G.J. Guillemin, B.E. Tuch, Effect of prolonged gelling time on the intrinsic properties of barium alginate microcapsules and its biocompatibility, J. Microencapsul. 28 (6) (2011) 499–507.
[34] T.E. Mollnes, O.-L. Brekke, M. Fung, H. Fure, D. Christiansen, G. Bergseth, V. Videm, K.T. Lappegård, J.r. Köhl, J.D. Lambris, Essential role of the C5a receptor in E coli–induced oxidative burst and phagocytosis revealed by a novel lepirudin-based human whole blood model of inflammation, Blood 100 (5) (2002) 1869–1877.
[35] Z. Zhuang, Y. Zhang, S. Sun, Q. Li, K. Chen, C. An, L. Wang, J.J.J.P. van den Beucken, H. Wang, Control of matrix stiffness using methacrylate–gelatin hydrogels for a macrophage-mediated inflammatory response, ACS Biomater. Sci. Eng. 6 (5) (2020) 3091–3102.
[36] B. Thu, P. Bruheim, T. Espevik, O. Smidsrød, P. Soon-Shiong, G. Skjåk-Bræk, Alginate polycation microcapsules: I. Interaction between alginate and polycation, Biomaterials 17 (10) (1996) 1031–1040.
[37] B. Thu, P. Bruheim, T. Espevik, O. Smidsrød, P. Soon-Shiong, G. Skjåk-Bræk, Alginate polycation microcapsules: II. Some functional properties, Biomaterials 17 (11) (1996) 1069–1079.

[38] K.Y. Lee, D.J. Mooney, Hydrogels for tissue engineering, Chem. Rev. 101 (7) (2001) 1869–1880.
[39] D.E. Discher, D.J. Mooney, P.W. Zandstra, Growth factors, matrices, and forces combine and control stem cells, Science 324 (5935) (2009) 1673–1677.
[40] G. Chan, D.J. Mooney, Ca2+ released from calcium alginate gels can promote inflammatory responses in vitro and in vivo, Acta Biomater. 9 (12) (2013) 9281–9291.
[41] J.E. Melvik, M. Dornish, Use of alginate matrices to control cell growth, in: FMC Biopolymer AS: United States Patent, 7, 2005, pp. 1–12. 790,193.
[42] Ø. Arlov, G. Skjåk-Bræk, Sulfated alginates as heparin analogues: a review of chemical and functional properties, Molecules 22 (5) (2017).
[43] J. Wu, Y.Q. Wu, D. Ricklin, B.J. Janssen, J.D. Lambris, P. Gros, Structure of complement fragment C3b-factor H and implications for host protection by complement regulators, Nat. Immunol. 10 (7) (2009) 728–733.
[44] S. Bettoni, E. Bresin, G. Remuzzi, M. Noris, R. Donadelli, Insights into the effects of complement factor H on the assembly and decay of the alternative pathway C3 proconvertase and C3 convertase, J. Biol. Chem. 291 (15) (2016) 8214–8230.
[45] I. Freeman, A. Kedem, S. Cohen, The effect of sulfation of alginate hydrogels on the specific binding and controlled release of heparin-binding proteins, Biomaterials 29 (22) (2008) 3260–3268.
[46] K. Peter, M. Schwarz, C. Conradt, T. Nordt, M. Moser, W. Kübler, C. Bode, Heparin inhibits ligand binding to the leukocyte integrin Mac-1 (CD11b/CD18), Circulation 100 (14) (1999) 1533–1539.
[47] A. Koenig, K. Norgard-Sumnicht, R. Linhardt, A. Varki, Differential interactions of heparin and heparan sulfate glycosaminoglycans with the selectins. Implications for the use of unfractionated and low molecular weight heparins as therapeutic agents, J. Clin. Invest 101 (4) (1998) 877–889.
[48] B. Mulloy, J. Hogwood, E. Gray, R. Lever, C.P. Page, Pharmacology of heparin and related drugs, Pharmacol. Rev. 68 (1) (2016) 76–141.
[49] G. Kopplin, A.M. Rokstad, H. Mélida, V. Bulone, G. Skjåk-Bræk, F. Aachmann, Structural characterization of fucoidan from laminaria hyperborea: assessment of coagulation and inflammatory properties and their structure–function relationship, ACS Appl. Bio. Mater. 1 (6) (2018) 1880–1892.
[50] J.C. Doloff, O. Veiseh, R. de Mezerville, M. Sforza, T.A. Perry, J. Haupt, M. Jamiel, C. Chambers, A. Nash, S. Aghlara-Fotovat, J.L. Stelzel, S.J. Bauer, S.Y. Neshat, J. Hancock, N.A. Romero, Y.E. Hidalgo, I.M. Leiva, A.M. Munhoz, A. Bayat, B.M. Kinney, H.C. Hodges, R.N. Miranda, M.W. Clemens, R. Langer, The surface topography of silicone breast implants mediates the foreign body response in mice, rabbits and humans, Nat. Biomed. Eng. (2021).
[51] M. Lekka, D. Sainz-Serp, A.J. Kulik, C. Wandrey, Hydrogel microspheres: influence of chemical composition on surface morphology, local elastic properties, and bulk mechanical characteristics, Langmuir 20 (23) (2004) 9968–9977.
[52] L. Tang, J.W. Eaton, Fibrin(ogen) mediates acute inflammatory responses to biomaterials, J. Exp. Med. 178 (6) (1993) 2147–2156.
[53] J. Zdolsek, J.W. Eaton, L. Tang, Histamine release and fibrinogen adsorption mediate acute inflammatory responses to biomaterial implants in humans, J. Transl. Med. 5 (2007) 31.
[54] R.A. Adams, M. Passino, B.D. Sachs, T. Nuriel, K. Akassoglou, Fibrin mechanisms and functions in nervous system pathology, Mol. Interv. 4 (3) (2004) 163–176.
[55] L. Tang, T.P. Ugarova, E.F. Plow, J.W. Eaton, Molecular determinants of acute inflammatory responses to biomaterials, J. Clin. Invest. 97 (5) (1996) 1329–1334.
[56] Y.A. Mørch, S. Holtan, I. Donati, B.L. Strand, G. Skjåk-Bræk, Mechanical properties of C-5 epimerized alginates, Biomacromolecules 9 (9) (2008) 2360–2368.
[57] M. Otterlei, K. Østgaard, G. Skjåk-Bræk, O. Smidsrød, P. Soon-Shiong, T. Espevik, Induction of cytokine production from human monocytes stimulated with alginate, J. Immunother 10 (4) (1991) 286–291 1991.
[58] T. Flo, L. Ryan, E. Latz, O. Takeuchi, B. Monks, E. Lien, Ø. Halaas, S. Akira, G. Skjåk-Bræk, D. Golenbock, T. Espevik, Involvement of toll-like receptor (TLR) 2 and TLR4 in cell activation by mannuronic acid polymers, J. Biol. Chem. 277 (2002) 35489–35495.

Paper III

Materials Today Bio 17 (2022) 100490

Contents lists available at ScienceDirect

Materials Today Bio

journal homepage: www.journals.elsevier.com/materials-today-bio

MS-proteomics provides insight into the host responses towards alginate microspheres

Abba E. Coron [a,b,d], Davi M. Fonseca [b,c], Animesh Sharma [b,c], Geir Slupphaug [b,c,1], Berit L. Strand [a,1], Anne Mari A. Rokstad [b,d,e,1,*]

[a] The Norwegian Biopolymer Laboratory (NOBIPOL), Department of Biotechnology and Food Science, Norwegian University of Science and Technology (NTNU), N-7491, Trondheim, Norway
[b] Department of Clinical and Molecular Medicine, NTNU, N-7491, Trondheim, Norway
[c] Proteomics and Modomics Experimental Core (PROMEC), NTNU and the Central Norway Regional Health Authority, N-7491, Trondheim, Norway
[d] Centre of Molecular Inflammation Research (CEMIR), Department of Clinical and Molecular Medicine, NTNU, N-7491, Trondheim, Norway
[e] Centre of Obesity, Clinic of Surgery, St. Olav's University Hospital, NO-7006, Trondheim, Norway

ARTICLE INFO

Keywords:
Alginate hydrogel microspheres
Proteomics
Protein adsorption
Complement
Coagulation
Immune profiling

ABSTRACT

Protein adsorption to biomaterial surfaces is considered a determining factor for the host response. Here we detail the protein adsorption profiles of alginate hydrogel microspheres relevant for cell therapy using mass spectrometry (MS)-based proteomics. The investigated microspheres include sulfated alginate (SA), high G alginate (HiG), and poly-L-lysine coated alginate (AP), which previously have been shown to exhibit different inflammatory and fibrotic responses. The biological significance was assessed in lepirudin-anticoagulated human whole blood (hWB) by functional analysis of the acute-phase responses (complement and coagulation). Proteomic profiling revealed distinct signatures for the microspheres, wherein Ingenuity Pathway Analysis identified complement and coagulation as the top enriched canonical pathways. The levels of complement and coagulation activators and inhibitors were distinctly different, which was reflected in the functional hWB analyses: SA was highly enriched with inhibitory factors of complement and coagulation (e.g. C1 inhibitor, factor H, antithrombin-III, heparin cofactor 2), other heparin-binding proteins and factors promoting fibrinolysis (factor XII, plasma kallikrein), conforming to an anti-inflammatory and anti-fibrotic profile. HiG enriched moderate levels of complement inhibitors, conforming to a low-inflammatory and pro-fibrotic profile. AP showed the most prominent enrichment of complement activators (e.g. C3, properdin, C-reactive protein) and low levels of inhibitors, conforming to a pro-inflammatory and highly pro-fibrotic profile. In conclusion, the extensive enrichment of inhibitory acute-phase proteins on SA could be a determining factor for its reduced host response. The interactions between the plasma proteins and hydrogel surfaces shown herein point to proteomics as an important supplement to existing *in vitro* and *in vivo* methods for designing biocompatible alginate-based hydrogels.

1. Introduction

The use of alginate hydrogel microspheres for immunoisolation in cell therapy holds great promise for treating various medical conditions, e.g. type 1 diabetes or acute liver failure, mitigating the need for systemic immunosuppressive treatment after graft transplantation [1–3]. However, implantation of biomaterials may result in acute and chronic inflammatory responses that lead to fibrotic tissue development, as part of the foreign body response [4]. For microspheres used in cell therapy, pericapsular fibrotic overgrowth (PFO) constitutes a major challenge, in which immune cells (neutrophils, macrophages) and fibroblasts hinder the diffusion of nutrients and oxygen, thus compromising the viability and function of the encapsulated cells [5,6]. Insight into the mechanistic cues associated with PFO will advance the development of high-performance, biocompatible materials for cell and tissue transplantation, with further impact on diagnostic sensors and implants. The initial protein adsorption to implanted biomaterials is considered a determining factor for the subsequent host responses [4,7,8]. Here, we investigate the protein adsorption profiles of three types of alginate microspheres that have previously been used or are promising candidates

* Corresponding author. NTNU, Faculty of Medicine and Health Sciences, CEMIR, NO-7491, Trondheim, Norway.
E-mail address: anne.m.rokstad@ntnu.no (A.M.A. Rokstad).
[1] Equal contribution.

https://doi.org/10.1016/j.mtbio.2022.100490
Received 22 July 2022; Received in revised form 8 November 2022; Accepted 9 November 2022
Available online 11 November 2022

for clinical transplantation [1,9,10], which we recently assessed in terms of inflammatory and fibrotic potentials using *in vitro* and *in vivo* models [10]. Proteomics could serve as a complementary method to understand the initial protein adsorption important for the design and selection of alginate microspheres with reduced host responses.

Alginate hydrogels are ionically crosslinked networks (e.g. with Ca^{2+}, Sr^{2+}, Ba^{2+}) of linear, anionic polysaccharides that consist of (1,4)-linked α-L-mannuronate (M) and β-D-guluronate (G) residues. The hydrogel is formed under physiological conditions, and the high water content (98–99%) allows for rapid diffusion of nutrients and oxygen to encapsulated cells, ensuring cell viability and function. Although generally regarded as biocompatible, the detailed design of alginate-based microspheres ultimately determines the onset of PFO and the long-term function of encapsulated cells *in vivo* [2,5]. Microspheres that are prone to PFO include the widely studied high G alginate microbeads [1,2,10,11], where the PFO response is exacerbated by coating with polyamines (e.g. poly-L-lysine; PLL) [2,12,13]. The prominent PFO response of PLL-coated microspheres [2,12] can be ascribed to surface-deposited complement C3, leading to leukocyte adhesion and subsequent induction of pro-inflammatory cytokines [14–16]. Several studies have demonstrated the involvement of complement activation/deposition (including complement C3) on biomaterial surfaces in promoting leukocyte activation/adhesion [14,15,17–20], pro-inflammatory cytokine induction [14–17] as well as inflammatory cell recruitment or fibrotic tissue formation after implantation [17,19]. Mitigation of the PFO response has been achieved by modulating microsphere composition using intermediate G alginates [10,11,21] or chemically modified alginates [2,10,22,23]. Alginates modified by chemical sulfation have been shown to display anti-inflammatory properties [10,24,25] and bind growth factors [24,26] and anti-complement factor H [25]. In a recent study [10], we reported minimal PFO for microbeads containing a mixture of sulfated alginate and high G alginate (SA) using the immunocompetent C57BL/6JRj mouse model. Contrastingly, PFO was found on high G alginate microbeads (HiG) and to an even larger extent on PLL-coated high G alginate microbeads (AP). In detail, the anti-fibrotic SA as well as the fibrotic HiG induced overall low cytokine and complement responses *in vitro* and minimal C3 deposition *in vivo*. The highly fibrotic AP induced higher pro-inflammatory cytokine responses and significant complement activation *in vitro* and displayed marked C3 deposition *in vivo*. Fibrin(ogen) deposition on the microspheres was found to coincide with PFO, further pointing to distinct protein deposition as a potential contributing factor to PFO. In the current proteomic study, we further analyse these microspheres with respect to protein adsorption in human plasma and link the proteomic findings to the inflammatory and fibrotic potentials of the different materials.

Mass spectrometry (MS)-based proteomic analysis represents an efficient and highly sensitive approach to identify protein adsorption profiles on biomaterial surfaces [7], and thus provides an additional means to predict biological performance and potentially reduce *in vivo* experimentation. To date, there is a limited number of proteomic studies that have addressed the adsorption of plasma or serum proteins to hydrogels [20,27,28], and neither of these encompassed alginate-based hydrogels or microspheres. Previous studies using MS-based proteomics have linked protein adsorption to the immune reactivity [20] or fibrotic tissue development [27] of poly(ethylene glycol) (PEG) hydrogels. The latter revealed an initial adsorption of acute-phase proteins for highly fibrotic PEG hydrogels explanted from mice [27]. More generally, there are few studies that directly correlate biomaterial protein adsorption using proteomics with *in vivo* performance [7,29]. In a collection of studies (e.g. Refs. [30,31]), Romero-Gavilán and co-workers characterise distinct protein layers on titanium-based implants using human serum. The authors correlate the differentially adsorbed proteins (mainly complement related) to the level of fibrotic tissue development and osseointegration in rabbits. Using the same animal model and calcium-doped materials, they also found distinct enrichment of proteins associated with coagulation, inflammation, and osteogenic functions, which were linked to the materials' regenerative potential *in vivo* [32]. Buck et al. showed that surface functionalisation of poly(ether ether ketone) (PEEK) implants significantly altered the adsorption of serum proteins (predominantly acute-phase proteins and apolipoproteins), where implantation into rats revealed similar levels of osseointegration despite different macrophage responses *in vitro* [33]. The protein adsorption to nanoparticles and its effect on biological performance *in vivo* has also been described [34–36].

Protein adsorption is a complex and dynamic process in which proteins attach and detach depending on the properties of the surface, proteins, and surrounding solution [37,38]. Protein adsorption has been linked to the biomaterials' chemical properties [39], surface charge [8] and topography [40]. In addition to non-covalent surface interactions (e.g. electrostatic, hydrophobic) that can result in conformational changes potentially affecting the bioactivity of adsorbing proteins, the proteins may also *react* with the biomaterial surface as well as surface-associated proteins. These features are well-recognised for the complement and coagulation proteins, which are critical components of the acute-phase responses in host defence [41]. Adsorbed complement activators and inhibitors have been suggested to be strong indicators for the biocompatibility of biomaterial surfaces [8,42]. The current study was designed to preserve the proteolytic cascades of complement and coagulation by using the anticoagulant lepirudin. This anticoagulant does not interfere with the complement proteins or coagulation proteins upstream of thrombin, in contrast to heparin which interferes with both systems [43,44]. In addition, the anticoagulants citrate and EDTA, commonly used in studies assessing the binding of plasma proteins to biomaterials, also interfere with the reactivity of the complement and coagulation systems by chelating calcium. Lepirudin has been used as an anticoagulant in several studies on inflammatory responses in whole blood, including studies on dialysis membranes [45], glucose sensors [46], polyvinyl chloride surfaces [47], and alginate microspheres [14–16,48].

Here, we present the first study on LC-MS/MS-based quantitative profiling of plasma proteins adsorbed to alginate hydrogel microspheres using a physiologically relevant human plasma model. Three types of microspheres were selected based on their different PFO responses and inflammatory potentials known from previous work [10]: HiG (low-inflammatory and fibrotic), SA (low-inflammatory and anti-fibrotic) and AP (pro-inflammatory and highly fibrotic). Unique protein signatures were identified for the different alginate microspheres. Immune profiles of the microspheres were detailed by combining proteomics and functional studies on initial inflammatory responses, with a particular focus on the acute-phase proteins of the complement and coagulation systems. This study represents a novel approach for elucidating proteomic profiles of alginate-based hydrogels that gives insight into the host-material interactions at the protein level, with potential relevance to PFO.

2. Materials and methods

2.1. Materials

Ultra-pure (UP) sodium alginates (endotoxin ≤43 EU/g) were from Novamatrix (Sandvika, Norway). UP-low-viscosity high G (LVG) alginate (68% guluronate [G], duplet fraction [F_{GG}] = 0.57, triplet fraction [F_{GGG}] = 0.53, average G-block length [$N_{G>1}$] = 16, weight average molecular weight [Mw] = 237 kDa) was used as gelling alginate. UP-medium-viscosity high G (MVG) alginate (66% G, F_{GG} = 0.55, F_{GGG} = 0.50, $N_{G>1}$ = 13, weight average Mw = 235 kDa) was used to produce sulfated alginate. Determination of the alginate chemical composition by H^1-NMR [49,50] and molecular weight by SEC-MALLS [51] has previously been described. Preparation of alginates and alginate microspheres included analytical grade $CaCl_2$, $BaCl_2$, NaCl, and formamide from Merck (Darmstadt, Germany). Poly-L-lysine (PLL) hydrochloride (Mw = 15–30 kDa) and chlorosulfonic acid (99%) were from Sigma-Aldrich (St. Louis, MO, USA). D(-)-Mannitol was from VWR International BVBA (Leuven,

Belgium) and non-pyrogenic sterile saline (0.9% NaCl) from B. Braun (Melsungen, Germany). Sulfated UP-MVG alginate was purified using Millistak+® CR40 activated carbon filter from Millipore (Billerica, MA, USA) and endotoxin-tested by QCL-1000™ Endpoint Chromogenic LAL Assay from Lonza (Walkersville, MD, USA). Human plasma and whole blood were anticoagulated with lepirudin (Refludan) from Celgene Europe (Boudry, Switzerland). Proteomic sample preparations employed the following (chemicals were at least pro analysis): urea, CHAPS hydrate, thiourea, DTT, ammonium bicarbonate, iodoacetamide, and solid-phase extraction disks (Empore C18, 47 mm) from Sigma-Aldrich; LC/MS grade: methanol, formic acid, acetonitrile, water, and Pierce trypsin from Thermo Fisher Scientific, USA; chloroform from VWR International S.A.S., France. For protein deposition studies by CLSM, FITC-conjugated polyclonal rabbit anti-human C3c (F0201) and C1q (F0254), including control antibody polyclonal rabbit-anti-mouse immunoglobulins (F0232), were from Dako (Glostrup, Denmark). Unconjugated polyclonal sheep anti-human FXII was from Nordic Diagnostica Service AB (HTI, Kungsbacka, Sweden), and secondary CF633-conjugated polyclonal donkey anti-sheep IgG was from Sigma-Aldrich. In the human whole blood experiment, assays used were enzyme-linked immunosorbent assay (ELISA) kit for Human Terminal Complement Complex (TCC) from Hycult Biotech (Uden, Netherlands), and ELISA kit Enzygnost® F1+2 monoclonal from Siemens Healthcare Diagnostics (Marburg, Germany). Low-activating polypropylene vials were from NUNC (Roskilde, Denmark). Glass control (BD vacutainer glass) was from Belliver Industrial Estate (Plymouth, UK), and PBS with $CaCl_2$ and $MgCl_2$ was purchased from Sigma-Aldrich.

2.2. Sulfation of alginate

Alginate was sulfated as previously described [24]. Briefly, chlorosulfonic acid was carefully added to a suspension of alginate (3.0 g) and formamide (120 mL) to a final concentration of 2.91% v/v. The mixture was incubated at 60 °C under continuous agitation for 2.5 h. Alginate was precipitated using cold acetone, centrifuged (10 °C, 3600×*g*, 7 min), redissolved in Milli-Q water and pH-neutralised. The alginate solution was dialysed against 100 mM NaCl, four times against Milli-Q water, and freeze-dried. The sulfur content of the alginate was determined to be 8.5% by high-resolution inductively coupled plasma mass spectrometry (HR-ICP-MS) at SINTEF, Trondheim, Norway. The degree of sulfation was estimated to be 0.83, as previously described [24]. Sulfated alginate was purified using an active carbon filter, and the level of endotoxins (LAL assay) was measured to 3.126 EU/mL.

2.3. Preparation of alginate microspheres

Three different microspheres were prepared using the same alginate formulations as in our recent study on PFO [10], comprising unmodified alginate (HiG), a mixture of 20% sulfated alginate and 80% unmodified alginate (SA), and unmodified alginate with PLL-coating (AP). Alginate solutions (5 mL) of 1.8% (w/v) were dripped into a gelling bath containing either 50 mM $CaCl_2$ with 1 mM $BaCl_2$ (HiG and SA) or 50 mM $CaCl_2$ (AP). All formulations were made using an electrostatic droplet generator operated at 7 kV, with a flow rate of 10 mL/h and needle size of 0.4 mm [52]. All solutions were sterile filtered, and the microspheres were prepared under sterile conditions. Alginate and gelling solutions were dissolved in 0.3 M and 0.15 M mannitol, respectively, and pH-adjusted to 7.2–7.3. Alginate microbeads were left for 10 min after the last formed droplet and washed in 0.9% NaCl (30 mL). AP-microspheres were subsequently incubated in 0.1% PLL dissolved in 0.9% NaCl (25 mL, pH = 7.35) for 10 min, and washed in 0.9% NaCl (30 mL). Each batch of microspheres was added 0.9% NaCl (50 mL) and aliquoted into samples containing 0.5 mL microspheres. Lastly, each aliquot was washed with 0.9% NaCl (2 × 1 mL) and further aliquoted into samples containing 50 μL microspheres. Microsphere diameters (mean ± SD of $n = 30$) were measured to 579 ± 17 μm (HiG), 565 ± 35 μm (SA) and 538 ± 34 μm (AP).

2.4. Proteomic sample preparation

2.4.1. Incubation of microspheres in human lepirudin-plasma

Alginate microspheres (50 μL) were incubated in pooled ($N = 7$) lepirudin-plasma (300 μL) for 24 h at 37 °C under rotation, with five replicates for each type of microsphere. Human blood was anticoagulated by adding lepirudin (50 μg/mL), centrifuged (1880×*g*, 15 min), and harvested plasma stored at -80 °C. Control samples comprised microspheres (50 μL) incubated in 300 μL 0.9% NaCl (saline control) and a pooled plasma control sample (10 μL). Low-activating polypropylene vials were used for all samples. Microspheres were washed in 0.9% NaCl (2 × 500 μL) to remove non-adsorbing proteins. Samples were stored in 0.9% NaCl (100 μL) at 4 °C. The storage solution was removed before analysis.

2.4.2. Primary elution of adsorbed plasma proteins (E-fraction)

Microspheres and control samples were incubated in 2D-PAGE buffer (100 μL, 7.0 M Urea, 2.0 M thiourea, 2.5% CHAPS, 25 mM DTT) for 2 h on a rotary shaker (37 °C, 400 rpm), and eluates were transferred to new tubes. 2D-buffer incubation was repeated (5 min), and the respective eluates were pooled. Eluates were stepwise added methanol (800 μL), chloroform (200 μL) and water (600 μL) with intermittent vortexing, and then centrifuged (16 000×*g*, 15 min). The top aqueous layer was removed, and methanol (800 μL) was added, followed by vortexing and centrifugation (16 000×*g*, 60 min). The supernatant was removed, and the pellet with remaining solution was evaporated to dryness. 50 mM ammonium bicarbonate (Ambic; 100 μL) was added to the pellet, and samples were vortexed. Supernatants were stepwise added 0.5 M DTT (4 μL, 30 min), 0.2 M iodoacetamide (30 μL, 30 min in the dark), 0.5 M DTT (8 μL, 20 min), incubated overnight on a rotary shaker (37 °C, 400 rpm) in 12.5 ng/μL trypsin in 44 mM Ambic (100 μL), and evaporated to dryness.

2.4.3. On-microsphere trypsination of residual plasma proteins (T-fraction)

Following the primary elution, microspheres were washed in 50 mM Ambic (200 μL) for 1 h on a rotary shaker (24 °C, 400 rpm) and further washed in 50 mM Ambic (2 × 200 μL). Microspheres were added 50 mM Ambic (100 μL) and stepwise treated with DTT/iodoacetamide/DTT as described above. Samples were washed in 50 mM Ambic (200 and 100 μL, respectively), resuspended in 50 mM Ambic (100 μL), and incubated overnight on a rotary shaker (37 °C, 400 rpm) in 12.5 ng/μL trypsin in 44 mM Ambic (100 μL). Released tryptic peptides were transferred to new tubes. Microspheres were washed in 50 mM Ambic (50 μL), and residual released peptides were pooled with respective samples. Tryptic eluates were evaporated to dryness.

2.4.4. Preparation of peptides in E- and T-fractions

Dried peptides were reconstituted in 0.1% formic acid in water (60 μL). Stage tip columns consisting of three C-18-filters were prewashed with methanol (3 × 50 μL), centrifuged (1500×*g*, 3 min) for each wash, equilibrated with 0.1% formic acid in water (3 × 100 μL), and centrifuged (1500×*g*, 2 min) for each equilibration step. Peptide samples were centrifuged (16 000×*g*, 25 min), supernatants loaded onto separate stage tip columns and centrifuged (1500×*g*, 4 min). Flow-through solutions were reloaded to stage tip columns and centrifuged (1500×*g*, 3 min). Stage tip columns were washed with 0.1% formic acid (2 × 60 μL), centrifuged (1500×*g*, 3 min) for each wash, and flow-throughs were discarded. Peptides were eluted from the stage tip column using 0.1% formic acid in 70% acetonitrile (2 × 40 μL), centrifuged (1500×*g*, 1 min) for each elution, and evaporated to dryness. Dried peptides were reconstituted in 0.1% formic acid in water (60 μL), vortexed, and agitated for 1–3 h (4 °C, 900 rpm). Samples were centrifuged (16 000×*g*, 15 min), and supernatants (30 μL) were transferred to MS-vials for LC-MS/MS analysis.

2.5. Liquid chromatography-tandem mass spectrometry (LC-MS/MS)

LC-MS/MS was performed on an EASY-nLC 1000 UPLC system (Thermo Scientific) interfaced with an Orbitrap Elite mass spectrometer (Thermo Scientific) via a Nanospray Flex ion source (Thermo Scientific). Peptides were injected onto an Acclaim PepMap100C18 trap column (75 μm i.d., 2 cm long, 3 μm, 100 Å, Thermo Scientific) and further separated on an Acclaim PepMap100C18 analytical column (75 μm i.d., 50 cm long, 2 μm, 100 Å, Thermo Scientific) using a 120-min multi-step gradient (3 min 2%–6% B, 92 min 6%–30% B, 5 min 30%–40% B, 5 min 40%–100% B and 15 min at 100% B; where B is 0.1% formic acid in acetonitrile and A is 0.1% formic acid in water) at 250 nL/min. Peptides were analysed in positive ion mode under data-dependent acquisition using the following parameters: Electrospray voltage 2.5 kV, CID fragmentation with normalised collision energy 35 and 10 ms activation time. Each MS scan (400–1600 m/z, 1 m/z isolation width, profile) was acquired at a resolution of 120 000 FWHM in the Orbitrap analyser, followed by rapid MS/MS scans (2 m/z isolation width, centroid) triggered for the 15 most intense ions, with a 40 s dynamic exclusion and analysed in the linear ion trap. Charge exclusion was set to unassigned, and 1.

2.6. Proteomic data analysis

LC-MS/MS data were initially collected from 5 replicates for each type of alginate microsphere, one saline control and one plasma control. A selection of samples was re-injected into the LC/MS due to some replicates displaying unsatisfactory chromatographic separation (namely, few and broad peaks). Initial data analysis (similar to the one described below) was performed for all collected data, i.e. initial injections and re-injections. This initial analysis culminated in the heatmap of z-scaled median transformed label-free quantification (LFQ) values with base 2 of the sample population, Supplementary Fig. S1. Considering the chromatographic quality and grouping of samples, we removed outliers resulting in the following number of replicates for each microsphere fraction: 3 (HiG_E), 4 (HiG_T), 4 (SA_E), 2 (SA_T), 4 (AP_E) and 5 (AP_T); our analyses and findings are based on these. Preview 2.3.5 (Protein Metrics Inc. https://www.proteinmetrics.com) was used to determine optimal search criteria for the raw files. These parameters were plugged into MaxQuant [53] v 1.5.8.3, which utilises the MaxLFQ algorithm [54] mapping the spectra over Human canonical proteome including isoforms (downloaded in March 2017 [55]). The following search parameters were used: enzyme specified as trypsin with a maximum of 2 missed cleavages allowed, deamidation of asparagine/glutamine, oxidation of methionine, N-terminal acetylation as variable- and carbamidomethylation of cysteine as fixed modification. Mass tolerance for FTMS-MS and ITMS-MS/MS was set to 20 ppm and 0.5 Da, respectively, with false discovery rate (FDR) < 0.01 (high confidence) for peptide spectra matches (PSM), peptide as well as protein group identification. LFQ values for identified protein groups were log-transformed with base 2. Filtered technical replicates were collapsed to their median value, each representing a biological replicate for a set condition. Proteins included in the final dataset were identified by two or more peptides at a fixed FDR protein level of 1.0%. The cut-off for $\log_2$-transformed LFQ values was set to 16.0 as per the MS-equipment discovered noise-sensitivity level. Proteins assigned with negative PSM scores, identified only by a site, as well as duplicates and known contaminants such as keratins, were removed from the dataset. Protein groups identified in >70% of replicates of at least one group were retained. For the cluster analysis, $\log_2$ LFQ values were z-scaled (except Fig. 1B). The obtained values are relative to the median of the whole expression profile and scaled to variation reflecting relative over- and under-expression. Raw file clustering was based on column-wise Z-scaling. The Euclidean distance between the expression vector was used for the hierarchical clustering (http://coxdocs.org/doku.php?id=perseus:user:activities:MatrixAnalysis:ClusteringPCA:HierarchicalCluster) using a k-means algorithm for pre-processing and average linkage for grouping. Median $\log_2$ LFQ intensities representing sample types were presented to Ingenuity® Pathway Analysis (IPA; QIAGEN Inc., https://www.qiagenbioinformatics.com/products/ingenuity-pathway-analysis [56]) to identify top canonical pathways, using an intensity threshold of 16.0. Raw files have been deposited to the ProteomeXchange Consortium [57] via the PRIDE partner repository with the dataset identifier PXD009135 (https://www.ebi.ac.uk/pride/archive/projects/PXD009135) and Notur/NorStore Project NN9036K/NS9036K, respectively.

2.7. Adsorption of plasma proteins to alginate microspheres evaluated by confocal laser scanning microscopy (CLSM)

Alginate microspheres (50 μL) were incubated in pooled ($N = 4$) lepirudin-plasma (300 μL) for 24 h at 37 °C under rotation and subsequently washed in 0.9% NaCl (2 × 500 μL). Microspheres were stained for complement factors C1q (polyclonal rabbit anti-human C1q/FITC, 50 μg/mL), C3c (polyclonal rabbit anti-human C3c/FITC, 50 μg/mL), or coagulation FXII by unconjugated polyclonal sheep anti-human FXII (50 μg/mL) and secondary staining with polyclonal donkey anti-sheep IgG/CF633 (20 μg/mL). Controls for non-specific antibody binding were polyclonal rabbit-anti-mouse immunoglobulins/FITC (50 μg/mL) and polyclonal donkey anti-sheep IgG/CF633 (20 μg/mL). All incubations were performed for 30 min (37 °C, under rotation) with subsequent washing in 0.9% NaCl (2 × 500 μL). Samples were stored in 0.9% NaCl (200 μL) before analysis and protected from light. Protein deposition was assessed by CLSM (Zeiss LSM 510 Meta, Carl Zeiss MicroImaging GmbH, Göttingen, Germany) using a C-Apochromat 10 × /0.45w objective and pinhole of 30.1 μm. 2D images were captured by optical cross-sections through the microsphere equator. 3D images were constructed from sections through the entire microsphere using z-stacks and ImageJ software (National Institutes of Health, New York, USA). An argon laser with an excitation wavelength of 488 nm at 20% laser power, emission at 500–550 nm, and gain 515, were used for FITC-conjugated antibodies. A helium-neon laser with an excitation wavelength of 633 nm at 50% laser power, emission over 650 nm, and gain 530, were used for the CF633-conjugated antibody.

2.8. Complement and coagulation reactivity of microspheres in human whole blood

Initial complement and coagulation responses to microspheres upon blood contact were evaluated using lepirudin-anticoagulated human whole blood, as previously described [44] and with modifications for microspheres [14]. In brief, aliquoted samples of either microspheres (50 μL) in 0.9% NaCl (50 μL) or controls (baseline, PBS [background] and glass) were added 0.9% NaCl (100 μL). All samples were further added PBS with $CaCl_2$ and $MgCl_2$ (100 μL). Blood was collected from healthy donors ($N = 5$) in low-activating polypropylene vials containing the anticoagulant lepirudin (50 μg/mL). Samples were incubated in blood (500 μL) for 4 h (37 °C, continuous rotation), and EDTA was added to a final concentration of 10 mM to inactivate the complement and coagulation responses. For the baseline sample, EDTA-inactivation was performed prior to blood incubation. Samples were centrifuged (4 °C, 1880×g, 15 min), plasma was harvested and stored at -20 °C before analysis. Complement activation was measured by the enzyme-linked immunosorbent assay (ELISA) kit for detecting soluble TCC. The assay was performed in accordance with the provided protocol. Coagulation activation was assessed by the level of prothrombin cleavage fragment F1+2 (PTF1.2) by ELISA kit Enzygnost® F1+2, monoclonal. Analysis was performed following the producer's protocol but included modifications to the plasma dilutions (1:10–1:1000).

2.9. Statistical analyses

In the proteomic analysis, plasma proteins on microspheres were statistically analysed with R [58], using $\log_2$-transformed LFQ values for

group comparisons. For enrichment against the plasma control, a one-sample Student's T-test [59] was employed with the assumption that the null values were 0. Protein groups missing from all microspheres and identified in the plasma control were categorised as *repelled* by microspheres with values 0. Values only represented in one group were also set as 0 in subsequent Benjamini-Hochberg corrections [60]. Only protein groups with FDR <0.1 were considered for further analysis. Protein hydrophobicity and isoelectric points (pI) were calculated using the Peptides software package [61] with the Kyte-Doolittle scale for hydrophobicity and Bjellqvist scale for pI.

For the human whole blood experiment, repeated measures one-way ANOVA with Geisser-Greenhouse correction and Tukey's multiple comparison test was used to define statistical differences between selected sample groups. Data were log-transformed before analysis due to low sample numbers ($N = 5$). Differences between sample groups were considered significant at $p < 0.05$.

2.10. Ethics

The use of blood and plasma from volunteers has been granted by the Regional Ethics Committee of Mid-Norway under REC Central (REK2009/2245), following their recommended guidelines.

3. Results

3.1. Proteomic analysis of human plasma proteins adsorbed to alginate microspheres

Adsorbed plasma proteins were identified by high-resolution LC-MS/MS as outlined in Fig. 1A. Label-free quantification of peptides (E-/T-fractions and controls) identified a total of 676 protein groups with relative protein abundances given as $\log_2$ LFQ intensity values. Hierarchical clustering of quantified proteins revealed distinct protein adsorption profiles for alginate microspheres HiG, SA, and AP, and the E- and T-fractions thereof (Fig. 1B). Proteins quantified by replicate analysis of each microsphere type invariantly clustered together, indicating high reproducibility of our method. For confident identification of proteins, the initial dataset was further processed using strict conditions: $\log_2$ LFQ value cut-off at 16.0, peptide count of at least 2 for identified proteins and the removal of peptides assigned with negative PSM-scores, duplicates and known contaminants. This resulted in a final dataset of 241 confidently identified protein groups (Supplementary Table S1), wherein 236 proteins were identified on the alginate microspheres. In the unfractionated plasma control, 128 proteins were identified and 5 of these proteins were not found on the microspheres. Hence, a total of 113 proteins were exclusively identified on the microspheres and thus enriched above their detection level in unfractionated plasma in our LC-MS/MS setup. A higher number of proteins were identified on microspheres HiG and SA compared to AP: HiG (167 E-/149 T-proteins), SA (182 E-/139 T-proteins) and AP (120 E-/114 T-proteins). As shown in Fig. 1C, several adsorbed plasma proteins were uniquely distributed between the E- and T-fractions. Of the 236 adsorbed proteins, 49 proteins were only identified in the E-fractions and 34 proteins were only identified in the T-fractions. It is reasonable to anticipate that the proteins uniquely identified in the T-fractions represent the proteins that bind most strongly to the microspheres.

3.2. Enrichment of plasma proteins on alginate microspheres

Plasma proteins identified in the current study were assigned their reported concentrations in human plasma using the Peptide Atlas (PA; https://www.proteinatlas.org/humanproteome/blood/proteins+detected+in+ms, accessed Nov. 2021) and the Plasma Proteome Database (PPD; http://www.plasmaproteomedatabase.org, v. 06_2015 retrieved Oct. 2018). The PA (plasma non-glyco 2017 build [62]) presents protein concentrations for 3222 proteins quantified by MS-based plasma proteomics with estimations from spectral counts. The PPD [63] contains published plasma and serum concentrations for 1278 proteins quantified by different methods, wherein plasma protein quantifications by MS spectral counts were only considered. Of the 241 proteins confidently identified in our dataset, plasma concentrations for 198 proteins have been deposited in PA and PPD combined. Proteins that were not reported in the respective databases were mainly immunoglobulin derived. In Fig. 2, the quantified proteins in this study are shown alongside their reported protein concentrations in human plasma. The most abundant proteins (plasma concentrations >1 μg/mL) were identified both in the plasma control and on the microspheres, whereas less abundant proteins (plasma concentrations <1 μg/mL) were selectively identified on the microspheres. This suggests that distinct subsets of plasma proteins were significantly enriched on the different alginate microspheres. Among the 113 enriched proteins below the cut-off or not detected in plasma, 32 proteins were exclusively detected in the T-fractions of the microspheres. The plasma concentrations for 25 of these proteins are reported and in the range 0.00029–13.0 μg/mL (PA or PPD), reflecting a high degree of enrichment on the microspheres.

A detailed illustration of the distinct protein adsorption profiles compared to plasma is included in Fig. 3. As shown in Fig. 3A, the protein profiles of the microspheres in terms of relative abundance ($\log_2$ LFQ values) were different from that of the plasma control. For the majority of the less abundant proteins in the plasma control, a marked enrichment on the microspheres is evident. Proteins below the cut-off or not detected in plasma and quantified on the microspheres are shown in Fig. 3B. Interestingly, among the proteins that were not detected in plasma, many escaped elution in the first step (E-fraction) but were readily quantified in the T-fractions, indicating strong and selective binding to the distinct microsphere types.

The number of significantly enriched proteins relative to plasma for microspheres HiG, SA, and AP across the E-/T-fractions were 106, 128, and 88 proteins, respectively (Fig. 4A). SA had the highest number of uniquely enriched proteins (40), compared to HiG (20) and AP (10). Further information on their binding strengths could be derived from the distribution between E- and T-fractions. Interestingly, two proteins were found to be significantly depleted compared to plasma (not detected in either E- or T-fractions); coagulation factor XIII A chain (F13A1) was depleted on all microspheres, and pregnancy zone protein (PZP) was depleted on AP.

Proteins uniquely identified on either HiG, SA, or AP microspheres were further analysed with respect to their physicochemical properties: hydrophobicity/hydrophilicity and charge/isoelectric point (pI) (Fig. 4B). Overall, most of the uniquely adsorbed proteins were hydrophilic in nature (GRAVY score below zero). Also, most acidic proteins (i.e. net negative charge at physiological pH) were found in the E-fractions. In contrast, most basic proteins (i.e. net positive charge at physiological pH) were found in the T-fractions. The latter was especially evident for HiG, in which most proteins observed in the T-fraction were basic and could be explained by opposite charge interactions. Much fewer basic proteins were observed for AP, in agreement with the overall charge neutralisation offered by poly-L-lysine. The number of acidic proteins binding to SA was markedly higher than for HiG. This was somewhat surprising since sulfation increases the number of negatively charged groups on the microbeads. However, most of these proteins have previously been reported to bind heparin or heparan sulfate (Fig. 4B, marked by orange circles). This points to a specific role of the sulfate groups in binding these proteins and likely also contributes to the higher number of uniquely identified proteins on SA.

3.3. Different microspheres display distinct adsorption profiles of proteins in the complement and coagulation pathways

The biological relevance of adsorbed plasma proteins was further analysed to elucidate potential immune profiles for the different microspheres. Ingenuity® Pathway Analysis (IPA) is presented in Table 1,

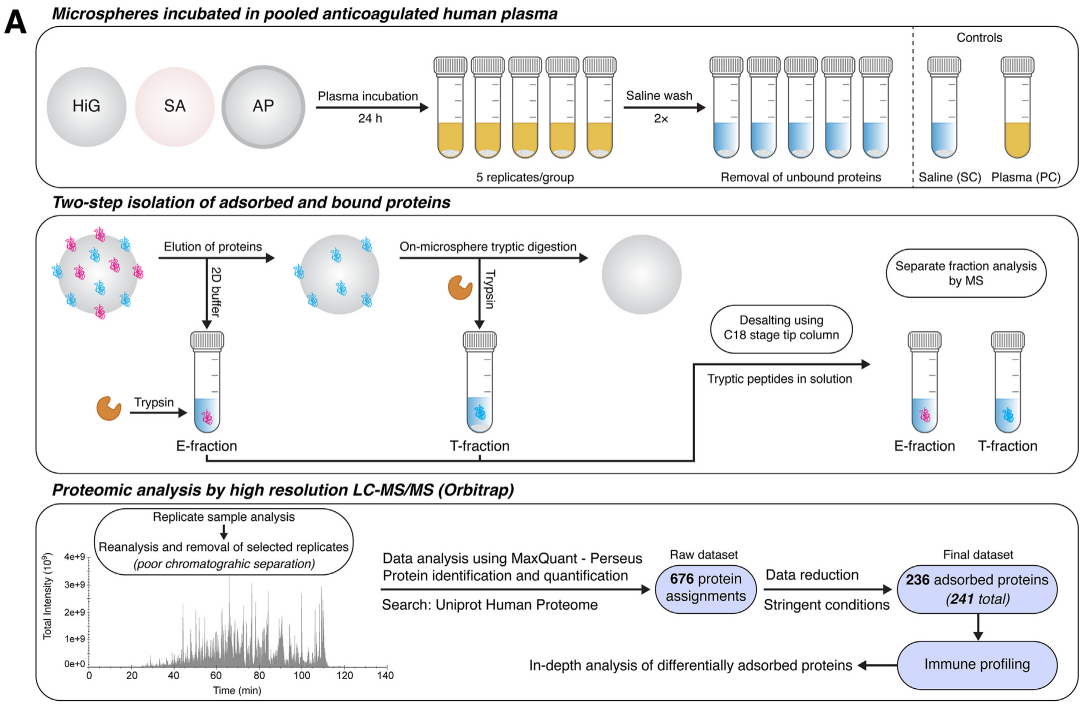

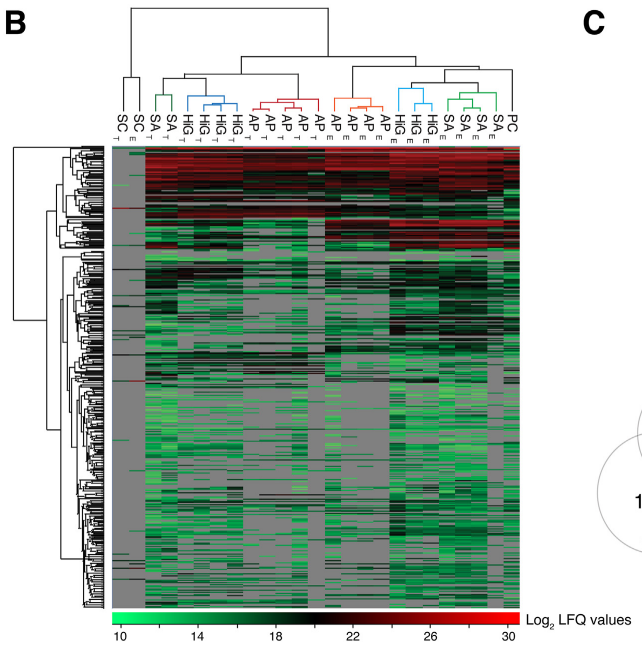

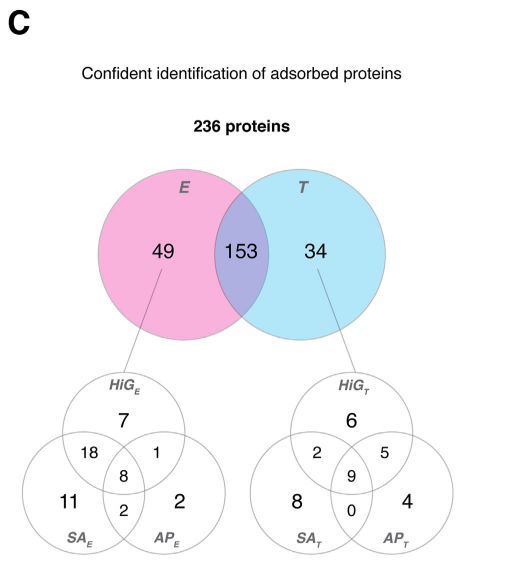

(caption on next page)

Fig. 1. Proteomic analysis of human plasma proteins adsorbed to alginate microspheres after incubation in lepirudin-plasma (24 h). (**A**) Workflow of the proteomic study using liquid chromatography-tandem mass spectrometry (LC-MS/MS). Identification and quantification of plasma proteins adsorbed to alginate microspheres HiG, SA, and AP, separated into eluted (E)- and on-microsphere trypsinated (T)-fractions. Control samples included saline (SC; microspheres in saline) and plasma (PC; unfractionated lepirudin-plasma). (**B**) Heatmap showing identified protein adsorption profiles for the alginate microspheres. Pairwise Pearson's correlation coefficient was used on the raw dataset to calculate the Euclidean distance for hierarchical clustering of proteins (*rows*) and samples (*columns*). Protein abundances are coloured based on $\log_2$ label-free quantification (LFQ) intensity values, indicated by a colour scale bar (*bottom*). Not detected proteins are indicated in grey. (**C**) Venn diagrams show 236 differentially adsorbed proteins between microsphere fractions (E vs T) and between microsphere types. (For interpretation of the references to colour in this figure legend, the reader is referred to the Web version of this article.)

showing the ten most abundant proteins and top canonical pathways identified for the microspheres. The most abundant protein of the plasma control was albumin (ALB), which was also ranked the highest for HiG and AP, but not for SA (ranked third). Besides ALB, protein abundances on the microspheres did not correspond to the unfractionated plasma control, again highlighting the specific protein adsorption to the microspheres. IPA further revealed the top canonical pathways assigned to the bound plasma proteins, including acute-phase response signalling, the complement and coagulation systems, and proteins linked to numerous metabolic pathways such as lipid metabolism (LXR/RXR and FXR/RXR activation). Specifically, bound proteins showed a high degree of overlap with complement and coagulation pathways. Several of these proteins were highly abundant (Table 1) and significantly enriched relative to the plasma control (Fig. 4). Thus, further investigations were made regarding the involvement of complement, coagulation, and other potentially relevant proteins, signifying the immune profiles of HiG, SA, and AP (Fig. 5).

In Fig. 5A, adsorbed proteins of the complement system are classified according to their associated pathway (classical, lectin, alternative) or function [68,69]. Microbeads HiG and SA were specifically enriched with proteins of the classical and lectin pathways. This was especially evident for the C1 complex (complement C1q with its associated proteases C1r and C1s), involved in the initiation of the classical pathway. C1q comprises subunits C1QA, C1QB and C1QC, which were 152-197-fold enriched on HiG (values given relative to plasma control), 13-140-fold on SA and 2-9-fold on AP, whereas the proteases (C1R, C1S) were only enriched on HiG (17-27-fold) and SA (65-122-fold). In agreement with this, the level of C1q surface-recruiting protein serum amyloid P-component (APCS) was highly pronounced on HiG (>193-fold) and SA (>230-fold), as well as lower-level enrichment of immunoglobulin G1 (IGHG1) and C-reactive protein (CRP). AP had the highest enrichment of CRP, being >3-fold above the other microbeads. The proteins comprising the classical C3 convertase (C4B, C2 [A]), which is activated by the C1 complex, were more prominent on HiG and SA. Proteins of the lectin pathway, including mannose-binding protein C (MBL2), ficolin-2 (FCN2), collectin-11 (COLEC11) and mannan-binding lectin serine protease 1 (MASP1), were also identified on HiG and/or SA but below the detection level in the plasma control. In addition to activators of the classical and lectin pathways, we observed selective enrichment of inhibitors for these pathways on HiG and SA. Plasma protease C1 inhibitor (C1IN), which inhibits the C1 complex and MASPs, respectively, was enriched on SA (7-fold) and HiG (2-fold). C4-binding protein (C4BPA/C4BPB complex), an inhibitor of the classical pathway, was exclusively enriched on SA (>2-fold). The selective enrichment of proteins from the alternative pathway was, however, not as evident on HiG and SA as compared to AP. This pathway is the main driving force of terminal complement activity, involving complement component 3 (C3) and complement factors B (CFB), D (CFD) and properdin (CFP). C3 plays a central role in complement activation, acting as a point of convergence for all three pathways and fuelling the amplification process. CFB and CFD both contribute to the activity of C3. CFP can serve as a local initiator of the pathway by recruiting C3 to the surface and also plays a vital role in stabilising the alternative C3 convertase. AP had the highest enrichment of C3 and CFP, roughly 5-fold above HiG and SA. Notably, CFP was not detected in plasma and was exclusively enriched in the T-fractions, indicating strong binding. Crucial inhibitors of C3 activity include complement factor H (CFH) and I (CFI). CFH was significantly enriched on SA (>44-fold) and to some extent on HiG (>2-fold), while below the plasma control for AP. CFI was enriched (~2-fold) on all microspheres. Complement components of the terminal complex (TCC; C5, C6, C7, C8, C9) were enriched (2-59-fold) on all microspheres. Inhibitors of TCC assembly, including clusterin (CLU) and vitronectin (VTN), were most pronounced on SA (CLU: 40-fold, VTN: >6-fold). Carboxypeptidase-N (CPN; CPN1/CPN2), which degrades anaphylatoxins (C3a, C5a) to their desArg forms, was distinctively enriched (catalytic subunit CPN1) on SA.

The coagulation protein profiles are summarised in Fig. 5B. Proteins of the contact activation (intrinsic) pathway [70], including plasma kallikrein (KLKB1), kininogen-1 (KNG1), coagulation factors XII (F12), XI (F11) and IX (F9), were all enriched on the microspheres and especially evident on SA. Here F12, which initiates the pathway, was enriched >64-fold on SA compared to >3-fold and >4-fold on HiG and AP, respectively. Proteins of the tissue factor (extrinsic) pathway, including factor III (F3) and VII (F7), were not detected in the dataset. The common coagulation proteins, factors X (F10) and V (F5), were distinct for SA and HiG. Vitamin K-dependent protein C (PROC) that functions as an anticoagulant when activated, including its cofactor vitamin K-dependent protein S (PROS1), were particularly enriched on SA. As part of the clotting process, prothrombin (factor II) is proteolytically cleaved to form thrombin (factor IIa) that converts fibrinogen into fibrin. Prothrombin/thrombin (F2) was most enriched on AP (>5-fold), followed by HiG (2-fold) and SA (<2-fold). Inhibitors of thrombin include antithrombin-III (AT3), which inhibits several coagulation factors, and heparin cofactor 2 (HCF2). Notably, SA showed the highest enrichment of AT3 (>12-fold) and HCF2 (4-fold). Plasmin is generated from the zymogen plasminogen on the surface of fibrin clots as part of the fibrinolytic system, which has also been implicated in complement-independent cleavage of C5 and C3 [69]. Plasminogen/-plasmin (PLG) was exclusively enriched in the T-fraction of AP (4-fold).

Fig. 5C displays adsorbed proteins with various biological functions that may be relevant to the PFO outcomes of the microspheres. These proteins include extracellular matrix (ECM)-associated proteins, apolipoproteins, monocyte-associated proteins and cytokines or chemoattractants. For the ECM proteins, ECM protein 1 (ECM1) was extensively enriched on SA (>170-fold) and to some extent on HiG (7-fold), and tenascin-X (TNXB) was distinctively identified on SA. Further, the ECM degrading proteins: matrix metalloproteinase-2 (MMP2) and -9 (MMP9) and neutrophil elastase (ELANE; Table S1) were highly enriched and unique for SA. The tissue inhibitors of metalloproteinase 1 (TIMP1) and 2 (TIMP2), which regulate the MMPs, were exclusively enriched on SA and HiG. Several apolipoproteins (not all shown; see Table S1 for full list of proteins) were either unique or most enriched on SA, including apolipoprotein E (APOE) and H (APOH). Proteins involved in monocyte activation by lipopolysaccharide (LPS) include the LPS-binding protein (LBP) and monocyte differentiation antigen CD14, which were enriched on all three microspheres. The pro-inflammatory cytokines, including platelet factor 4 (PF4), PF4 variant 1 (PF4V1) and leukocyte cell-derived chemotaxin-2 (LECT2), and the chemoattractant azurocidin (AZU1), were enriched above the detection level in plasma and consistently more pronounced or exclusive for HiG and AP.

A selection of the identified proteins is presented in a heatmap (Fig. 5D), showing the relative protein abundances between the three types of microspheres across the E- and T-fractions. Samples from each type of microsphere formed distinct clusters, and the largest dissimilarity

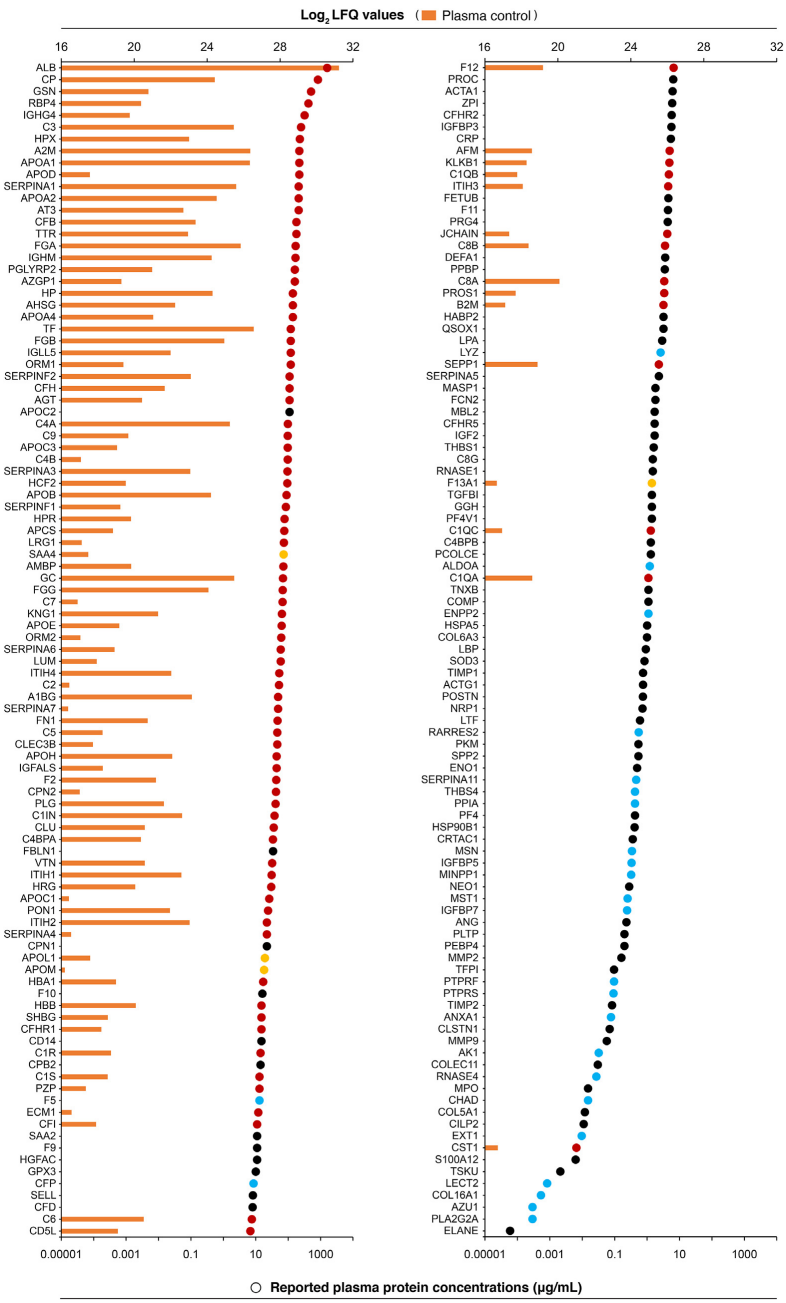

Fig. 2. Human plasma proteins identified in this study ranked according to their reported plasma protein concentrations retrieved from the Peptide Atlas [62] and Plasma Proteome Database [63]. Proteins quantified in the unfractionated plasma control are presented as orange bars (*upper axis*) and reported plasma protein concentrations are indicated by dots (*lower axis*). The identified proteins are further categorised (*colouring of dots*) according to their distinct detection: microspheres* (*black*), on-microsphere trypsinated (T)-fractions (*blue*), plasma control (*yellow*), and both on microspheres and in plasma control (*red*). In the current work, a total of 241 plasma proteins were confidently identified, of which 198 proteins were reported with plasma concentrations determined by MS spectral counts. Proteins are denoted by gene names.*Proteins identified in either eluted (E) or E- and T-fractions.

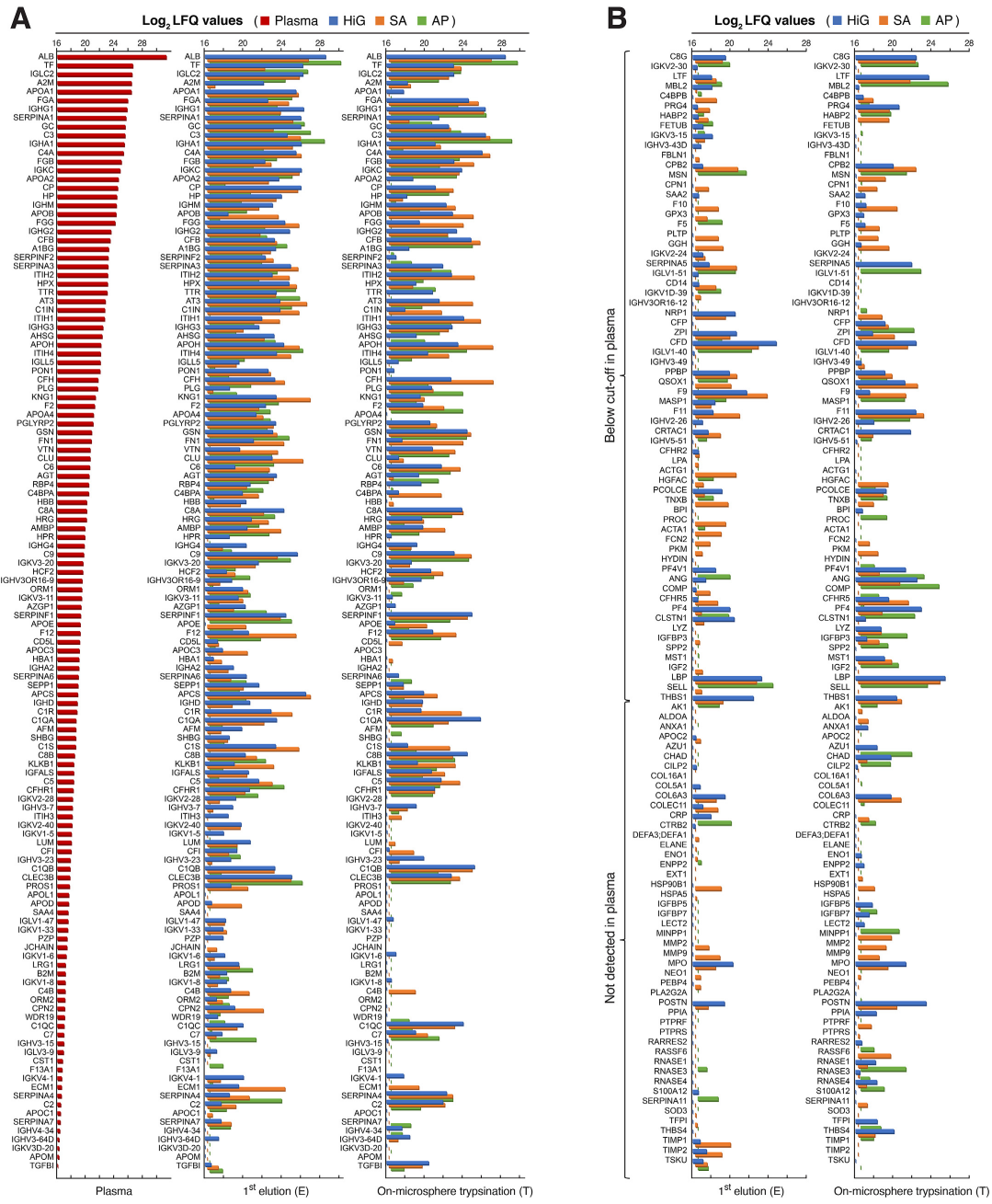

Fig. 3. Enrichment of plasma proteins on alginate microspheres after incubation in human lepirudin-plasma (24 h). Protein abundances, represented as $\log_2$ LFQ values, for 241 proteins identified for the microspheres (HiG, SA, AP) and unfractionated plasma control. Microsphere samples comprised separate fractions of eluted (E) and on-microsphere trypsinated (T) proteins. (**A**) Quantified proteins in the plasma control ranked according to their detection level (*descending order*), including the respective protein profiles of the microspheres. (**B**) Enriched proteins on the microspheres, which were below the cut-off or not detected in the plasma control. Proteins are denoted by gene names.

Table 1
The upper panel shows the 10 most abundant plasma proteins binding to the different alginate microspheres (E- and T-fractions) with indicated log_2 LFQ values. The lower panel shows top canonical pathways (IPA analysis) associated with the proteins identified in each fraction from the microspheres and per cent overlap with each pathway. LXR = Liver X Receptor, RXR = Retinoid X Receptor, FXR = Farnesoid X Receptor. *Number of proteins assigned to pathway (IPA).

10 most abundant plasma proteins *(Log_2 LFQ values)*							
Plasma control	HiG $_E$	HiG $_T$	SA $_E$	SA $_T$	AP $_E$	AP $_T$	
ALB *(31.2)*	**ALB** *(28.5)*	**ALB** *(26.7)*	**APCS** *(26.7)*	**CFH** *(27.1)*	**ALB***(29.6)*	**ALB** *(29.5)*	
TF *(26.6)*	**APCS** *(26.4)*	**C3** *(26.6)*	**KNG1** *(26.7)*	**APOH** *(27.1)*	**C3** *(27.9)*	**C3** *(28.9)*	
IGLC2 *(26.4)*	**IGHG1** *(26.2)*	**IGHG1** *(26.5)*	**ALB** *(26.5)*	**ALB** *(26.9)*	**GC** *(26.4)*	**IGHG1** *(26.1)*	
A2M *(26.4)*	**IGLC2** *(26.1)*	**C4A** *(26.2)*	**AT3** *(26.3)*	**C3** *(26.8)*	**TF** *(26.2)*	**LTF** *(25.1)*	
APOA1 *(26.3)*	**TF** *(26.1)*	**C1QA** *(26.0)*	**CLU** *(25.9)*	**C4A** *(26.8)*	**SERPINA1** *(25.8)*	**CFB** *(24.7)*	
FGA *(25.8)*	**IGKC** *(26.0)*	**C1QB** *(25.4)*	**C4A** *(25.7)*	**IGHG1** *(26.1)*	**APOH** *(25.7)*	**C9** *(24.3)*	
IGHG1 *(25.7)*	**IGHA1** *(26.0)*	**LBP** *(25.4)*	**C3** *(25.6)*	**ITIH1** *(25.8)*	**CLEC3B** *(25.6)*	**ANG** *(24.2)*	
SERPINA1 *(25.6)*	**CP** *(25.9)*	**SERPINF1** *(25.1)*	**IGLC2** *(25.5)*	**CFB** *(25.7)*	**TTR** *(25.3)*	**GSN** *(24.0)*	
GC *(25.5)*	**SERPINA1** *(25.9)*	**CFB** *(25.0)*	**APOH** *(25.5)*	**FGA** *(25.6)*	**HPX** *(24.9)*	**APOH** *(24.0)*	
C3 *(25.5)*	**GC** *(25.9)*	**FGA** *(24.7)*	**IGKC** *(25.5)*	**ITIH2** *(25.1)*	**IGKC** *(24.5)*	**PLG** *(23.7)*	
Top canonical pathways *(overlap)*							
24.4%	26.1%	24.4%	25.6%	21.1%	22.2%	19.4%	Acute phase response *(180*)*
51.4%	62.2%	62.2%	64.9%	59.5%	51.4%	48.6%	Complement system *(37*)*
42.9%	48.6%	54.3%	57.1%	45.7%	42.9%	42.9%	Coagulation system *(35*)*
30.6%	29.8%	25.6%	33.9%	19.0%	26.4%	19.8%	LXR/RXR Activation *(121*)*
29.4%	27.8%	23.0%	29.4%	15.9%	24.6%	18.3%	FXR/RXR Activation *(126*)*

in the immune profiles was found between SA and the two other microspheres, HiG and AP. From the cluster analysis of adsorbed proteins, the first level of grouping predominantly separates pro-inflammatory proteins (upper group, encompassing complement mediators and cytokines) from other proteins (lower group, encompassing complement inhibitors and coagulation proteins). Illustratively, proteins of the pro-inflammatory group are clearly most abundant on AP, and proteins of the more anti-inflammatory group are more abundant on SA. HiG represents an intermediate profile between the respective groups. Moreover, the clustering of IGHG1 with C1q (C1QA, C1QB, C1QC) may indicate immunoglobulin-mediated classical complement activation for HiG and SA, whereas the clustering of C1IN with the C1q proteases (C1R, C1S) may indicate the subsequent inactivation of the classical pathway for these microbeads.

3.4. Complement and coagulation assessments by CLSM and human whole blood assay

The deposition of complement and coagulation proteins on the microspheres was studied by CLSM, and functional responses were assessed in a human whole blood assay (Fig. 6). The binding of C1q was distinct for microspheres HiG and SA (Fig. 6A). Complement C3c, a stable C3-conversion product, was exclusively detected on the surface of AP (Fig. 6B), in accordance with the proteomics data showing a high and selective enrichment of C3 and CFP (stabilises C3-convertases) on these microspheres (Fig. 5A). The binding of FXII was detected for all three microspheres, accumulated in the order SA > AP > HiG (Fig. 6C). The non-specific binding of antibodies to the microspheres was negligible (Fig. 6D). On a general note, the protein depositions at the outer layer of the microspheres indicate surface binding rather than passive diffusion into the hydrogels (i.e. absorption). In summary, the CLSM analyses are in agreement with the MS analyses.

In the human whole blood assay, complement and coagulation reactivity was determined by levels of TCC and prothrombin fragment 1 + 2 (PTF1.2), respectively. Whereas no significant TCC induction was observed for SA, low induction was observed for HiG ($p < 0.01$) and a strong induction for AP ($p < 0.001$) compared to baseline (Fig. 6E). The saline control for TCC (not shown) was significantly elevated ($p < 0.01$) above baseline and SA, whereas not statistically different from HiG and AP. Conversely, the activation of coagulation was most pronounced for SA ($p < 0.01$), followed by AP and HiG ($p < 0.05$) compared to baseline (Fig. 6F). The PTF1.2-response for SA as well as for the positive control (glass, not shown) were also significantly ($p < 0.01$) elevated above the saline control (not shown).

A graphical summary of proposed complement and coagulation mechanisms for the three types of alginate microspheres is presented in Fig. 7, with a basis on elucidated proteomic immune profiles (Fig. 5) and functional data on complement and coagulation reactivity (Fig. 6). Details are outlined in the figure legend.

4. Discussion

Here, we use high-resolution LC-MS/MS to identify distinct protein adsorption profiles for three types of alginate microspheres relevant for immune isolation in cell therapy, which we recently reported exhibit different inflammatory and PFO responses: HiG (low-inflammatory and fibrotic), SA (low-inflammatory and anti-fibrotic), and AP (pro-inflammatory and highly fibrotic) [10]. A total of 236 proteins were differentially adsorbed to the microspheres, and in-depth analyses of the proteins revealed unique immune profiles. In detail, the microspheres showed differences in enriched complement and coagulation factors with inhibitory or activating roles. Of specific importance is the prominent enrichment of inhibitors of complement and coagulation on SA, coinciding with minimal PFO. These findings were supported by functional assessments in human whole blood (hWB) involving total complement and coagulation activation. The current work establishes MS-based quantitative proteomics as a valuable tool, in conjunction with established *in vitro* and *in vivo* methods, to identify potential drivers of inflammation and PFO for alginate-based hydrogels. In the following, we discuss our methodological strategy and the effect of hydrophobicity/hydrophilicity and charge/isoelectric point. Further, we include an in-depth discussion of specific proteins involved in the complement and coagulation cascades that were prominent in the canonical pathway analysis, as well as other proteins that may be relevant in PFO development.

The competitive displacement of adhering surface proteins by other proteins with higher binding affinities is commonly referred to as the Vroman effect [37,75]. Consequently, the protein adsorption behaviour of a material depends on the composition of the protein solution and the exposure time. In the current study, we chose a strategy that preserved the reactive complement proteins and coagulation factors in human plasma, which sets an important premise for the subsequent protein displacements. To distinguish between weaker and stronger bound proteins, we chose to employ a two-step detachment procedure (primary

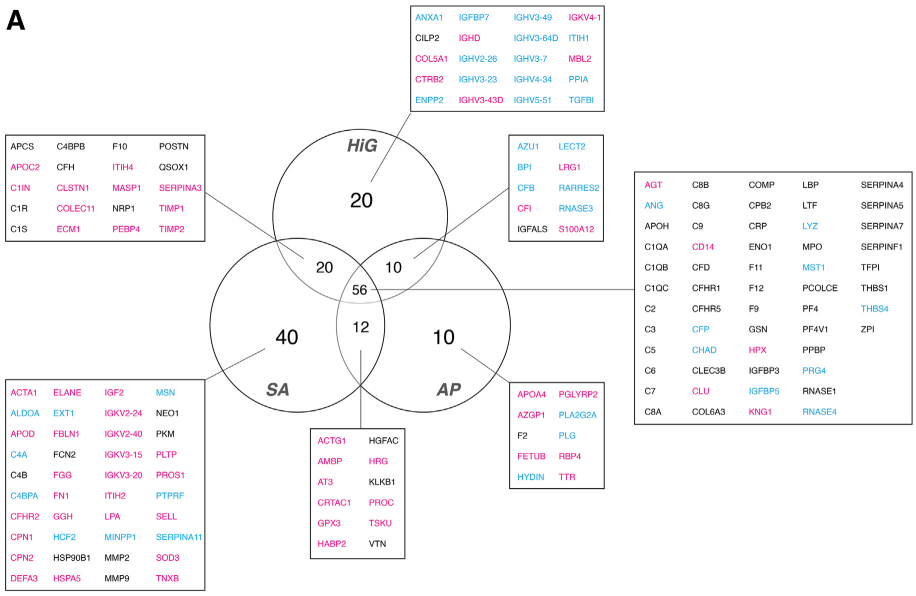

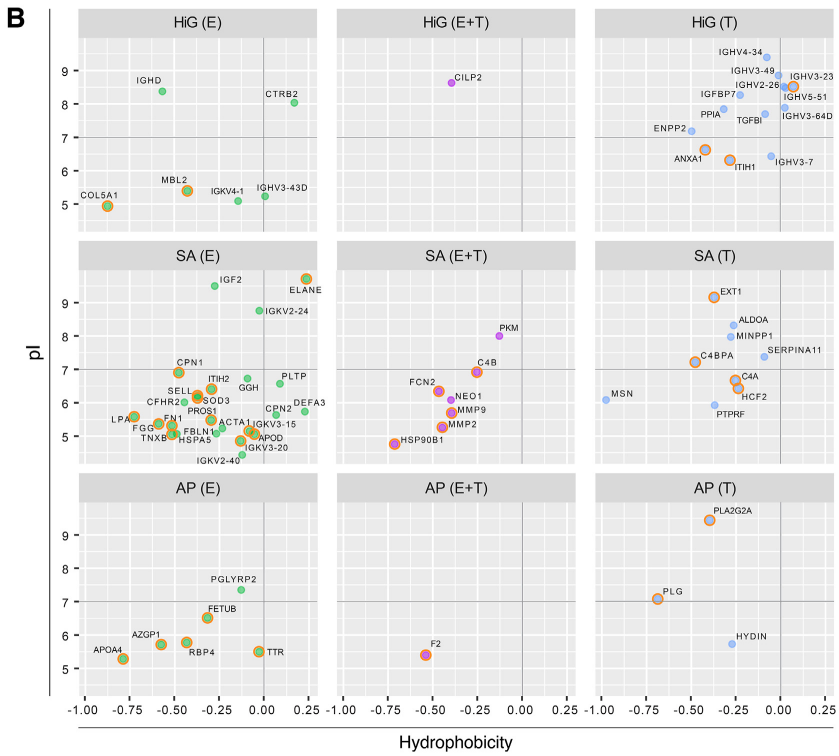

(caption on next page)

Fig. 4. Significantly enriched plasma proteins on alginate microspheres (HiG, SA, AP) after incubation in lepirudin-plasma (24 h). (**A**) Venn diagrams showing enriched proteins on the microspheres (E- and T-fractions) compared to the unfractionated plasma control. The statistical significance is given by corrected p-value (FDR) ≤ 0.1 and enrichment by $\geq$ 2-fold change. Colour assignments correspond to protein enrichment in the following microsphere fractions: eluted (E)-fraction (*pink*), on-microsphere trypsinated (T)-fraction (*blue*), and both (E + T) fractions (*black*). Proteins are listed alphabetically using their gene names. (**B**) Uniquely enriched proteins are characterised by their hydrophobicity score (*x-axis*) and isoelectric point (pI) (*y-axis*). The average hydrophobicity/hydrophilicity of the proteins was calculated using the Kyte-Doolittle method with GRAVY scoring (-2 [hydrophilic] $< 0 <$ 2 [hydrophobic]). pI was calculated along the primary sequence of the protein using the Bjellqvist scale [61]. Heparin- or heparan sulfate-binding proteins [64–67] are encircled in orange.

elution [E] and secondly on-microsphere trypsination [T]). The T-fraction represents the proteins with the overall strongest binding, which is supported by the many proteins below the detection level in plasma selectively identified in the T-fraction. The highly abundant plasma proteins were predominantly identified in the E-fraction. The enrichment of proteins from plasma was evident for all the studied microspheres. However, the number of different proteins was highest on the anti-fibrotic SA and lowest on the pro-fibrotic AP. This indicates that the number of proteins by itself is not a driver of the host response, but rather the type of proteins and their capability to react with the material surface, as will be discussed in later sections.

Hydrogels constitute a unique class of hydrophilic materials, comprising water-swollen networks of hydrophilic polymers. Their protein adsorption behaviour is thus not directly comparable to that of other non-hydrogel hydrophilic materials, such as functionalised solid surfaces that are more widely described in the literature ([76] and references therein). The three types of hydrogel microspheres in this study primarily differ in their functional groups, which also dictate the surface charges. The alginate (present in all the microspheres) is negatively charged at physiological pH due to the presence of carboxylate groups (-COO^-), while the sulfated alginate (in SA) carries additional negative charges from the chemically introduced sulfate groups (-SO_4^{2-}) at C2 and/or C3 [24]. Complexation of the alginate hydrogel with poly-L-lysine (PLL; AP), which contains positively charged amino groups (-NH_3^+) at physiological pH, decreases the net negative charge at the capsule surface of AP [5]. The number of significantly enriched proteins increased with the negative charge of the microspheres (SA > HiG > AP) (Fig. 4A), pointing to charge interactions as important drivers for the observed protein binding. There was a trend towards a more positive charge of the proteins in the T-fraction, supporting that opposing charge interactions play an important role in promoting the strongest binding to the microspheres. The high number of negatively charged proteins uniquely binding to the microspheres may be explained by positively charged surface patches that could dictate their binding despite an overall net negative charge [38]. One such example is the known sugar-binder inter-alpha-trypsin inhibitor heavy chain 1 (ITIH1). This protein contains a positively charged lysine cluster aligned on top of a β-sheet on the protein surface (PDB: 6FPY) [77], which might explain the strong association to HiG. The inclusion of sulfated alginate in the alginate microbeads (SA) resulted in an overall increase in adsorbed proteins as well as uniquely enriched proteins in the E-fraction. Notably, the majority (>63%) of the negatively charged proteins binding to SA have previously been reported to bind heparin and/or heparan sulfate [64–67]. Heparin and heparan sulfate are sulfated glycosaminoglycans (GAGs) that interact with a wide range of proteins in the regulation of different biological processes such as the immune response or response to wounding [64]. The structure-function properties of sulfated alginate have been associated with those of heparin and heparan sulfate [24,78], and sulfated alginate has previously been shown to bind several heparin-binding proteins [24,26].

Alginate hydrogels have water-swollen, porous structures (~2% [w/v] polymer concentration) that could allow proteins to penetrate below the microsphere surface [79]. Coating alginate microbeads with PLL decreases the pore size of the microspheres [80], which could contribute to the lower number of proteins on AP. Previous studies on the surface topography of alginate microspheres using atomic force microscopy (AFM) revealed similar average surface roughness for Ca- or Ba-alginate microbeads and alginate-PLL-alginate microspheres [81]. In a recent AFM study, we showed that the inclusion of oxidized alginate in soft alginate hydrogels leads to an increase in surface roughness [82]. Like oxidized alginate, sulfated alginate also contributes poorly to the ionic network of the hydrogel [83,84]. Thus, higher surface roughness could potentially be expected for SA when compared to HiG. However, the effect of topography as a driver for protein adsorption in the studied microspheres remains elusive.

Complement is considered a key contributor to biomaterial-induced host responses [41]. The coagulation cascade may influence the host response by direct activation through the contact pathway or through crosstalk with the complement system [71]. Ingenuity pathway analysis (IPA) identified the acute-phase response and the complement and coagulation cascades as the top enriched canonical pathways for all three microspheres. However, the protein adsorption does not necessarily reflect a biological response, since the acute-phase effectors which include most of the complement and coagulation proteins depend on distinct conformational changes to elicit their biological functions [41,85]. Thus, we interpret the proteomics data (Fig. 5) alongside the functional data in hWB with assessments of total complement and coagulation activation (Fig. 6). In agreement with our findings, initial *in vivo* adsorption of acute-phase proteins was also reported for fibrotic PEG hydrogels explanted from mice [27]. This supports the significance of active proteolytic cascades in the early phases of the host response and fibrotic tissue development, as well as the relevance of using lepirudin plasma *in vitro*.

In brief, the complement system consists of an intricate network of effectors and regulators. Driven by conformational changes, complement activation could be initiated through the alternative, classical, or lectin pathways. This culminates in the formation of convertases, which in turn generate the complement effectors, including opsonins (e.g. C1q, C3b), anaphylatoxins (e.g. C3a, C5a), and terminal complement complex (TCC) [68,69]. The potent biological effects of these effectors are tightly regulated by inhibitors, consisting of cellular receptors or soluble humoral factors that also bind to GAGs on cell surfaces [68,86,87]. In the current study, SA showed insignificant terminal complement activation (TCC formation) in hWB, which represents the functional endpoint of complement activation. This conforms with the enrichment of complement inhibitors in the proteomic analysis, including C1 inhibitor (C1IN), factor H (CFH), C4-binding protein (C4BP), clusterin (CLU), vitronectin (VTN), and carboxypeptidase-N (CPN). Interestingly, the catalytic subunit of CPN, which serves to mitigate the pro-inflammatory, chemotactic signalling of the anaphylatoxins C3a and C5a [69], was exclusively enriched on SA. The abundant enrichment of CFH on SA is intriguing as it is involved in the inhibition of complement at the level of C3. It is acknowledged that CFH can bind directly to polyanions such as sulfated GAGs and sialic acid on host cells [85]. It has also been demonstrated that C1IN directly binds to heparin [88] which exhibits properties similar to sulfated alginate. The enrichment of complement inhibitors to SA (containing sulfated alginate) is likely biologically significant, as shown by the low TCC response and could at least partly be related to a direct binding of these factors. In addition, low levels of C3 in both proteomics (enriched >2-fold from plasma) and CLSM analyses, together with a pronounced enrichment of CFH (>44-fold) for SA, indicates that the balance of activating and inhibiting proteins is important for the biological outcome. This is further apparent when comparing to AP, which showed low levels of the complement inhibitors while the highest deposition of C3 and properdin (CFP). This further coincides with a significant TCC response in hWB. The abundant plasma protein C3 is crucial for downstream complement activation, where CFP serves to

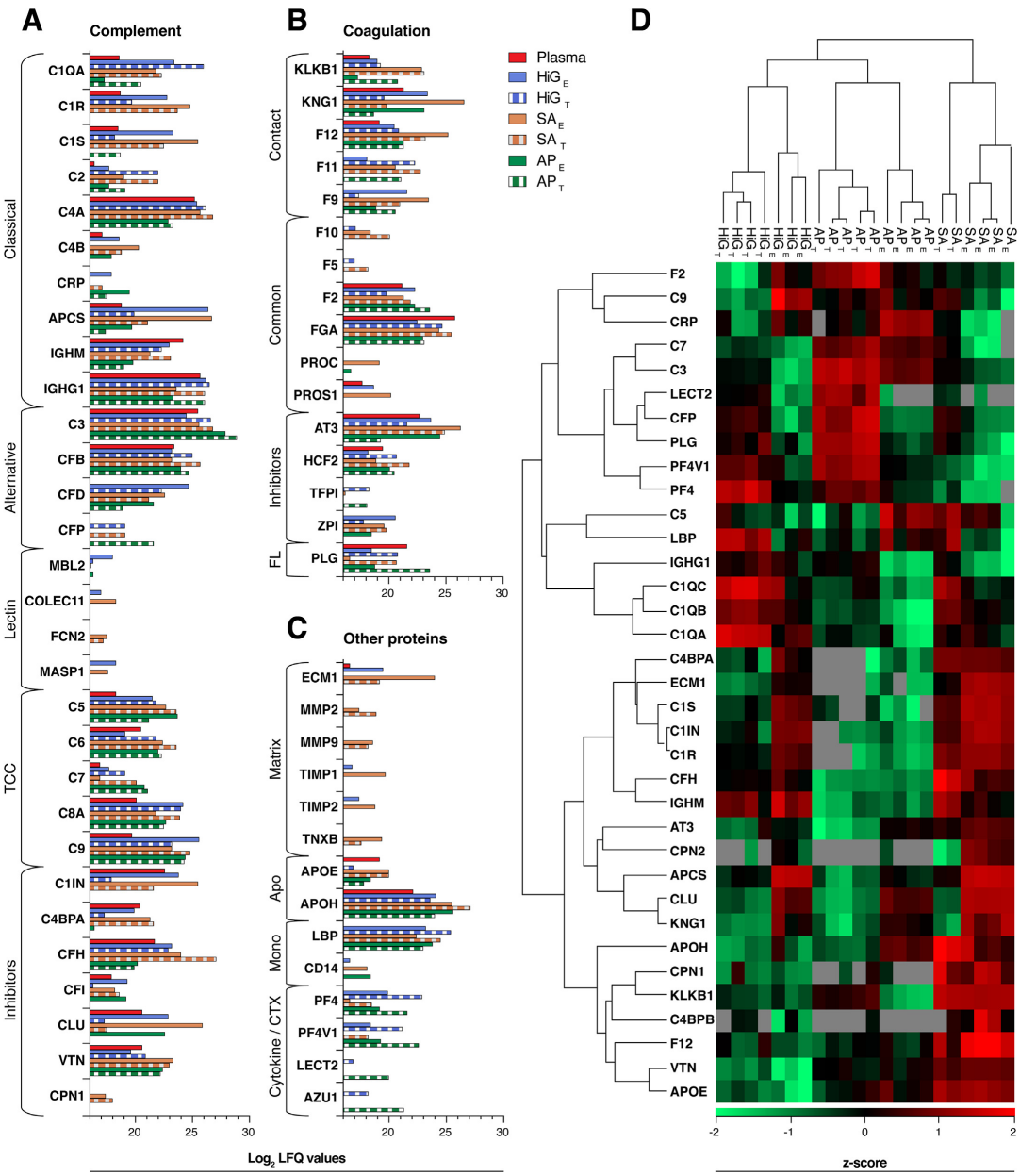

Fig. 5. Immune profiling of adsorbed plasma proteins on alginate microspheres. Isolated proteins from eluted (E)- and trypsinated-on-microsphere (T)-fractions of the microspheres (HiG, SA, AP) and the plasma control. (**A**) Adsorbed proteins of the complement system, (**B**) coagulation system, and (**C**) other potentially relevant proteins grouped with their associated pathway or mechanistic function. Protein abundance is given as $\log_2$ LFQ values, where a difference of 1 equals a 2-fold change. (**D**) Selected adsorbed plasma proteins are presented in the heatmap using z-scored $\log_2$ LFQ values. The median score is zero (*black*), and the grey colour indicates not detected proteins. Proteins are denoted by gene names. TCC = terminal complement complex, FL = fibrinolytic system, Matrix = extracellular matrix-associated, Apo = apolipoproteins, Mono = monocyte associated, CTX = chemoattractant.

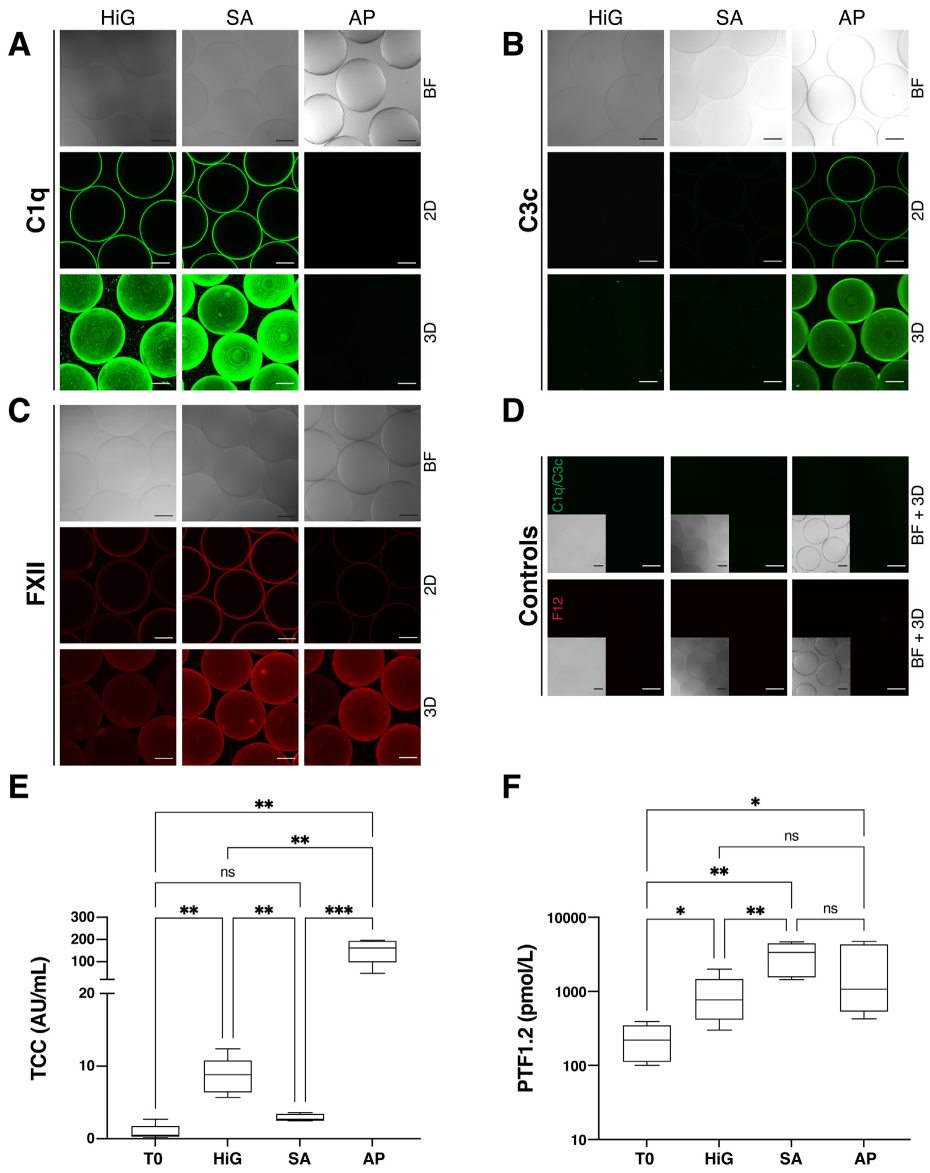

Fig. 6. Evaluation of complement and coagulation proteins and responses on/to alginate microspheres. Detection of complement (C1q, C3c) and coagulation proteins (FXII) in human plasma by CLSM (**A-D**) and activation in human whole blood by terminal complement complex (TCC) and prothrombin fragment 1 + 2 (PTF1.2) (**E, F**). CLSM images show antibody-stained alginate microspheres HiG, SA, and AP after incubation (24 h) in lepirudin-anticoagulated human plasma. Microspheres were FITC-stained (*green*) against complement C1q (**A**) and C3c (**B**) and CF633-stained (*red*) against coagulation FXII (**C**), and non-specific antibody binding was assessed (**D**). Captured images include brightfield (BF), equatorial (2D)-sections and (3D)-projections of z-stacked images. Scale bar: 200 μm. Activation of complement by TCC-induction (**E**) and coagulation by PTF1.2 formation (**F**) was assessed after incubation (4 h) in lepirudin-anticoagulated human whole blood. Controls measured (median ± SEM), but not shown, included positive control for PTF1.2 (glass): 759 954 ± 197 581 pmol/L, and saline control: 12.9 ± 5.2 AU/mL (TCC) and 401 ± 169 pmol/L (PTF1.2). Data are expressed in box plots with values from five donors. Significant values are given as $p \leq 0.05$ (*), $p \leq 0.01$ (**), $p \leq 0.001$ (***) between indicated sample groups. T0 represents the experimental baseline. (For interpretation of the references to colour in this figure legend, the reader is referred to the Web version of this article.)

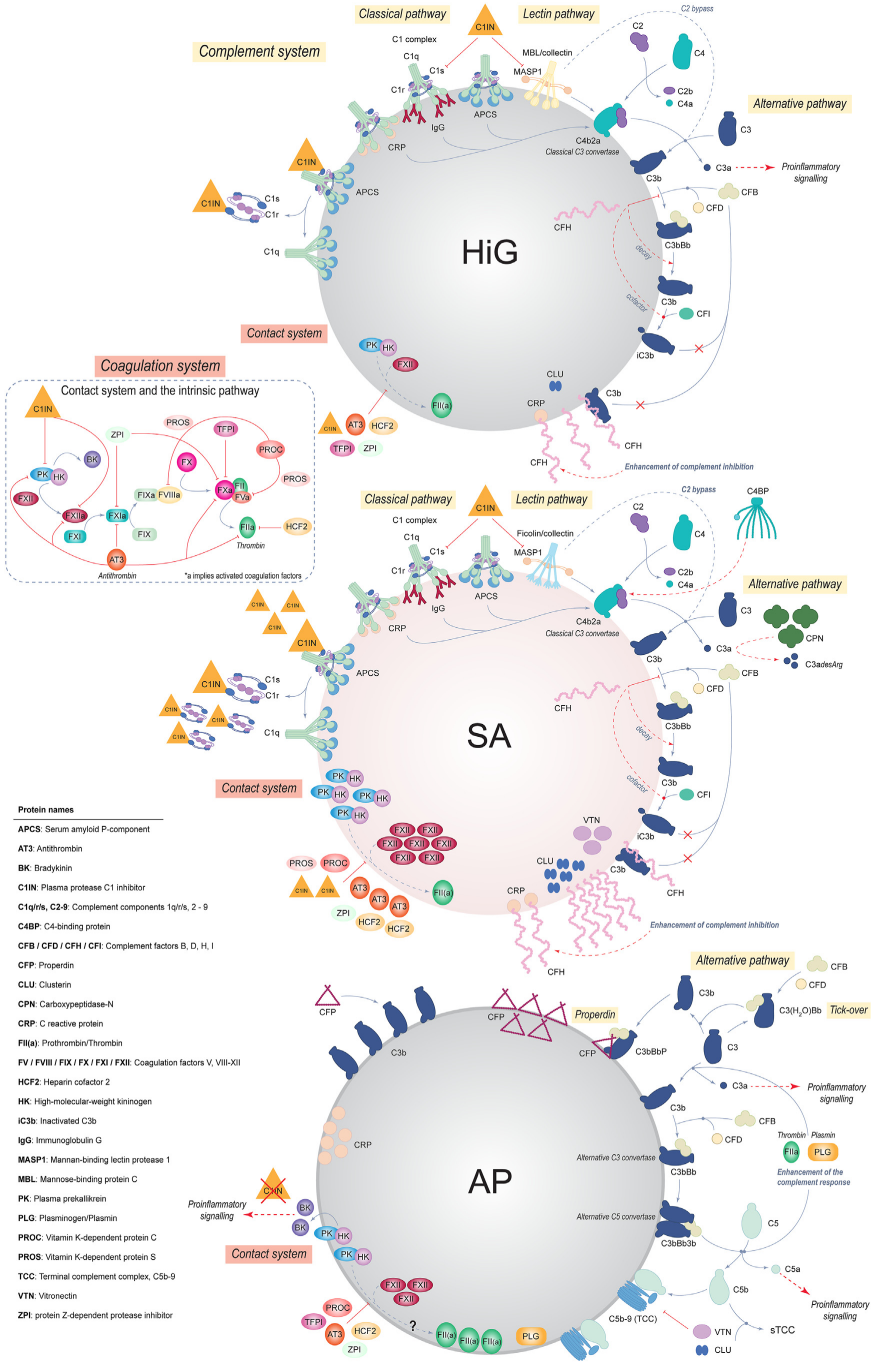

(caption on next page)

Fig. 7. Proposed mechanisms of complement and coagulation responses on the alginate microspheres based on proteomic and CLSM analyses as well as functional data from human whole blood (hWB). The complement and coagulation systems are interconnected protein defence systems [71], consisting of sequential activation of zymogens to active proteinases during inflammatory responses. **The complement system** is activated by three distinct pathways: classical, lectin and alternative, which have been thoroughly described elsewhere [68,69]. HiG and SA are significantly enriched with proteins of both the classical (e.g. C1q and APCS) and lectin pathways (MBL/collectins/ficolins), which may suggest an initial complement activation. However, low levels of C3 indicate a prompt attenuation of this potential complement response through initial regulators. SA is unique in the high abundance of adsorbed complement inhibitors (C1IN, CFH, CFI, C4BP, CPN, CLU, VTN). HiG is enriched with fewer inhibitors (C1IN, CFH, CFI, CLU) and to a lesser extent. HiG, and especially SA, exhibit low terminal complement activity (fluid-phase TCC; sTCC) in hWB, despite being enriched with proteins involved in TCC formation, which suggest inactivation of TCC or adsorption of non-assembled TCC-components. AP displays pronounced enrichment of CFP and C3, indicating complement initiation and propagation through the alternative pathway. Moreover, enrichment of prothrombin/thrombin (FII [a]) and plasminogen/plasmin (PLG) also present the additional possibility of a complement-independent activation of C3 and C5. AP is distinct in the absence or low levels of initial complement inhibitors. This is in accordance with a persisting complement response and subsequent terminal complement activity, shown for these microspheres by the high levels of adsorbed proteins involved in TCC formation and the significant TCC response in hWB. **The coagulation system** is activated through two mechanisms: the extrinsic (tissue factor) pathway (not discussed here) and the intrinsic (contact activation) pathway, which has been described elsewhere [70,72–74]. All the microspheres activate coagulation to some extent, as seen by the functional hWB data. SA has an overall moderate coagulation reactivity but the highest coagulation (prothrombin fragment 1 + 2) response among the microspheres. Being highly enriched with proteins of the intrinsic pathway, such as FXII, suggests coagulation activation through the contact system. SA is also enriched with numerous coagulation inhibitors (AT3, HCF2, C1IN, PROC, ZPI), which likely diminishes this activation. HiG shares a similar coagulation profile to SA in types of enriched proteins, although at significantly lower abundances and with some variation in adsorbed inhibitors (i.e. PROC, TFPI). Distinctively, AP is enriched with all the contact system proteins, except for C1IN, which potentially allows for pro-inflammatory signalling by BK. Further enrichments include several coagulation inhibitors (AT3, HCF2, PROC, ZPI, TFPI). AP shows the highest enrichment of FII(a) yet distinctively lacks central proteins (FX, FV) of the intrinsic pathway. Hence, the observed coagulation reactivity in hWB indicates tissue factor-dependent initiation [48], closely linked to complement activation.

stabilise the C3 protein in its active form (C3 convertase) [68]. Thus, the data indicates that the C3 convertase is built at the surface of AP, with further downstream activation of the complement cascade leading to the formation of TCC. Previously, we have shown that the binding of C3 to the surface of AP leads to the adhesion of leukocytes *in vitro* with subsequent secretion of pro-inflammatory cytokines [15,16]. In agreement with our previous work, the proteomics study by Wang et al. on human serum proteins adsorbed to PEG hydrogels revealed the binding and activation of C3, where the inactivation of C3 (incubation in C3-inactivated serum) led to a reduction in the attachment of human monocytes *in vitro* [20].

In the functional assay (hWB) herein, HiG induced a low TCC response yet significantly elevated above that of SA. The proteomic analysis may provide insight into the subtle differences in inflammatory potentials of the microspheres, showing that the enriched complement inhibitors were significantly less abundant on HiG compared to SA (Fig. 7). Intriguingly, both microspheres showed an extensive enrichment of C1q (classical pathway), as well as being enriched with proteins of the lectin pathway, which could indicate an initial complement recognition. However, if this recognition leads to complement activation it is likely subdued at an early stage, in accordance with enriched inhibitors (C1IN), lower-level enrichment of C3, minimal C3c deposition verified by CLSM and, importantly, low TCC induction in the functional hWB assay. In support, the cluster analysis of bound proteins showed a potential inactivation of C1 complex (C1q/C1r/C1s) by grouping its inhibitor (C1IN) with the C1q-associated proteases (C1r, C1s). C1IN is known to bind these proteases, forming an inactive covalent complex that dissociates from C1q and hinders downstream complement activation [69]. Interestingly, C1q was more enriched on HiG whereas C1IN was more enriched on SA, which might explain the slightly lower complement activation of SA in hWB. It has previously been shown that sulfated polysaccharides (e.g. sulfated GAGs and dextran sulfate) potentiate C1IN activity [89]. The anti-inflammatory effects of C1IN encompass the regulation of the classical and lectin complement pathways, as well as the coagulation (contact pathway) and fibrinolytic systems [86].

In the assessment of the total coagulation activation in hWB (prothrombin factor 1 + 2; PTF1.2), we found an elevated response for SA. The proteomics data showed a marked enrichment of the initiators of the contact pathway on SA, including coagulation factor XII (FXII), plasma kallikrein (KLKB1) and high-molecular-weight kininogen (KNG1), thus pointing to an initiation through the contact pathway. Still, the coagulation response of SA is considered moderate in comparison to the glass control, which is a prominent activator of FXII [48]. This could be explained by the enrichment of C1IN, which also regulates the contact pathway. In addition, SA was enriched with several coagulation inhibitors, especially antithrombin-III (AT3) and heparin cofactor 2 (HCF2). This finding points to a similarity to heparin that mediates its anticoagulation effect through the binding of AT3 [90].

In the following sections, we discuss the proteomics data in connection with the previously reported PFO outcomes and focus on the poorly understood differences in PFO between HiG and SA, the former being prone to PFO as opposed to the latter exhibiting minimal PFO *in vivo* [10]. Their elucidated immune profiles present similar protein identities, except for a few regulatory proteins, yet they display distinct protein abundances. These subtle differences might tip the balance toward a PFO response as seen for HiG. In detail, SA was unique in its abundant and strong association to a multitude of complement inhibitors, which were less prominent on HiG. Importantly, this includes the binding of complement factor H (CFH) that was profoundly more enriched on SA compared to HiG and, contrastingly, not enriched on AP. The abundant enrichment of CFH is particularly interesting as it serves a protective role against complement-targeted destruction in the host [68], and CFH enrichment strategies have previously been used to improve the biocompatibility of biomaterials [91]. In addition, an extensive enrichment of serum amyloid-P component (APCS) was found on HiG and SA. APCS is involved in several aspects of innate immunity, including inhibiting the differentiation of fibrocytes and pro-fibrotic macrophages, and has been proposed as a potential anti-fibrotic therapeutic [92]. The strong binding of IgG (e.g. IGHG1) and other immunoglobulins was consistently more pronounced on HiG. The classical pathway, mediated by the action of C1q and its numerous pattern recognition molecules, is strongly initiated by IgG or IgM [68]. Cluster analysis of the proteomics data grouped IgG with C1q (Fig. 5D), which was most prominent for HiG and could indicate a relatively higher degree of C1q activation. As discussed above, the clustering of C1IN with the C1q-associated proteases was most prominent for SA and could point to a relatively larger degree of C1q inactivation. Thus, the potential activation state of C1q might prove relevant for the PFO outcomes of HiG (fibrotic) and SA (anti-fibrotic). Complement proteins (such as C3) play a central role in fibrotic tissue development [17,19], and we recently demonstrated the *in vivo* deposition of C3 on highly PFO-prone AP microspheres [10]. In the proteomics study herein, AP displayed the highest enrichment of C3 and, intriguingly, the acute-phase protein C-reactive protein (CRP). CRP is involved in classical complement activation [68] and has further been shown to promote cell-mediated responses with potential recruitment of inflammatory cells [93]. Romero-Gavilán et al. found that CRP, as well as C1q, was most abundant on titanium-based implants that were prone to fibrotic responses, wherein the authors postulate that the ratio of complement activators and inhibitors may determine the *in vivo* outcome [30].

The fibrinolytic system is known to restrict the propagation of blood clots by dissolving fibrin during wound healing processes. In our previous *in vivo* experiments [10], the accumulation of fibrin(ogen) on the microspheres was found to coincide with PFO, where SA exhibited a significantly lower degree of PFO and fibrin(ogen) deposition than HiG and AP. In the current study, specific regulatory factors of fibrinolysis [94], involving the activation of plasminogen to form the active fibrinolytic enzyme plasmin, could indicate that SA has a higher inherent potential for fibrinolysis. The levels of the plasminogen activators FXII and KLKB1 were markedly higher on SA, and the plasmin inhibitor alpha-2-macroglobulin (A2M) was strikingly more depleted, compared to HiG and AP (Supplementary Fig. S2).

The significantly enriched heparin-binding proteins which were unique for the anti-fibrotic SA include the matrix metalloproteinases (MMPs [MMP2, MMP9]), neutrophil elastase (ELANE) and tenascin-X (TNXB). The ECM degrading enzymes MMP2 and MMP9 have been found to inhibit, and also promote, fibrosis in different fibrotic disease models [95,96]. Interestingly, the MMPs and their regulators (TIMPs) were enriched on SA, while only the latter was enriched on HiG. The intricate balance between MMPs and TIMPs and their potential roles in fibrosis might prove relevant for biomaterial-mediated fibrotic responses and, in effect, the fibrotic outcome for SA and HiG. The neutrophil-derived protease ELANE modulates innate immunity and inflammation, where excessive activity has been shown to hamper phagocytic recognition and clearance through the digestion of opsonins and opsonin receptors [97]. The ECM glycoprotein TNXB plays an important role in ECM architecture and tissue integrity, which has been shown to have anti-adhesive properties [98]. Several apolipoproteins involved in lipid metabolism, among others [99], were detected on the microspheres, which were consistently more pronounced on SA compared to HiG and AP. Interestingly, the apolipoproteins E (APOE) and H (APOH; β2-glycoprotein 1) have been reported to have anti-fibrotic effects [100,101].

In summary, the previous sections have highlighted proteins that may have an impact on the PFO responses seen *in vivo* [10], with a particular focus on HiG and SA. Sulfated alginate reduces the fibrotic host response towards empty and cell-containing microbeads compared to high G alginate [3,10], demonstrating the significance of using biomaterials with low inflammatory potential in cellular therapies that depend on the free diffusion of oxygen and nutrients to encapsulated cells. In this study, the binding of inhibitors (e.g. C1IN and CFH) and heparin-binding proteins to SA are striking. Recruiting CFH to biomaterial surfaces has previously been shown to attenuate biomaterial-mediated inflammatory responses [91], thus underscoring the clinical relevance of surface-associating proteins in terms of biocompatibility. Importantly, as the proteomic analysis does not provide information on the activation state of the proteins, it needs to be supported with functional studies. Here, we focused on the proteolytically active cascades of complement and coagulation in human whole blood. The proteomics data serves to deepen our understanding of the mechanisms of activation by providing insight into the binding of activators and inhibitors to the biomaterial surface. This culminates in the biological effects seen as complement or coagulation activation *in vitro* or fibrotic tissue development *in vivo*.

5. Conclusion

The current study is the first to document the adsorption of human plasma proteins on alginate hydrogel microspheres using LC-MS/MS-based proteomics. In conjunction with functional data of complement and coagulation activation in human whole blood, the proteomic analysis signifies a physiologically relevant method for elucidating protein-based immune profiles of alginate hydrogel materials. Utilising lepirudin-based plasma enables the investigation of proteolytic activable cascades of the complement and coagulation systems, which are critical activators of the host immune system. Protein profiling revealed novel details on the selective protein binding to the different alginate-based materials, and that could help explain their different PFO outcomes shown in previous studies. The abundant binding of complement and coagulation inhibitors to SA conforms to a low-inflammatory and anti-fibrotic profile. Moderate levels of inhibitors to HiG conform to a low-inflammatory but pro-fibrotic profile. In contrast, the enrichment of complement activators in combination with low amounts of inhibitors on AP conforms to a pro-inflammatory and pro-fibrotic profile. The current work presents a step forward in understanding the underlying mechanisms of the inflammatory and PFO responses towards alginate-based microspheres. SA possibly evades fibrosis through the extensive binding of acute-phase inhibitors. Heparin-binding proteins enriched on SA may have additional anti-fibrotic effects. Ultimately, the method and results presented in this study can serve as tools to tailor novel biocompatible alginate materials intended for cell-based therapies as well as other therapeutic or diagnostic applications.

Credit author statement

Abba E. Coron: Conceptualisation, Methodology, Validation, Formal analysis, Investigation, Writing – original draft, Writing – review & editing, Visualisation. **Davi M. Fonseca**: Conceptualisation, Methodology, Validation, Investigation, Writing – review & editing. **Animesh Sharma**: Conceptualisation, Methodology, Validation, Formal analysis, Resources, Writing – review & editing. **Geir Slupphaug**: Conceptualisation, Methodology, Validation, Resources, Writing – review & editing, Funding acquisition. **Berit L. Strand**: Conceptualisation, Methodology, Validation, Resources, Writing – review & editing, Supervision, Project administration, Funding acquisition. **Anne Mari A. Rokstad**: Conceptualisation, Methodology, Validation, Investigation, Resources, Writing – review & editing, Supervision, Project administration, Funding acquisition.

Funding

This work was supported by the Norwegian University of Science and Technology (NTNU), Faculty for Natural Science, The Liaison Committee for Education, Research, and Innovation in Central Norway (Regional Health Authority, Samarbeidsorganet) under grant 46056819, CEMIR NFR grant 223255, NTNU Health project "Tailored biomaterials with reduced immune responses", and the Chicago Diabetes Project (www.chicagodiabetesproject.org). PROMEC is funded by the Faculty of Medicine at NTNU and Central Norway Regional Health Authority. PROMEC is a member of the National Network of Advanced Proteomics Infrastructure (NAPI), which is funded by the RCN INFRASTRUKTUR-program (295910).

Declaration of competing interest

The authors declare that they have no known competing financial interests or personal relationships that could have appeared to influence the work reported in this paper.

Data availability

Data will be made available on request.

Acknowledgements

We thank professor emeritus Gudmund Skjåk-Bræk, NTNU, for support on the development of sulfated alginate as well as on previous work on alginate microspheres. Professor Jose Oberholzer, University of Virginia, is acknowledged for continuous support in the development of encapsulation systems for type 1 diabetes. Øystein Arlov at the SINTEF research institute is credited for providing guidance in the sulfation of alginate and measuring the sulfur content (HR-ICP-MS) of the sulfated alginate.

Appendix A. Supplementary data

Supplementary data to this article can be found online at https://doi.org/10.1016/j.mtbio.2022.100490.

References

[1] D. Jacobs-Tulleneers-Thevissen, M. Chintinne, Z. Ling, P. Gillard, L. Schoonjans, G. Delvaux, B.L. Strand, F. Gorus, B. Keymeulen, D. Pipeleers, Sustained function of alginate-encapsulated human islet cell implants in the peritoneal cavity of mice leading to a pilot study in a type 1 diabetic patient, Diabetologia 56 (7) (2013) 1605–1614.

[2] M.A. Bochenek, O. Veiseh, A.J. Vegas, J.J. McGarrigle, M. Qi, E. Marchese, M. Omami, J.C. Doloff, J. Mendoza-Elias, M. Nourmohammadzadeh, A. Khan, C.-C. Yeh, Y. Xing, D. Isa, S. Ghani, J. Li, C. Landry, A.R. Bader, K. Olejnik, M. Chen, J. Hollister-Lock, Y. Wang, D.L. Greiner, G.C. Weir, B.L. Strand, A.M.A. Rokstad, I. Lacik, R. Langer, D.G. Anderson, J. Oberholzer, Alginate encapsulation as long-term immune protection of allogeneic pancreatic islet cells transplanted into the omental bursa of macaques, Nat Biomed Eng 2 (11) (2018) 810–821.

[3] A.M. Syanda, V.I. Kringstad, S.J.I. Blackford, J.S. Kjesbu, S.S. Ng, L. Ma, F. Xiao, A.E. Coron, A.M.A. Rokstad, S. Modi, S.T. Rashid, B.L. Strand, Sulfated alginate reduces pericapsular fibrotic overgrowth on encapsulated cGMP-compliant hPSC-hepatocytes in mice, Front. Bioeng. Biotechnol. 9 (2022).

[4] J.M. Anderson, A. Rodriguez, D.T. Chang, Foreign body reaction to biomaterials, Semin. Immunol. 20 (2) (2008) 86–100.

[5] A.M.A. Rokstad, I. Lacík, P. de Vos, B.L. Strand, Advances in biocompatibility and physico-chemical characterization of microspheres for cell encapsulation, Adv. Drug Deliv. Rev. 67–68 (2014) 111–130.

[6] O. Veiseh, J.C. Doloff, M. Ma, A.J. Vegas, H.H. Tam, Andrew R. Bader, J. Li, E. Langan, J. Wyckoff, W.S. Loo, S. Jhunjhunwala, A. Chiu, S. Siebert, K. Tang, J. Hollister-Lock, S. Aresta-Dasilva, M. Bochenek, J. Mendoza-Elias, Y. Wang, M. Qi, D.M. Lavin, M. Chen, N. Dholakia, R. Thakrar, I. Lacík, Gordon C. Weir, J. Oberholzer, D.L. Greiner, R. Langer, D.G. Anderson, Size- and shape-dependent foreign body immune response to materials implanted in rodents and non-human primates, Nat. Mater. 14 (6) (2015) 643–651.

[7] Z. Othman, B. Cillero Pastor, S. van Rijt, P. Habibovic, Understanding interactions between biomaterials and biological systems using proteomics, Biomaterials 167 (2018) 191–204.

[8] A.E. Engberg, P.H. Nilsson, S. Huang, K. Fromell, O.A. Hamad, T.E. Mollnes, J.P. Rosengren-Holmberg, K. Sandholm, Y. Teramura, I.A. Nicholls, B. Nilsson, K.N. Ekdahl, Prediction of inflammatory responses induced by biomaterials in contact with human blood using protein fingerprint from plasma, Biomaterials 36 (2015) 55–65.

[9] P. Soon-Shiong, R.E. Heintz, N. Merideth, Q.X. Yao, Z. Yao, T. Zheng, M. Murphy, M.K. Moloney, M. Schmehl, M. Harris, et al., Insulin independence in a type 1 diabetic patient after encapsulated islet transplantation, Lancet 343 (8903) (1994) 950–951.

[10] A.E. Coron, J.S. Kjesbu, F. Kjærnsmo, J. Oberholzer, A.M.A. Rokstad, B.L. Strand, Pericapsular fibrotic overgrowth mitigated in immunocompetent mice through microbead formulations based on sulfated or intermediate G alginates, Acta Biomater. 137 (2022) 172–185.

[11] S.K. Tam, J. Dusseault, S. Bilodeau, G. Langlois, J.-P. Hallé, L.H. Yahia, Factors influencing alginate gel biocompatibility, J. Biomed. Mater. Res. 98A (1) (2011) 40–52.

[12] B.L. Strand, L. Ryan, P.I.t. Veld, B. Kulseng, A.M. Rokstad, G. Skjåk-Bræk, T. Espevik, Poly-L-lysine induces fibrosis on alginate microcapsules via the induction of cytokines, Cell Transplant. 10 (3) (2001) 263–275.

[13] A. King, S. Sandler, A. Andersson, The effect of host factors and capsule composition on the cellular overgrowth on implanted alginate capsules, J. Biomed. Mater. Res. 57 (3) (2001) 374–383.

[14] A.M. Rokstad, O.-L. Brekke, B. Steinkjer, L. Ryan, G. Kolláriková, B.L. Strand, G. Skjåk-Bræk, I. Lacík, T. Espevik, T.E. Mollnes, Alginate microbeads are complement compatible, in contrast to polycation containing microcapsules, as revealed in a human whole blood model, Acta Biomater. 7 (6) (2011) 2566–2578.

[15] P. Ørning, K.S. Hoem, A.E. Coron, G. Skjåk-Bræk, T.E. Mollnes, O.-L. Brekke, T. Espevik, A.M. Rokstad, Alginate microsphere compositions dictate different mechanisms of complement activation with consequences for cytokine release and leukocyte activation, J. Contr. Release 229 (2016) 58–69.

[16] A.M. Rokstad, O.-L. Brekke, B. Steinkjer, L. Ryan, G. Kolláriková, B.L. Strand, G. Skjåk-Bræk, J.D. Lambris, I. Lacík, T.E. Mollnes, T. Espevik, The induction of cytokines by polycation containing microspheres by a complement dependent mechanism, Biomaterials 34 (3) (2013) 621–630.

[17] V. Vaithilingam, B. Steinkjer, L. Ryan, R. Larsson, B.E. Tuch, J. Oberholzer, A.M. Rokstad, Vitro and in vivo biocompatibility evaluation of polyallylamine and macromolecular heparin conjugates modified alginate microbeads, Sci. Rep. 7 (1) (2017), 11695.

[18] A.K. McNally, J.M. Anderson, Complement C3 participation in monocyte adhesion to different surfaces, Proc. Natl. Acad. Sci. U. S. A. 91 (21) (1994) 10119–10123.

[19] I. Kourtzelis, S. Rafail, R.A. DeAngelis, P.G. Foukas, D. Ricklin, J.D. Lambris, Inhibition of biomaterial-induced complement activation attenuates the inflammatory host response to implantation, Faseb. J. 27 (7) (2013) 2768–2776.

[20] X. Wang, D.R. Schmidt, E.J. Joyce, W.J. Kao, Application of MS-based proteomics to study serum protein adsorption/absorption and complement C3 activation on poly(ethylene glycol) hydrogels, Journal of biomaterials science, Polym. Ed. 22 (10) (2011) 1343–1362.

[21] S.A. Safley, N.S. Kenyon, D.M. Berman, G.F. Barber, M. Willman, S. Duncanson, N. Iwakoshi, R. Holdcraft, L. Gazda, P. Thompson, I.R. Badell, A. Sambanis, C. Ricordi, C.J. Weber, Microencapsulated adult porcine islets transplanted intraperitoneally in streptozotocin-diabetic non-human primates, Xenotransplantation 25 (6) (2018), e12450.

[22] Q. Liu, A. Chiu, L.H. Wang, D. An, M. Zhong, A.M. Smink, B.J. de Haan, P. de Vos, K. Keane, A. Vegge, E.Y. Chen, W. Song, W.F. Liu, J. Flanders, C. Rescan, L.G. Grunnet, X. Wang, M. Ma, Zwitterionically modified alginates mitigate cellular overgrowth for cell encapsulation, Nat. Commun. 10 (1) (2019) 5262.

[23] A.J. Vegas, O. Veiseh, J.C. Doloff, M. Ma, H.H. Tam, K. Bratlie, J. Li, A.R. Bader, E. Langan, K. Olejnik, P. Fenton, J.W. Kang, J. Hollister-Locke, M.A. Bochenek, A. Chiu, S. Siebert, K. Tang, S. Jhunjhunwala, S. Aresta-Dasilva, N. Dholakia, R. Thakrar, T. Vietti, M. Chen, J. Cohen, K. Siniakowicz, M. Qi, J. McGarrigle, A.C. Graham, S. Lyle, D.M. Harlan, D.L. Greiner, J. Oberholzer, G.C. Weir, R. Langer, D.G. Anderson, Combinatorial hydrogel library enables identification of materials that mitigate the foreign body response in primates, Nat. Biotechnol. 34 (3) (2016) 345–352.

[24] Ø. Arlov, F.L. Aachmann, A. Sundan, T. Espevik, G. Skjåk-Bræk, Heparin-Like properties of sulfated alginates with defined sequences and sulfation degrees, Biomacromolecules 15 (7) (2014) 2744–2750.

[25] Ø. Arlov, G. Skjåk-Bræk, A.M. Rokstad, Sulfated alginate microspheres associate with factor H and dampen the inflammatory cytokine response, Acta Biomater. 42 (2016) 180–188.

[26] I. Freeman, A. Kedem, S. Cohen, The effect of sulfation of alginate hydrogels on the specific binding and controlled release of heparin-binding proteins, Biomaterials 29 (22) (2008) 3260–3268.

[27] M.D. Swartzlander, C.A. Barnes, A.K. Blakney, J.L. Kaar, T.R. Kyriakides, S.J. Bryant, Linking the foreign body response and protein adsorption to PEG-based hydrogels using proteomics, Biomaterials 41 (2015) 26–36.

[28] Y. Yamada, G. Fichman, J.P. Schneider, Serum protein adsorption modulates the toxicity of highly positively charged hydrogel surfaces, ACS Appl. Mater. Interfaces 13 (7) (2021) 8006–8014.

[29] J. Kim, Systematic approach to characterize the dynamics of protein adsorption on the surface of biomaterials using proteomics, Colloids Surf. B Biointerfaces 188 (2020), 110756.

[30] F. Romero-Gavilán, A.M. Sánchez-Pérez, N. Araújo-Gomes, M. Azkargorta, I. Iloro, F. Elortza, M. Gurruchaga, I. Goñi, J. Suay, Proteomic analysis of silica hybrid sol-gel coatings: a potential tool for predicting the biocompatibility of implants in vivo, Biofouling 33 (8) (2017) 676–689.

[31] N. Araújo-Gomes, F. Romero-Gavilán, I. Lara-Sáez, F. Elortza, M. Azkargorta, I. Iloro, M. Martínez-Ibañez, J.J. Martín de Llano, M. Gurruchaga, I. Goñi, J. Suay, A.M. Sánchez-Pérez, Silica–gelatin hybrid sol–gel coatings: a proteomic study with biocompatibility implications, J. Tissue Eng. Regen. Med. 12 (7) (2018) 1769–1779.

[32] I. García-Arnáez, F. Romero-Gavilán, A. Cerqueira, F. Elortza, M. Azkargorta, F. Muñoz, M. Mata, J.J.M. de Llano, J. Suay, M. Gurruchaga, I. Goñi, Correlation between biological responses in vitro and in vivo to Ca-doped sol-gel coatings assessed using proteomic analysis, Colloids Surf. B Biointerfaces 220 (2022), 112962.

[33] E. Buck, S. Lee, Q. Gao, S.D. Tran, F. Tamimi, L.S. Stone, M. Cerruti, The role of surface chemistry in the osseointegration of PEEK implants, ACS Biomater. Sci. Eng. 8 (4) (2022) 1506–1521.

[34] C. Sacchetti, K. Motamedchaboki, A. Magrini, G. Palmieri, M. Mattei, S. Bernardini, N. Rosato, N. Bottini, M. Bottini, Surface polyethylene glycol conformation influences the protein corona of polyethylene glycol-modified single-walled carbon nanotubes: potential implications on biological performance, ACS Nano 7 (3) (2013) 1974–1989.

[35] D.H. Jo, J.H. Kim, J.G. Son, K.S. Dan, S.H. Song, T.G. Lee, J.H. Kim, Nanoparticle-protein complexes mimicking corona formation in ocular environment, Biomaterials 109 (2016) 23–31.

[36] J. Lazarovits, S. Sindhwani, A.J. Tavares, Y. Zhang, F. Song, J. Audet, J.R. Krieger, A.M. Syed, B. Stordy, W.C.W. Chan, Supervised learning and mass spectrometry predicts the in vivo fate of nanomaterials, ACS Nano 13 (7) (2019) 8023–8034.

[37] L. Vroman, A.L. Adams, Identification of rapid changes at plasma-solid interfaces, J. Biomed. Mater. Res. 3 (1) (1969) 43–67.

[38] M. Rabe, D. Verdes, S. Seeger, Understanding protein adsorption phenomena at solid surfaces, Adv. Colloid Interface Sci. 162 (1) (2011) 87–106.

[39] M.-N. Abdallah, S.D. Tran, G. Abughanam, M. Laurenti, D. Zuanazzi, M.A. Mezour, Y. Xiao, M. Cerruti, W.L. Siqueira, F. Tamimi, Biomaterial surface proteomic signature determines interaction with epithelial cells, Acta Biomater. 54 (2017) 150–163.

[40] M. Hammad, W. Rao, J.G.W. Smith, D.G. Anderson, R. Langer, L.E. Young, D.A. Barrett, M.C. Davies, C. Denning, M.R. Alexander, Identification of polymer surface adsorbed proteins implicated in pluripotent human embryonic stem cell expansion, Biomater. Sci. 4 (9) (2016) 1381–1391.

[41] K.N. Ekdahl, J.D. Lambris, H. Elwing, D. Ricklin, P.H. Nilsson, Y. Teramura, I.A. Nicholls, B. Nilsson, Innate immunity activation on biomaterial surfaces: a mechanistic model and coping strategies, Adv. Drug Deliv. Rev. 63 (12) (2011) 1042–1050.

[42] B. Nilsson, K.N. Ekdahl, T.E. Mollnes, J.D. Lambris, The role of complement in biomaterial-induced inflammation, Mol. Immunol. 44 (1–3) (2007) 82–94.

[43] A. Landsem, H. Fure, D. Christiansen, E.W. Nielsen, B. Østerud, T.E. Mollnes, O.L. Brekke, The key roles of complement and tissue factor in Escherichia coli-

induced coagulation in human whole blood, Clin. Exp. Immunol. 182 (1) (2015) 81–89.
[44] T.E. Mollnes, O.-L. Brekke, M. Fung, H. Fure, D. Christiansen, G. Bergseth, V. Videm, K.T. Lappegard, J.r. Kohl, J.D. Lambris, Essential role of the C5a receptor in E coli–induced oxidative burst and phagocytosis revealed by a novel lepirudin-based human whole blood model of inflammation, Blood 100 (5) (2002) 1869–1877.
[45] A. Hovland, R. Hardersen, E.W. Nielsen, T. Enebakk, D. Christiansen, J.K. Ludviksen, T.E. Mollnes, K.T. Lappegård, Complement profile and activation mechanisms by different LDL apheresis systems, Acta Biomater. 8 (6) (2012) 2288–2296.
[46] A. Sokolov, B.C. Hellerud, E.A. Johannessen, T.E. Mollnes, Inflammatory response induced by candidate biomaterials of an implantable microfabricated sensor, J. Biomed. Mater. Res. 100A (5) (2012) 1142–1150.
[47] K.T. Lappegård, G. Bergseth, J. Riesenfeld, A. Pharo, P. Magotti, J.D. Lambris, T.E. Mollnes, The artificial surface-induced whole blood inflammatory reaction revealed by increases in a series of chemokines and growth factors is largely complement dependent, J. Biomed. Mater. Res. 87 (1) (2008) 129–135.
[48] C. Gravastrand, S. Hamad, H. Fure, B. Steinkjer, L. Ryan, J. Oberholzer, J.D. Lambris, I. Lacík, T.E. Mollnes, T. Espevik, O.-L. Brekke, A.M. Rokstad, Alginate microbeads are coagulation compatible, while alginate microcapsules activate coagulation secondary to complement or directly through FXII, Acta Biomater. 58 (2017) 158–167.
[49] H. Grasdalen, B. Larsen, O. Smidsrød, A p.m.r., Study of the composition and sequence of uronate residues in alginates, Carbohydr. Res. 68 (1) (1979) 23–31.
[50] H. Grasdalen, High-field, 1H-n.m.r. spectroscopy of alginate: sequential structure and linkage conformations, Carbohydr. Res. 118 (1983) 255–260.
[51] I.M.N. Vold, K.A. Kristiansen, B.E. Christensen, A study of the chain stiffness and extension of alginates, in vitro epimerized alginates, and periodate-oxidized alginates using size-exclusion chromatography combined with light scattering and viscosity detectors, Biomacromolecules 7 (7) (2006) 2136–2146.
[52] B.L. Strand, O. Gåserød, B. Kulseng, T. Espevik, G. Skjåk-Baek, Alginate-polylysine-alginate microcapsules: effect of size reduction on capsule properties, J. Microencapsul. 19 (5) (2002) 615–630.
[53] J. Cox, M. Mann, MaxQuant enables high peptide identification rates, individualized p.p.b.-range mass accuracies and proteome-wide protein quantification, Nat. Biotechnol. 26 (12) (2008) 1367–1372.
[54] J. Cox, M.Y. Hein, C.A. Luber, I. Paron, N. Nagaraj, M. Mann, Accurate proteome-wide label-free quantification by delayed normalization and maximal peptide ratio extraction, termed MaxLFQ, Mol. Cell. Proteomics 13 (9) (2014) 2513–2526.
[55] C. The UniProt, Update on activities at the universal protein resource (UniProt) in 2013, Nucleic Acids Res. 41 (D1) (2012) D43–D47.
[56] A. Krämer, J. Green, J. Pollard Jr., S. Tugendreich, Causal analysis approaches in ingenuity pathway analysis, Bioinformatics 30 (4) (2014) 523–530.
[57] J.A. Vizcaíno, A. Csordas, N. del-Toro, J.A. Dianes, J. Griss, I. Lavidas, G. Mayer, Y. Perez-Riverol, F. Reisinger, T. Ternent, Q.-W. Xu, R. Wang, H. Hermjakob, Update of the PRIDE database and its related tools, Nucleic Acids Res. 44 (D1) (2016) D447–D456, 2016.
[58] R. R Core Team, A Language and Environment for Statistical Computing, R Foundation for Statistical Computing, 2017. https://www.R-project.org/.
[59] Student, The probable error of a mean, Biometrika 6 (1) (1908) 1–25.
[60] Y. Benjamini, Y. Hochberg, Controlling the false discovery rate: a practical and powerful approach to multiple testing, J. Roy. Stat. Soc. B 57 (1) (1995) 289–300.
[61] D. Osorio, P. Rondón-Villarreal, R. Torres, Peptides: a package for data mining of antimicrobial peptides, R Journal 7 (1) (2015) 4–14.
[62] J.M. Schwenk, G.S. Omenn, Z. Sun, D.S. Campbell, M.S. Baker, C.M. Overall, R. Aebersold, R.L. Moritz, E.W. Deutsch, The human plasma proteome draft of 2017: building on the human plasma PeptideAtlas from mass spectrometry and complementary assays, J. Proteome Res. 16 (12) (2017) 4299–4310.
[63] V. Nanjappa, J.K. Thomas, A. Marimuthu, B. Muthusamy, A. Radhakrishnan, R. Sharma, A. Ahmad Khan, L. Balakrishnan, N.A. Sahasrabuddhe, S. Kumar, B.N. Jhaveri, K.V. Sheth, R. Kumar Khatana, P.G. Shaw, S.M. Srikanth, P.P. Mathur, S. Shankar, D. Nagaraja, R. Christopher, S. Mathivanan, R. Raju, R. Sirdeshmukh, A. Chatterjee, R.J. Simpson, H.C. Harsha, A. Pandey, T.S.K. Prasad, Plasma Proteome Database as a resource for proteomics research: 2014 update, Nucleic Acids Res. 42 (Database issue) (2014) D959–D965.
[64] A. Ori, M.C. Wilkinson, D.G. Fernig, A systems biology approach for the investigation of the heparin/heparan sulfate interactome, J. Biol. Chem. 286 (22) (2011) 19892–19904.
[65] A. Gómez Toledo, J.T. Sorrentino, D.R. Sandoval, J. Malmström, N.E. Lewis, J.D. Esko, A systems view of the heparan sulfate interactome, J. Histochem. Cytochem. 69 (2) (2021) 105–119.
[66] D.R. Sandoval, A. Gomez Toledo, C.D. Painter, E.M. Tota, M.O. Sheikh, A.M.V. West, M.M. Frank, L. Wells, D. Xu, R. Bicknell, K.D. Corbett, J.D. Esko, Proteomics-based screening of the endothelial heparan sulfate interactome reveals that C-type lectin 14a (CLEC14A) is a heparin-binding protein, J. Biol. Chem. 295 (9) (2020) 2804–2821.
[67] B.T. Kim, H. Kitagawa, J. Tanaka, J. Tamura, K. Sugahara, In vitro heparan sulfate polymerization: crucial roles of core protein moieties of primer substrates in addition to the EXT1-EXT2 interaction, J. Biol. Chem. 278 (43) (2003) 41618–41623.
[68] D. Ricklin, G. Hajishengallis, K. Yang, J.D. Lambris, Complement: a key system for immune surveillance and homeostasis, Nat. Immunol. 11 (9) (2010) 785–797.
[69] N.S. Merle, S.E. Church, V. Fremeaux-Bacchi, L.T. Roumenina, Complement system Part I – molecular mechanisms of activation and regulation, Front. Immunol. 6 (262) (2015).
[70] A.T. Long, E. Kenne, R. Jung, T.A. Fuchs, T. Renné, Contact system revisited: an interface between inflammation, coagulation, and innate immunity, J. Thromb. Haemostasis 14 (3) (2016) 427–437.
[71] K. Oikonomopoulou, D. Ricklin, P.A. Ward, J.D. Lambris, Interactions between coagulation and complement–their role in inflammation, Semin. Immunopathol. 34 (1) (2012) 151–165.
[72] A.J. Gale, Continuing education course #2: current understanding of hemostasis, Toxicol. Pathol. 39 (1) (2011) 273–280.
[73] H. Weidmann, L. Heikaus, A.T. Long, C. Naudin, H. Schlüter, T. Renné, The plasma contact system, a protease cascade at the nexus of inflammation, coagulation and immunity, Biochim. Biophys. Acta Mol. Cell Res. 1864 (11 Pt B) (2017) 2118–2127.
[74] T.J. Girard, N.M. Lasky, E.A. Tuley, G.J. Broze Jr., Protein Z, protein Z-dependent protease inhibitor (serpinA10), and the acute-phase response, J. Thromb. Haemostasis : JTH 11 (2) (2013) 375–378.
[75] P. Wojciechowski, J.L. Brash, The Vroman effect in tube geometry: the influence of flow on protein adsorption measurements, Journal of biomaterials science, Polym. Ed. 2 (3) (1991) 203–216.
[76] E.A. Vogler, Protein adsorption in three dimensions, Biomaterials 33 (5) (2012) 1201–1237.
[77] D.C. Briggs, A.W.W. Langford-Smith, H.L. Birchenough, T.A. Jowitt, C.M. Kielty, J.J. Enghild, C. Baldock, C.M. Milner, A.J. Day, Inter-α-inhibitor heavy chain-1 has an integrin-like 3D structure mediating immune regulatory activities and matrix stabilization during ovulation, J. Biol. Chem. 295 (16) (2020) 5278–5291.
[78] Ø. Arlov, G. Skjåk-Bræk, Sulfated alginates as heparin analogues: a review of chemical and functional properties, Molecules 22 (5) (2017) 778.
[79] Ý.A. Mørch, I. Donati, B.L. Strand, Effect of Ca2+, Ba2+, and Sr2+ on alginate microbeads, Biomacromolecules 7 (5) (2006) 1471–1480.
[80] B. Kulseng, B. Thu, T. Espevik, G. Skjåk-Braek, Alginate polylysine microcapsules as immune barrier: permeability of cytokines and immunoglobulins over the capsule membrane, Cell Transplant. 6 (4) (1997) 387–394.
[81] M. Lekka, D. Sainz-Serp, A.J. Kulik, C. Wandrey, Hydrogel microspheres: influence of chemical composition on surface morphology, local elastic properties, and bulk mechanical characteristics, Langmuir 20 (23) (2004) 9968–9977.
[82] A. Akbarzadeh Solbu, A. Koernig, J.S. Kjesbu, D. Zaytseva-Zotova, M. Sletmoen, B.L. Strand, High resolution imaging of soft alginate hydrogels by atomic force microscopy, Carbohydr. Polym. 276 (2022), 118804.
[83] M.Ø. Dalheim, L.A. Omtvedt, I.M. Bjørge, A. Akbarzadeh, J.F. Mano, F.L. Aachmann, B.L. Strand, Mechanical properties of Ca-saturated hydrogels with functionalized alginate, Gels 5 (2) (2019) 23.
[84] E. Öztürk, Ø. Arlov, S. Aksel, L. Li, D.M. Ornitz, G. Skjåk-Bræk, M. Zenobi-Wong, Sulfated hydrogel matrices direct mitogenicity and maintenance of chondrocyte phenotype through activation of FGF signaling, Adv. Funct. Mater. 26 (21) (2016) 3649–3662.
[85] D. Ricklin, E.S. Reis, D.C. Mastellos, P. Gros, J.D. Lambris, Complement component C3 - the "Swiss Army Knife" of innate immunity and host defense, Immunol. Rev. 274 (1) (2016) 33–58.
[86] A.E. Davis III, F. Lu, P. Mejia, C1 inhibitor, a multi-functional serine protease inhibitor, Thromb. Haemostasis 104 (11) (2010) 886–893.
[87] C.Q. Schmidt, J.D. Lambris, D. Ricklin, Protection of host cells by complement regulators, Immunol. Rev. 274 (1) (2016) 152–171.
[88] M. Rajabi, E. Struble, Z. Zhou, E. Karnaukhova, Potentiation of C1-esterase inhibitor by heparin and interactions with C1s protease as assessed by surface plasmon resonance, Biochim. Biophys. Acta Gen. Subj. 1820 (1) (2012) 56–63.
[89] M. Dijk, J. Holkers, P. Voskamp, Bruno M. Giannetti, W.-J. Waterreus, Harrie A. van Veen, Navraj S. Pannu, How dextran sulfate affects C1-inhibitor activity: a model for polysaccharide potentiation, Structure 24 (12) (2016) 2182–2189.
[90] J. Hirsh, S.S. Anand, J.L. Halperin, V. Fuster, Mechanism of action and pharmacology of unfractionated heparin, Arterioscler. Thromb. Vasc. Biol. 21 (7) (2001) 1094–1096.
[91] Y.Q. Wu, H. Qu, G. Sfyroera, A. Tzekou, B.K. Kay, B. Nilsson, K. Nilsson Ekdahl, D. Ricklin, J.D. Lambris, Protection of nonself surfaces from complement attack by factor H-binding peptides: implications for therapeutic medicine, J. Immunol. 186 (7) (2011) 4269–4277.
[92] D. Pilling, R.H. Gomer, The development of serum amyloid P as a possible therapeutic, Front. Immunol. 9 (2018), 2328-2328.
[93] N.R. Sproston, J.J. Ashworth, Role of C-reactive protein at sites of inflammation and infection, Front. Immunol. 9 (2018).
[94] H. Lin, L. Xu, S. Yu, W. Hong, M. Huang, P. Xu, Therapeutics targeting the fibrinolytic system, Exp. Mol. Med. 52 (3) (2020) 367–379.
[95] M. Giannandrea, W.C. Parks, Diverse functions of matrix metalloproteinases during fibrosis, Dis Model Mech. 7 (2) (2014) 193–203.
[96] E. Leong, M. Bezuhly, J.S. Marshall, Distinct metalloproteinase expression and functions in systemic sclerosis and fibrosis: what we know and the potential for intervention, Front. Physiol. 12 (1426) (2021), 727451.

[97] J.A. Voynow, M. Shinbashi, Neutrophil elastase and chronic lung disease, Biomolecules 11 (8) (2021) 1065.
[98] U. Valcourt, L.B. Alcaraz, J.Y. Exposito, C. Lethias, L. Bartholin, Tenascin-X, Beyond the architectural function, Cell Adhes. Migrat. 9 (1–2) (2015) 154–165.
[99] T. Liu, J.-M. Chen, D. Zhang, Q. Zhang, B. Peng, L. Xu, H. Tang, ApoPred: identification of apolipoproteins and their subfamilies with multifarious features, Front. Cell Dev. Biol. 8 (2021), 621144.
[100] H. Cui, D. Jiang, S. Banerjee, N. Xie, T. Kulkarni, R.M. Liu, S.R. Duncan, G. Liu, Monocyte-derived alveolar macrophage apolipoprotein E participates in pulmonary fibrosis resolution, JCI Insight 5 (5) (2020), e134539.
[101] T. Wang, S.S. Chen, R. Chen, D.M. Yu, P. Yu, Reduced beta 2 glycoprotein I improves diabetic nephropathy via inhibiting TGF-β1-p38 MAPK pathway, Int. J. Clin. Exp. Pathol. 8 (3) (2015) 2321–2333.

Paper IV

Function of encapsulated rat islets in sulfated and intermediate G alginate in diabetic immunocompetent and immunodeficient mice

Joachim S. Kjesbu [a, †], Abba E. Coron [a, b, †], Peter Rios [c], Sofia Ghani [c], Douglas Isa [c], Ira Joshi [c], Matthew Bochenek [d], Anne M. A. Rokstad [b, e], José Oberholzer [f], Berit L. Strand [a, *]

[a] *NOBIPOL, Department of Biotechnology and Food Science, Norwegian University of Science and Technology, N-7491 Trondheim, Norway.*

[b] *Centre of Molecular Inflammation Research, Department of Clinical and Molecular Research, Norwegian University of Science and Technology, Trondheim, Norway.*

[c] *CellTrans Inc., Chicago, IL, USA.*

[d] *Department of Chemical Engineering, Massachusetts Institute of Technology, Cambridge, MA, USA.*

[e] *Centre for Obesity, Clinic of Surgery, St. Olav's University Hospital, NO-7006 Trondheim, Norway.*

[f] *Charles O. Strickler Transplant Center. Division of Transplantation, Department of Surgery, University of Virginia, VA 22903, USA.*

[*] Corresponding author

[†] The two authors contributed equally to this work

This paper is not yet published and is therefore not included.

ISBN 978-82-326-7534-0 (printed ver.)
ISBN 978-82-326-7533-3 (electronic ver.)
ISSN 1503-8181 (printed ver.)
ISSN 2703-8084 (online ver.)

NTNU

Norwegian University of
Science and Technology